Development of immunoassays for the rapid determination of the endocrine disruptor bisphenol A released from polymer materials and products

Dissertation

zur Erlangung des akademischen Grades:

Doctor rerum naturalium

(Dr. rer. nat.)

im Fach Chemie

Spezialisierung: Angewandte Analytik und Umweltchemie

eingereicht an der Mathematisch-Naturwissenschaftlichen Fakultät

der Humboldt-Universität zu Berlin

von Dipl.-Pharm. Anna Raysyan

Präsidentin der Humboldt-Universität zu Berlin

Prof. Dr.-Ing. Dr. Sabine Kunst

Dekan der Mathematisch-Naturwissenschaftlichen Fakultät

Prof. Dr. Elmar Kulke

Gutachter*innen: 1. Prof. Dr. Kannan Balasubramanian

2. Dr. Franziska Emmerling

3. Dr. Rudolf J. Schneider

Tag der mündlichen Prüfung: 23. September 2021

Die vorliegende Arbeit wurde im Zeitraum von September 2016 bis Mai 2021 an der Bundesanstalt für Materialforschung und -prüfung (BAM) sowie am Institut für Chemie der Humboldt-Universität zu Berlin unter der Betreuung von Herrn Priv.-Doz. Dr. Rudolf J. Schneider und Herrn Prof. Dr. Kannan Balasubramanian angefertigt.

“Nichts auf der Welt ist so mächtig wie eine Idee,

deren Zeit gekommen ist.”

Victor Hugo

(1802–1885)

Fig. i. The lateral flow device developed at BAM

Writing the thesis has been like brewing an espresso: a huge amount of material, experiments, and discussions have had to be concentrated down to produce an easy-to-consume final shot.

LIST OF PUBLICATIONS

1. **Anna Raysyan**, Inna A. Galvidis, Rudolf J. Schneider, Sergei A. Eremin, and Maksim A. Burkin. "Development of a latex particles-based lateral flow immunoassay for group determination of macrolide antibiotics in breast milk." Journal of Pharmaceutical and Biomedical Analysis 189 (2020): 113450. https://doi.org/10.1016/j.jpba.2020.113450

2. **Anna Raysyan**, Robin Moerer, Bianca Coesfeld, Sergei A. Eremin, and Rudolf J. Schneider. "Fluorescence polarization immunoassay for the determination of diclofenac in wastewater." Analytical and Bioanalytical Chemistry (2020): 1–9. https://doi.org/10.1007/s00216-020-03058-w

3. Ander Chapartegui-Arias, **Anna Raysyan**, Ana M. Belenguer, Carsten Jaeger, Teodor Tchipilov, Carsten Prinz, Carlos Abad, Sebastian Beyer, Rudolf J. Schneider, and Franziska Luise Emmerling. "Tailored Mobility in a Zeolite Imidazolate Framework (ZIF) Antibody Conjugate." Chemistry–A European Journal (2021), (in press). https://doi.org/10.1002/chem.202100803

4. **Anna Raysyan**, Rudolf J. Schneider, "Development of a rapid immunoassay to screen for the release of the endocrine disruptor bisphenol A from polymer materials." Biosensors (2021), (submitted)

5. **Anna Raysyan**, Sandro Zwigart, Sergei A. Eremin, Rudolf J. Schneider. "Highly sensitive detection of the endocrine disruptor bisphenol A by FPIA and ELISA immunoassay formats" Frontiers in Chemistry (2021), (in preparation)

Patent

Veröffentlichungsnummer: PCT/EP2021/050061;

Titel: Immunochemical device and lateral-flow immunoassay method for the determination of pharmaceutical residues and contaminants in breast milk

Presentations

1. **Anna Raysyan**, Rudolf J. Schneider, A dipstick immunoassay for the determination of bisphenol A releases from plastic materials, BAM-BfR Seminar, 14 February 2018, Berlin
2. **Anna Raysyan**, Rudolf J. Schneider, A fast dipstick immunoassay for the determination of DCF in the breast milk, BIONNALE, 20 June 2018, Berlin
3. **Anna Raysyan**, Rudolf J. Schneider, Falling Walls of complicated lab methods, Falling Walls Lab Adlershof, 28 September 2018, Berlin
4. **Anna Raysyan**, Rudolf J. Schneider, Falling Walls of complicated lab methods, Falling Walls Lab Conference (Final) 2018, 8–10 November 2018, Berlin
5. **Anna Raysyan**, Rudolf J. Schneider, Development of dipstick immunoassays for environmental and diagnostic applications missions from plastic materials, Arbeitskreistreffen Immunoassays, 26 November 2018, Hennigsdorf, Germany
6. **Anna Raysyan**, RaYs Assay, Chemistry Pitch Day 2019, 4 April 2019, Frankfurt am Main, Germany
7. **Anna Raysyan**, Rudolf J. Schneider, Enzyme membrane-based immunoassay and Fluorescence polarization immunoassay (FPIA) of AFB1 for quality assessment of pharmaceutical substances and medical herbs, The XXIIIth International Congress Phytopharm 2019, 1–3 July 2019, Saint Petersburg, Russia

Posters

1. **Anna Raysyan**, Rudolf J. Schneider, Development of a quick test to screen for bisphenol A, 20 March 2017, First European / 10th German BioSensor Symposium, Potsdam, Germany
2. **Anna Raysyan**, Robin Moerer, Bianca Coesfeld, Sergei A. Eremin, Rudolf J. Schneider, Fluorescence polarization immunoassay for determination of diclofenac in wastewater, Potsdam Days on Bioanalysis, 23 November 2017, Potsdam, Germany

3. **Anna Raysyan**, Rudolf J. Schneider, Development of a quick test to screen for bisphenol A release from polymer materials, Adlershofer Forschungsforum, 11 November 2017, Berlin

4. **Anna Raysyan**, Rudolf J. Schneider, An immunochromatographic assay for the determination of bisphenol A releases from plastic materials, International Biotech Innovation Days, 2 May 2018, Senftenberg, Germany

5. **Anna Raysyan**, Rudolf J. Schneider, Lateral Flow ImmunoAssays for the detection of bisphenol A emissions, 15 February 2019, Florence, Italy

6. **Anna Raysyan**, Rudolf J. Schneider, Development of a quick test to screen for bisphenol A release from polymer materials, Adlershofer Forschungsforum, 11 November 2019, Berlin

7. Emil Fuhry, **Anna Raysyan**, Michel Wehrhold, Tilman J. Neubert, Rudolf J. Schneider, Kannan Balasubramanian, Separation and detection of antioxidants using a graphene based electrochemical sensor platform, Chem2Dmat 2019, 3 September 2019, Dresden, Germany

TABLE OF CONTENTS

ZUSAMMENFASSUNG

Die Ereignisse des Jahres 2020 haben uns gezeigt, wie wichtig schnelle, benutzerfreundliche und kostengünstige Hilfsmittel zur Gesundheitsüberwachung sind. Aus den Erfahrungen mit der berüchtigten COVID-19-Pandemie wurde deutlich, dass die Verfügbarkeit eines Schnelltests das Schlüsselelement für ein zuverlässiges und robustes Gesundheitssystem ist. Diese einfache Technologie kann dazu beitragen, die Unsicherheit in den verschiedenen und manchmal sehr kontroversen statistischen Kennzahlen, mit denen das Gesundheitssystem in Zeiten einer Pandemie umgehen muss, erheblich zu verringern. Wenn es in Bezug auf COVID-19 möglich ist, eine große Anzahl von Menschen schnell und zuverlässig zu testen, würde dies den Druck auf das Gesundheitssystem verringern und gleichzeitig die störenden Auswirkungen der Pandemie auf Wirtschaft und Gesellschaft abschwächen.

Immunoassays wie LFIA, FPIA und ELISA (Lateral Flow Immunoassay, Fluoreszenzpolarisationsimmunoassay und Enzymimmunoassay) sind in vielen wichtigen Bereichen, wie der Diagnose von Krankheiten, der pharmazeutischen Industrie und der Umweltanalyse weit verbreitet. Die Verwendung von LFIA für ein schnelles Screening vor Ort bietet beispielsweise eine einfache und kostengünstige Alternative zu teuren, mühsamen und zeitaufwendigen instrumentellen Methoden und auch zu den komplizierteren Immunoassay-Formaten. Die Ergebnisse des LFIA können innerhalb von 10 bis 15 Minuten erhalten werden. Solche Verfahren, bei denen Membranen als feste Träger verwendet werden, haben sich als sehr vielversprechende Formate erwiesen und ermöglichen die Durchführung paralleler Assays in derselben Probe. In dieser Arbeit wurden Latex-Mikropartikel-basierte und Gold-Nanopartikel-basierte LFIA zum schnellen Nachweis von Bisphenol A (BPA) entwickelt. Ein Ziel dieser Arbeit war die Suche nach geeigneten Nitrocellulose-Membranen, Konjugatpads, Membranbehandlungen sowie nach einer geeigneten LFIA-Vorbehandlung zur Optimierung der Leistungseigenschaften des Assays. Die Ergebnisse eines LFIA-Tests können sowohl mit bloßem Auge als auch instrumentell interpretiert werden. Die visuellen Nachweisgrenzen (vLOD) wurden bei 10 µg/L gefunden. Die berechnete Nachweisgrenze (cLOD) der instrumentellen Auslesung betrug 0,14 µg/L. Die Synthese der erforderlichen Haptenproteinkonjugate und deren weitere Bewertung in einem ELISA-Aufbau führte zu einem hochempfindlichen Assay mit einer Nachweisgrenze von 0,05 µg/L. Eine zusätzliche Methode, der Mix-and-Read-FPIA zur Bestimmung von BPA, wurde entwickelt, und die Ergebnisse dieser Methode konnten innerhalb von 20 bis 30 Minuten erhalten werden. In dieser Studie wurden neue Tracer-Moleküle mit unterschiedlichen Strukturen synthetisiert, welche Fluorophore mit Derivaten des Analyten verbinden, einschließlich eines C_6-Spacers (Ahx). Der Einfluss der Ahx-Tracer-Brückenlänge auf die Assay-Empfindlichkeit wurde abgeschätzt. Die niedrigste Nachweisgrenze lag bei 1,0 µg/L mit einem Arbeitsbereich von 2 bis 155 µg/L.

Die Methoden wurden für reale Proben gegen LC-MS/MS als Referenzmethode mit guter Übereinstimmung mit LFIA, FPIA und ELISA validiert.

ABSTRACT

The events of the year 2020 have shown us the importance of fast, easy-to-use, and affordable health-tracking devices. From the experience with the notorious COVID-19 pandemic it became obvious that the availability of a rapid test is the key element for a reliable and robust healthcare system. This in fact simple technology can significantly reduce the uncertainty in the various and sometimes highly controversial statistical figures the healthcare system has to manage in times of a pandemic. With respect to COVID-19, if it is possible to test a large number of people quickly and in a reliable way, it would lift the pressure from the healthcare system and at the same time mitigate disruptive effects by the pandemic on the economic and social system.

Immunoassays, like LFIA, FPIA and ELISA (lateral flow immunoassay, fluorescence polarization immunoassay, enzyme immunoassay), have been widely used in many important fields, such as diagnosis of diseases, pharmaceutical industries, and environmental analysis. The use of LFIA for rapid on-site screening, for example, provides a simple and low-cost alternative to expensive, laborious, and time-consuming instrumental methods and also to the more sophisticated immunoassay formats. The results from LFIA can be obtained within 10 to 15 min. Such methods, which use membranes as solid supports, have proven to be very promising formats and allow parallel assays to be performed in the same sample. In this work, latex microparticles-based and gold nanoparticles-based LFIA for a rapid detection of bisphenol A (BPA) were developed. The work was focused on the search for suitable nitrocellulose membranes, conjugate pads, membrane treatments, as well as for a proper LFIA pre-treatment to optimize the performance properties of the assay. The results of an LFIA test can be interpreted both by naked eye and instrumentally. The visual limit of detection (vLOD) was found to be 10 µg/L. The calculated instrumental limit of detection (cLOD) was 0.14 µg/L. The synthesis of the required hapten-protein conjugates and further evaluation in an ELISA setup resulted in a highly sensitive assay with a limit of detection of 0.05 µg/L. An additional method, the mix-and-read FPIA for determination of BPA, was developed and results from this method could be obtained within 20 to 30 min. In this study, new tracer molecules with different structures that link fluorophores to derivatives of the analyte, were synthesized, including a C_6 spacer (Ahx). The influence of the Ahx tracer bridge length on the assay sensitivity was estimated. The lowest limit of detection was 1.0 µg/L with a working range from 2 to 155 µg/L.

The methods were validated for real samples against LC-MS/MS as reference method with good agreement with LFIA, FPIA, and ELISA.

ABBREVIATIONS AND ACRONYMS

A	
A	Parameter *A* of the sigmoidal curve, representing the maximum signal intensity
Ab	Antibody
Ag	Antigen
Ahx (C_6)	6-Aminohexanoic acid
AMF	4-Aminomethylfluorescein
B	
B	Parameter *B* of the sigmoidal curve, slope at the inflection point
BB	Borat buffer
BPA	Bisphenol A
BPB	Bisphenol B
BPF	Bisphenol F
BPS	Bisphenol S
BSA	Bovine serum albumin
BVA	Bisphenol valeric acid
C	
C	Parameter C of the sigmoidal curve, inflection point (in concentration units)
CAS	Chemical abstracts service
CR	Cross-reactivity
CV	Coefficient of variation
D	
D	Parameter *D* of the sigmoidal curve, representing the minimal signal intensity
DCC	Dicyclohexylcarbodiimide
DMF	*N*,*N*-Dimethylformamide
DMSO	Dimethyl sulfoxide
E	
EDC	*N*-(3-Dimethylaminopropyl)-*N´*-ethylcarbodiimide hydrochloride
ELISA	Enzyme-linked immunosorbent assay
EDTA	Ethylenediaminetetraacetic acid
F	
FDA	(U.S.) Food and Drug Administration
FPIA	Fluorescence polarization immunoassay
G	
GC-MS	Gas chromatography-mass spectrometry
GNP	Gold nanoparticles
H	
HRP	Horseradish peroxidase
I	

IC_{50}	Inhibition concentration. Concentration that is required for 50 % inhibition in vitro (analyte concentration at the half maximum signal intensity)
IgG	Immunoglobulin G
L	
LF	Lateral flow
LC-MS/MS	Liquid chromatography-tandem mass spectrometry
LFA	Lateral flow assay
LFIA	Lateral flow immunoassay
LMP	Latex microparticles
LOD	Limit of detection
M	
MAb	Monoclonal antibody
MALDI	Matrix-assisted laser desorption/ionisation
MRL	Maximum residue level
N	
NHS	*N*-hydroxysuccinimide
O	
OD	Optical density
P	
PAb	Polyclonal antibody
PBS	Phosphate buffered saline
R	
R^2	Coefficient of determination
rpm	Revolutions per minute
RT	Room temperature, 20 °C
S	
SD	Standard deviation
SPE	Solid-phase extraction
T	
TLC	Thin-layer chromatography
TMB	3,3',5,5'-tetramethylbenzidine
TOF/MS	Time-of-flight mass spectrometry
TRIS	Tris(hydroxymethyl)aminomethane

I. Introduction

The rapid increase in global population has accelerated the production of food, industrial products, and also the need for service activities. This has, in turn, contributed to the massive growth of the corresponding industrial sectors to meet the high demand for goods of all kind. Another effect is that the number of chemicals used in consumer products is steadily increasing, whereas understanding of their exposure pathways and associated human health risks often lag behind. Numerous studies on exposure to those chemicals have proven adverse health effects both on humans and animals. Some of the substances used in plastics production show effects on the hormone system and are therefore suspected to contribute to various diseases.

One of the most important chemicals used in the production of polycarbonate plastics and epoxy resins is bisphenol A. The substance was first synthesized in the late-nineteenth century by the Russian Aleksandr Pavlovich Dianin and it came into wider use in 1905 by Theodor Zincke from Marburg University, Germany. Today, bisphenol A (BPA) is one of the most important bulk chemicals in the world. The global volume of BPA consumption for different application areas was estimated at 7.7 million metric tons in 2015 and is expected to reach 10.6 million metric tons in 2022 at a compound annual growth rate (CAGR) of 4.8 % between 2016 and 2022 [1]. However, despite the large number of studies on the toxicity and hormonal activity of BPA, there are still open questions and thus considerable media attention regarding BPA toxicity.

1. Bisphenol A - Structure and use

Bisphenol A is an organic chemical synthesized by condensation of 2 mol phenol with one mol acetone in the presence of an acidic catalyst (**Figure 1**). The chemical formula is $C_{15}H_{16}O_2$ (**Figure 2**), with a molecular mass of 228.29 g/mol.

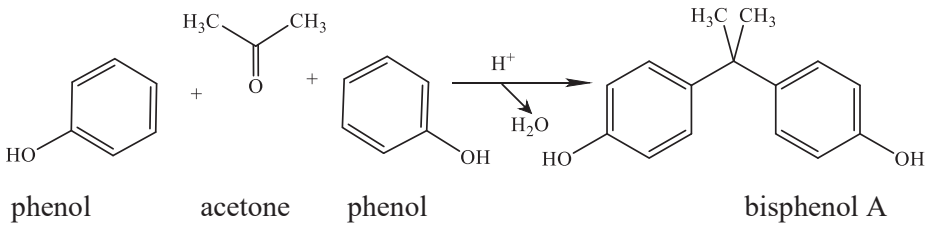

phenol acetone phenol bisphenol A

Figure 1. Reaction equation of the synthesis of BPA

BPA is a fairly water-soluble compound [2] (300 mg/L at room temperature) and dissociates in an alkaline environment (pK_a of BPA: 9.9–11.3).

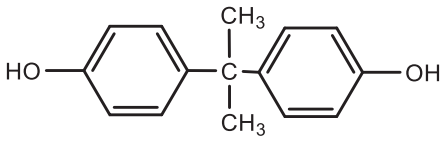

Figure 2. Chemical structure of bisphenol A

IUPAC name:
4,4'-dihydroxy-2,2-diphenylpropane
2,2-bis(4-hydroxyphenyl)propane
4-[2-(4-hydroxyphenyl)propane-2-yl]phenol

CAS name:
4,4′-(1-methylethylidene)bisphenol

Other names:
bisphenol A
bis(4-hydroxyphenyl)dimethyl methane
4,4′-dihydroxydiphenyl propane
diphenylolpropane

Polycarbonate plastic is used to make a variety of common consumer products, including baby bottles, sports equipment and medical devices, thermal [3] or recycled paper. Polycarbonate plastics are typically clear and rigid. Due to these properties, there are numerous applications for polycarbonate, such as CDs, food packaging materials, such as plastic containers for food and drinks, baby bottles, lining materials for dental sealants and orthodontic products, eyeglasses, sports safety equipment, medical equipment, visors for helmets, and microfibers [4, 5]. Epoxy resins are used as coatings for the inside of almost all food and beverage containers [6, 7] to prevent the contents from a direct contact and a possible reacting with the metal.

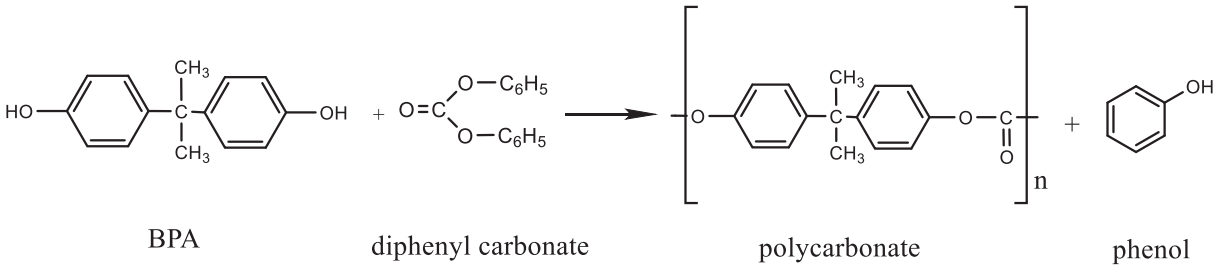

Figure 3. Reaction equation for the synthesis of polycarbonate resins

1.1. RELEASE AND HEALTH IMPLICATIONS

Bisphenol A can be easily released from its corresponding polymers by the following mechanism. The ester bond connecting the BPA molecules in polycarbonates or epoxy resins is hydrolyzed during heating or in acidic or alkaline medium. As a result, free BPA is released and can migrate into food, beverages and finally into the environment and may be taken up by the oral route. Moreover, migration is enhanced by repeated washing with detergents, rubbing and sterilization.

Bisphenol A can be easily absorbed by the oral route. It enters the animal and human body by ingesting foods and drinks that are contaminated with bisphenol A from polycarbonate bottles and cans coated with epoxy resins.

The human endocrine system controls many biological processes and is important for regulating homeostasis in the body. BPA has the capacity to mimic the effects of the female sex hormone estrogen and thus antagonize 17β-estradiol (E2), the most active estrogen (**Figure 4**). There is substantial evidence indicating that BPA has structural features that confer the ability to bind to both nuclear estrogen receptors (ERs), ERα and Erβ, which can trigger various physiological effects [8, 9]. It was found that BPA contributes to the risk of cancer [10], the development of mental problems, obesity, metabolic syndrome, and BPA possibly also contributes to infertility and subfertility. The mechanisms at the root of these multiple effects are numerous and involve BPA binding to membrane and nuclear estrogen receptors, interference with other nuclear and nonnuclear receptors [11, 12], and alterations in the synthesis or in the metabolism of hormones, as well as epigenetic deregulation.

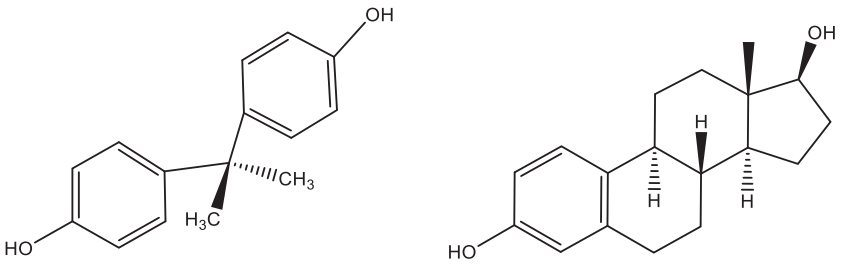

Bisphenol A 17β-estradiol

Figure 4. Chemical structure of BPA and estradiol

1.2. BISPHENOL A (BPA) REGULATIONS

BPA has become subject to product regulations because of growing concerns of toxicological significance from its potential to disrupt the hormone balance by mimicking estrogens. Canada was the first country to declare BPA as a toxic chemical in 2008 [13, 14]. For example, by 2020, the regulation body REACH mandates that thermal paper must not contain a BPA concentration equal to or greater than 0.02 % by weight.

A specific migration limit for BPA in food or food simulant has been set to 0.05 mg/kg of food (European Commission, Commission Regulation (EU) 2018/832 of 12 February 2018) [15]. Regulation 2018/213 [2] banned the use of BPA in the European Union for feeding bottles, plastic cups and packaging containing food intended to be used by infants and children younger than 3 years old.

In January 2015, the European Food Safety Authority [2] issued a new value of tolerable daily intake (TDI) of 4 μg/kg of body weight per day of BPA. Previously, the amount of BPA exposure that the EFSA considered "safe" was a TDI of 50 μg/kg of bodyweight (bw)/day (equivalent to 0.05 mg/kg of bw/day) [2]. The EFSA estimates an exposure of approximately 1.5 μg/(kg and day) in adults and 0.2–13 μg/(kg and day) in infants and children just from food sources alone. The Food and Agricultural Organization within the World Health Organization (FAO/WHO) issued a tolerable daily intake (TDI) of 1.5–4.2 μg BPA/kg bw/day in 2010 [16]. In 2012, the United States Food and Drug Administration (FDA) banned the use of BPA in baby bottles intended for children under 12 months [17, 18]. In July 2013, the FDA completely banned the use of BPA in coating compositions that are used in packaging materials for products to be used with infants. A study by Vandenberg et al. [19] in the United States proved that BPA was found in 93 % of the tested urine samples with detectable levels.

These regulations exemplarily demonstrate that early prevention of contaminations of food and environment from this toxin is necessary to protect human health.

1.3. ANALYTICAL METHODS TO QUANTIFY BISPHENOL A

Several analytical methods have been proposed to detect and quantify bisphenol A in plastic materials, food, and beverages. Bisphenol A analysis has frequently been performed by gas chromatography, mostly after derivatization, and liquid chromatography, applying mass spectrometric or fluorescence detection. An overview is given in **Table 1**.

Table 1 Analytical methods of determination for bisphenol A.

Instrumental methods	Substance	Sensitivity	Reference
LC-MS/MS	Beverages, water samples, plastic materials; milk samples; breast milk.	LOD 0.22 ng/mL	[20–24]
GC-MS(SIM) **GC-MS/MS**	Beverages: sweet corn, peas with carrots; human breast milk	LOD 3 pg/mL LOD 0.05 µg/kg	[25] [26]
UPLC-MS/MS **DLLME–UHPLC–MS/MS**	Dental materials human urine eggs	LOD 0.44 pmol/mL LOQ 1.10 pmol/mL LOD 0.02 µg/kg	[27] [28, 29]
HPLC-UV	Milk samples	LOD 3.05 µg/L	[30]

The sample preparation constitutes the key step to determine BPA in different matrices. Although the conventional analytical methods are usually very sensitive and accurate, they are technically complex, time-consuming, require costly and sophisticated instrumentation and do not allow for field portability or high-throughput analysis [31]. Hence, it is necessary to develop a sensitive, simple, cost-efficient, specific, portable, and rapid method for monitoring bisphenol A and in particular, for high sample through-put and on-site screening analysis.

2. IMMUNOCHEMICAL METHODS – STATE OF THE ART

Immunoassays display a platform for clinical diagnostics studies, biopharmaceutical analysis, environmental monitoring, and food testing, that quantifies and identifies unknown analytes in the sample based on antibody-antigen interactions [32].

Immunoassays offer several advantages, such as simplicity and specificity comparable with the conventional analytical methods. Immunoassays are cost-effective and more importantly, on-site analysis is also possible. The ease of automation, an efficient and high throughput, and the versatility in the applications of immunoassays have contributed to make this method more and more popular in recent years.

Antibodies are the essential reagents that play a critical role in various bioanalytical methods, such as immunoassays. A large part of biotechnological research deals exclusively with the production of antibodies [33, 34] , not only for science research or diagnostic purposes but also for therapeutic purposes.

2.1 Antibody structure and production

Antibodies are immune system-related proteins called immunoglobulins. Antibodies are divided into five major classes, IgM, IgG, IgA, IgD, and IgE, based on their constant region structure and immune function. The most common type of antibody for immunoassays is the IgG class of immunoglobulins. IgG antibodies are Y-shaped proteins (**Figure 5**) that consist of two light polypeptide chains (25 kDa) that are linked together by disulfide bonds and identical heavy polypeptide chains (50 kDa).

The light and heavy chains both have one variable domain (V_L and V_H, respectively), and additionally the light chain has a single constant domain (C_L and C_H, respectively), whereas the heavy chain contains three constant domains (CH_1, CH_2, CH_3). The two antigen-binding fragments (Fabs) are responsible for binding to the target, whereas the highly conserved Fc (fragment crystallizable) region interacts with effector molecules. Each variable domain (V_L and V_H) contains three hypervariable loops, known as complementarity determining regions (CDRs), evenly distributed between four less variable framework (FR) regions. It is the CDRs that provide a specific antigen recognition site on the surface of the antibody, and the hypervariability of these regions enables antibodies to recognize an almost unlimited number of antigens. From an analytical point of view,

the most relevant region is the paratope, also called antigen-binding site; that is the part of an antibody which recognizes and binds to an antigen [35]. The selectivity and sensitivity of an immunoassay are controlled by the nature of the antibody–antigen binding process.

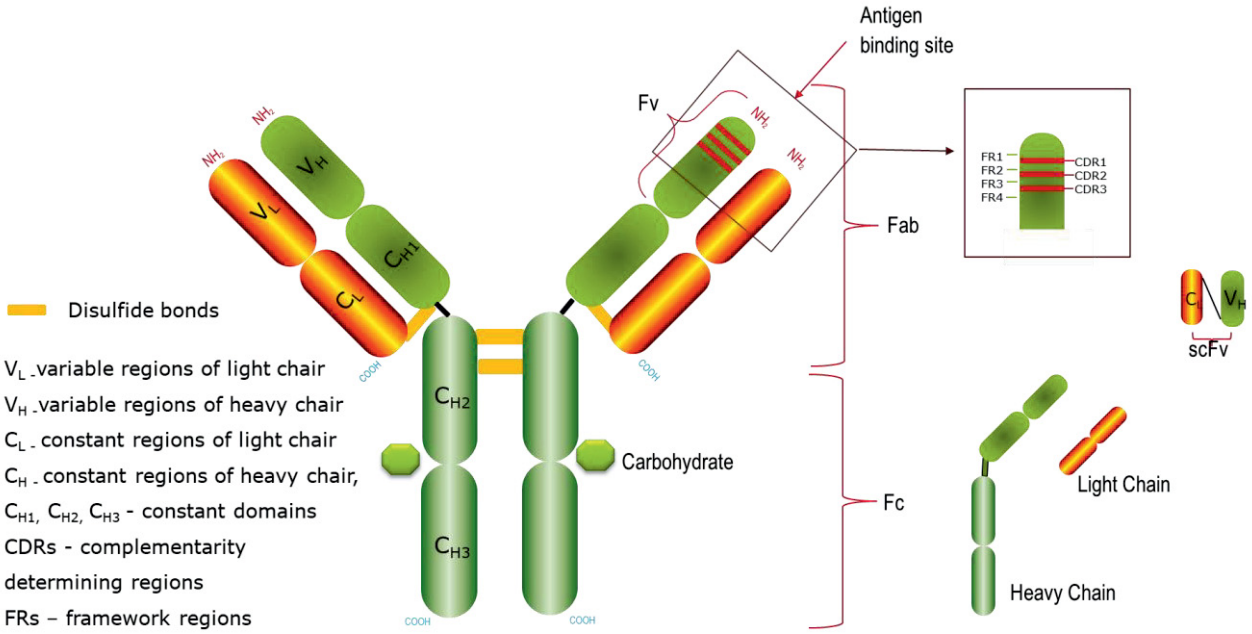

Figure 5. Structure of IgG

There are two primary types of antibody [36], namely monoclonal and polyclonal, which are determined by the means in which they are produced.

2.1.1. Polyclonal antibodies

Polyclonal antibodies are produced by injecting an immunogen into an animal with different epitopes that characterize the particular immunogen. Relatively large animals, such as rabbits, goats, sheep, guinea pigs, donkeys and fowl, have all been used for the generation of polyclonal antisera. The chosen subject used for the immunization depends on the type and quantity of antiserum required, on the previous success of the particular type of animal and on the cost and welfare of the animal. After being injected with a specific antigen to elicit a primary immune response, the animal is given a secondary even tertiary immunization to produce higher titers of antibodies against the particular antigen. Rabbits and sheep are frequently used for the production of polyclonal antiserum because they are cheap and easy to handle for immunization and bleeding purposes. Polyclonal antibody (IgG) production is relatively cost-effective and does not involve laborious

techniques. Polyclonal IgGs can bind to different epitopes of the same antigen, may cross-react with structurally related molecules, and there is little consistency between batches [33].

2.1.2 Monoclonal antibodies

Monoclonal antibodies are produced by the same clone of plasma B cells, and they bind to a unique specific epitope on the antigen. The first system for the production of monoclonal antibodies was reported by Köhler and Milstein in 1975 [37]. It provided an alternative method for antibody production, resulting in the isolation of a homogenous antibody population. The chosen subject used for the immunization is mouse or rat, then B lymphocytes are generally isolated from an immunized animal and the cells are fused with the myeloma cell to obtain an immortal population of hybridoma cells. The hybridoma cells are cultured in HAT ((hypoxanthine, aminopterin and thymidine)-supplemented media) medium in order to obtain large populations of monoclonal plasma B hybridoma cells. This HAT selection system was previously described by Littlefield et al. [38, 39]. Monoclonal antibody (IgG) can be harvested from culture vessels. Monoclonal IgG are expensive to produce, require skills to handle cell culture technology for the production and are time-consuming. Yet, assays based on monoclonal IgG may exert less cross-reactivity and it is straightforward to produce them reproducibly.

Small molecules, such as bisphenol A, are classified as haptens. A “hapten” is a low-molecular mass molecule that reacts with a specific antibody but cannot elicit an immune response unless conjugated to a large molecule, for example a protein. Designed haptens usually consist of a molecular “spacer” arm (linker) for their covalent attachment to carrier proteins. It has been proven that the structure of a hapten and the length of the hapten spacer has influence on affinity and specificity of the antibody and the sensitivity of the resulting immunoassays [40].

Low molecular weight and one antigenic determinant of hapten impede the simultaneous binding of two or more antibodies [41, 42]. Therefore, competitive immunoassays are the main format for detecting low-molecular weight compounds.

2.2. Enzyme-linked immunosorbent assay (ELISA)

Immunoassays can be divided into two groups: homogeneous and heterogeneous. A heterogeneous immunoassay, such as in the ELISA methods, are based on enzyme-catalyzed (horseradish peroxidase (HRP)) reaction resulting in the generation of an optical signal. By using chromogens, such as tetramethylbenzidine (TMB), the terminal measurement of absorbances by a simple UV-vis photometer is enabled [43].

2.2.1. Indirect competitive ELISA

In the indirect competitive ELISA, a hapten-protein conjugate is first immobilized on the surface of a flat-bottom well of a 96-well microtiter plate (MTP) possessing high protein-binding capacity (**Figure 6 A**).

Unoccupied binding sites are blocked with casein to prevent non-specific binding of the antibody. In the next step, analyte (BPA) is added. Then, analyte and hapten-protein conjugate compete for the binding sites of the primary antibody specific to BPA (anti-BPA IgG). When the analyte binds to the antibody, it remains in the solution and is removed with the next washing step. If the conjugate binds to the primary antibody, the antibody is fixed to the surface of the microtiter plate. For detection of the primary antibody, a secondary antibody (enzyme-labeled IgG specific to the primary antibody) is added. The quantification is carried out here again by measuring the absorbance. The amount of surface-bound antibody is indirectly proportional to the analyte concentration in the sample.

2.2.2. Sandwich ELISA

The sandwich ELISA measures the amount of analyte, which is bound between two antibodies. As in the assay two antibodies are required, the sandwich ELISA is restricted, because the analyte must contain at least two epitopes [43] and two different antibodies are needed.

To perform this assay, a “capture” antibody is immobilized on the surface of the well of an (MTP). Unoccupied binding sites are blocked with casein to prevent non-specific binding of the analyte. The analyte is then added and bound or captured by the “capture” antibody. Unbound analyte is removed with the next washing step and an enzyme-labeled “detection” antibody is added, which recognizes a distinctly different epitope on the analyte, thus completing the sandwich. The assay is then quantified by measuring the amount of detector antibody bound (an enzyme-labeled

antibody) using a colorimetric substrate (TMB). In this case, IgG can be an analyte. An example of the assay is demonstrated in **Figure 6 B**.

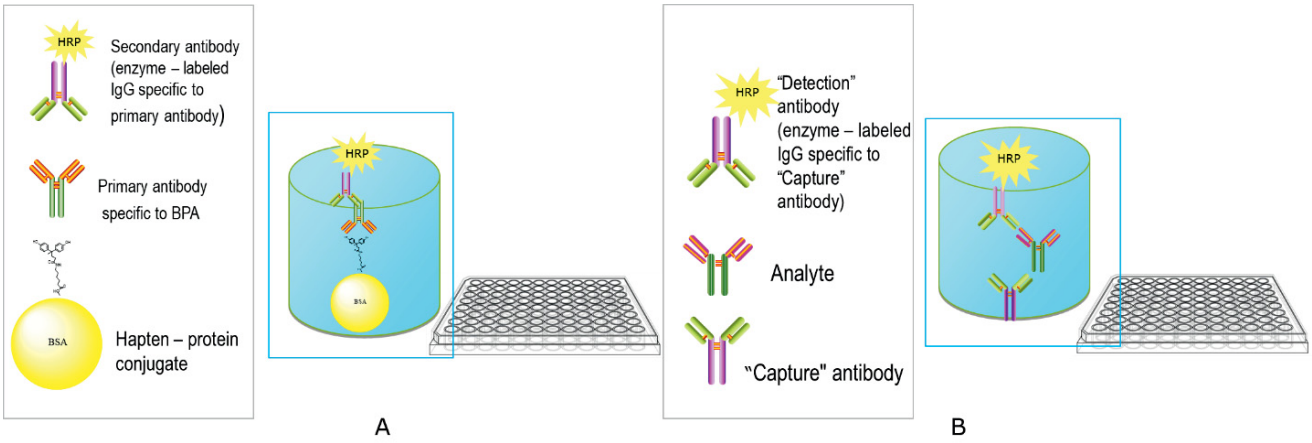

Figure 6 A. Schematic illustration of a competitive indirect ELISA for determination of BPA. **B**. Schematic illustration of a sandwich ELISA

2.3. Fluorescence polarization immunoassay (FPIA)

A prominent example of a competitive homogeneous immunoassay, the Fluorescence Polarization Immunoassay (FPIA), was first described by Dandliker and Feigen (1961) [44]. In contrast to ELISA, for the quantification of the antibody-antigen reaction the immobilization of reagents is not required, and the sample constituents are in contact with the antibody and tracer for a prolonged time. It can be performed in a single step and there is no need for any washing steps which makes the entire procedure easier and faster since the procedure is just mixing the reagents. So, FPIA is sometimes classified as a mix-and-read assay [45, 46]. Lastly, sample constituents that might interfere with the fluorescence measurement, either via intrinsic fluorescence or by quenching, have to be evaluated for their effect on assay performance.

The signal originates from observing the fluorescence emission of an analyte-fluorophore conjugate (the tracer) [47]. It is added to the sample and the mixture excited by plane-polarized light, produced via a polarizer between lamp and sample cuvette. The emitted fluorescence radiation is recorded via a photomultiplier in front of which another polarizer is positioned. An intensity value of the incident light is recorded ("parallel", $I_{\parallel}$) and then a second value after rotating the second polarizer by 90° ("perpendicular", $I_{\perp}$). Some instruments possess a second detector in 90° position which records $I_{\perp}$ simultaneously. The difference of both recordings divided by the sum of both

recordings (in the case of equal sensitivity in both directions) is called fluorescence polarization FP (reported in millipolarization units, mP) [48]. The following formula is used to calculate the degree of polarization (P) in millipolarization units (mP):

$$P = \frac{I_{par} - G \cdot I_{per}}{I_{par} + G \cdot I_{per}}$$

The phenomenon of FP is also known as anisotropy r. It only differs in the way of calculation; for anisotropy, the perpendicular intensity in the denominator is counted twice ($I_{\parallel} + 2I_{\perp}$).

This denominator term describes also the total fluorescence intensity of polarized light. The G factor is a measure of the instrument-specific geometry, which dependents on the applied wavelength. The G factor is determined by measuring the intensities in parallel and perpendicular polarizer settings, while the polarizer for the exciting light is rotated by 90° compared to normal polarization measurement. In other words, the ratio of the perpendicularly and parallelly measured intensities is the G factor [48].

Then, antibody is added in solution. Two extreme examples may illustrate the processes that take place:

If (a) no (or a small amount of) analyte is present in the solution, the larger fraction of the tracer binds to the antibody. As a result, its orientation in space, which before was in steady change due to Brownian motion, rotation and diffusion, is rather conserved: the registered intensity values of both detectors gradually decline while differing strongly from each other and after reading at a fixed time, a large polarization FP is registered.

If (b) there is a high analyte concentration in the mixture, mostly analyte molecules bind to the antibody added, the tracer remains largely "free" (and, therefore, subject to Brownian motion, fast rotation, and diffusion) so that in consequence the incident polarized light is transformed to depolarized fluorescence emission in all directions: little light hits the detector and $I\perp$ is similar to $I\parallel$, resulting in a small difference, i.e., a small value for the polarization FP. Plotting FP against the analyte concentration on a logarithmic scale results in a sigmoidal curve as with all immunoassays. As fluorophore, in the large majority of applications, fluorescein is used, and the instruments are adapted to its peak excitation at 494 nm and peak emission at 521 nm for measurement.[43, 49, 50]. According to the assay steps, FPIA is a technique where kinetics play an important role.

Therefore, the length of all incubation steps (i.e., the time after addition of the tracer and before addition of the antibody, and the time after which the read-out is recorded) has to be optimized in order to obtain a sensitive assay and controlled in order to obtain good reproducibility. The schematic principle of FPIA is shown in **Figure 7**. Plotting mP against the analyte concentration on a logarithmic scale results in a sigmoidal curve as with all immunoassays [46].

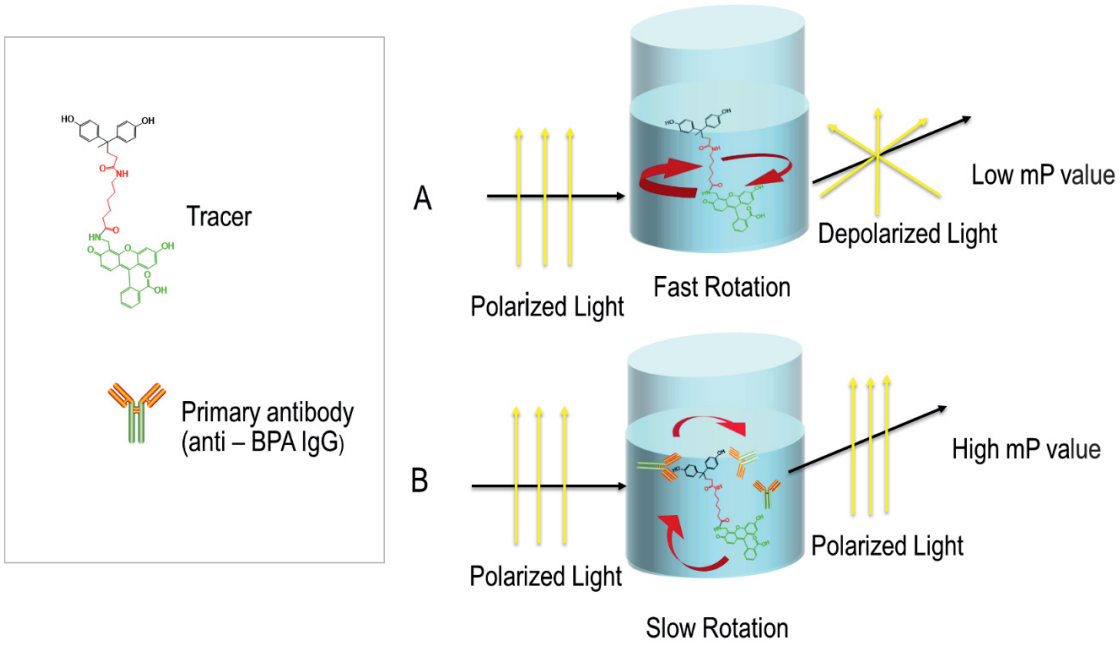

Figure 7. Schematic principle of FPIA for determination of BPA

2.4. Lateral flow immunoassay (LFIA)

The lateral flow immunoassay (LFIA), also known as dipstick assay or immunochromatographic assay (ICA), is a type of a membrane strip for detecting the presence of a target analyte in the sample. LFIAs have first been reported in the early 1980s; and in 1984, the first commercial lateral flow strip product was launched as a urine-based pregnancy test [51]. Due to low-cost materials in the manufacturing process, a relatively short assay development time, affordability, sensitivity, specificity, user-friendliness, speed, robustness, and equipment-free use (it has ability to be operated by people without professional training) the LFIA has become a widely used format. Lateral flow devices meet the World Health Organization's (WHO) criteria for point-of-care diagnostics and technology has been employed to develop a wide and growing range of tests for clinical, veterinary, agricultural, food industry and environmental applications [52, 53]. The qualitative method provides a positive response when the target analyte content is higher than a set threshold

and the results can be assessed with strip readers (color density scanners, fluorescence scanners), including smartphone-based strip readers [54–57].

According to Markets & Markets, (https://www.marketsandmarkets.com/), the lateral flow assay market was valued about 5 billion Euro in 2017 and is expected to reach 10 billion Euro by 2026. Nowadays, several different types of the lateral flow devices are available, such as for infectious diseases testing, mosquito-borne disease testing, influenza testing, sexually transmitted infection testing, HIV testing, HPV testing, chlamydia testing, gonorrhoea testing, syphilis testing, hepatitis testing, tuberculosis testing, and SARS-CoV-2 testing. The lateral flow assay market comprises hospitals and clinics, diagnostic laboratories, personal home care, pharmaceutical and biotechnology companies and private end users.

A database search for patent applications using Google Patent Search (https://patents.google.com/) with the search terms “lateral flow”, “lateral flow device” and “immunochromatography” for the years 2000 to 2019 yielded 5000 hits. According to the Google data base the annual numbers of patent applications follows a growing trend.

2.4.1. Elements of Lateral Flow Immunoassays

A Lateral flow immunoassay is based on different components, each serving one or more purposes. The LFIA strip includes a sample pad, a conjugate pad, a wicking or absorbent pad and a nitrocellulose membrane, which are all applied to a self-adhesive plastic backing card [56, 58]. **Figure 8** shows the typical configuration of an LFIA strip.

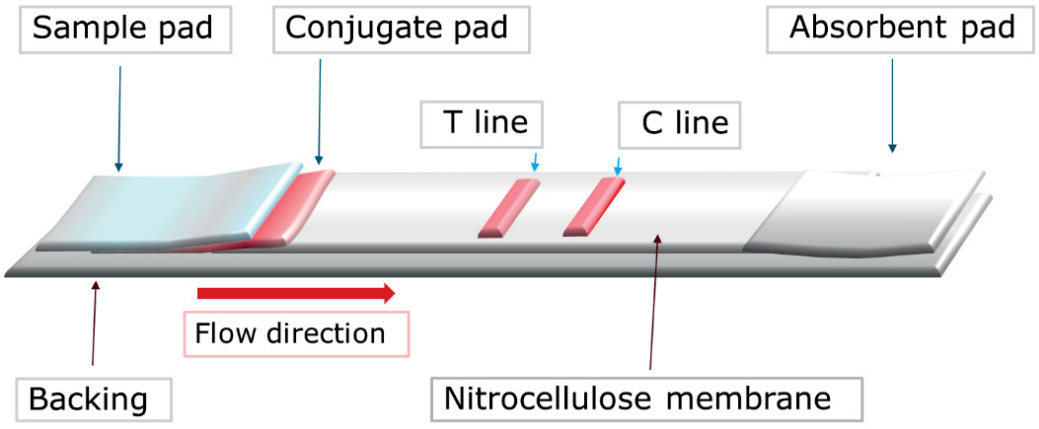

Figure 8. Configuration of a lateral flow immunoassay

Sample pad

The sample pad is commonly manufactured of rayon, glass fiber or cellulose (**Fig. 8**) (**Table 3**). The sample pad is the first material on the strip which has contact with the sample liquid. The main function of the membrane is to absorb the sample fluids and treat it such that it is compatible with the assay and that it will release the analyte with high efficiency to the analytical membrane via the conjugate release pad. Sample treatments include the filtering out of particulates, changing the pH of the sample, actively binding sample components that can interfere with the assay, and disrupting matrix components, such as mucins, in order to release the analyte to the assay [56, 59].

Conjugate pad

The conjugate pad is commonly manufactured of glass fiber (**Fig. 8**) (**Table 3**). For the best result, the material must be hydrophilic and allow a rapid flow rate. The role of the conjugate pad is to accept the antibody−gold nanoparticles (IgG−GNPs) or antibody−latex microparticles (IgG−LMPs) conjugate, hold it stable and release it when the liquid flows across it. To ensure optimal release and stability it is often necessary to pre-treat the conjugate pad [56, 60, 61].

Absorbent pad

The absorbent pad is usually manufactured of high-density cellulose (**Fig. 8**) (**Table 3**). The role of the pad is to wick the fluid through the membrane and to collect the processed liquid. The absorbent pad allows to increase the sample volumes, which results in increased test sensitivity. Moreover, proper choice of the absorbent pad could increase the speed of signal development or by limiting the liquid capacity it can be used to stop the liquid flow at a desired time. The choice of wicking material is generally dictated by absorptive capacity, cost, and capillarity [55, 56].

Nitrocellulose membrane

The nitrocellulose membrane is one of the most important materials used in lateral flow immunoassay devices (**Fig. 8**). The main function of the nitrocellulose membrane is to bind proteins at the test and control areas and to maintain their stability and activity. Proteins bind to nitrocellulose through a combination of electrostatic interactions (see structure in **Fig. 9**), especially through the interaction of the strong dipole of the nitrate ester with the strong dipole of the peptide bonds of the protein [55, 56, 62].

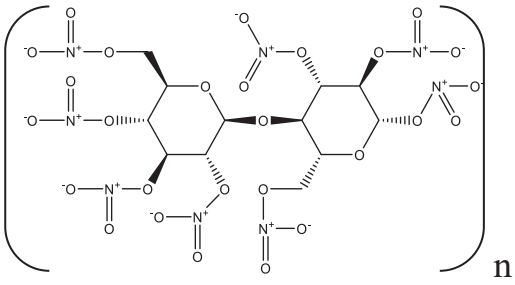

Figure 9. Chemical composition of a nitrocellulose polymer subunit

The nitrocellulose membranes are available in various pore sizes, porosities, and thicknesses (**Table 4**) [63].

Many factors affect the binding process, and these must be considered when developing assays and processing nitrocellulose membranes. Some of these factors are listed below [56, 63]:

(i) Membrane's protein binding capacity

It is determined by the amount of polymer surface area available for immobilization. The available surface area is determined by capillary flow rate, pore size, and thickness.

The capillary flow time is directly related to pore size. A larger pore size correlates with a faster flow and a smaller pore size correlates with slower flow across the membrane (**Table 4**). The membrane with smaller pore size (long capillary flow time) will increase the assay time. Slow speed increases the incubation time between the particles, the analyte, and the test line, which can increase the sensitivity. It is important to screen membranes for each assay from a variety of manufactures.

(ii) Reagent choices

The loading capacity of a protein (IgG, OVA, BSA, casein, gelatin etc.) on a given surface area depends on the protein's compactness in structure and its Stokes radius (effective diameter). For IgG, the approximate loading capacity is 1 μg/cm^2. Multiplying the loading capacity of IgG (1 μg/cm^2) by the surface area ratio of the membrane (50 – 200) produces an approximate IgG binding capacity of 50 – 200 μg/cm^2. In a typical test strip, the test line is 1 mm wide. If the strip is 1 cm wide, the amount of capture reagent that can be bound is 5 – 20 μg (0.1 cm width x 1 cm length = 0.1 cm^2).

(iii) Environment

Humidity and temperature should be optimized for increase the binding capacity of the membrane. Preliminary to striping/spotting, the nitrocellulose membrane needs to be equilibrated to a controlled humidity environment of ~50 % relative humidity (RH).

Nitrocellulose membranes that are too dry may result in spotty, non-uniform lines, whereas nitrocellulose that is too damp will result in a widened test line that may decrease the signal intensity. Usually, it is recommended that after receiving new membranes, to expose the membrane to the "wet room" environment overnight or for a period of 8 to 12 hours prior to striping.

(iv) Dispensing methods

For dispensing the proteins onto the nitrocellulose membrane either contact or non-contact dispensing systems can be used. The non-contact systems are preferable, they provide precise amounts of reagent to be as quantitative as possible. Important parameters for the spotting process include the reagent concentration and dispensing rate.

(v) Blocking reagents

The purpose of blocking a nitrocellulose membrane is to prevent the binding of proteins and label conjugate to the membrane at areas other than the test and control lines. It also serves other functions, including maintenance of hydration of membranes, modification of wicking rates, and stabilization of test and control line proteins.

(vi) Drying time and methods

These can affect the arrangement and activity of proteins on the membrane. After the striping/spotting, the membrane is exposed to an elevated temperature for some time (e.g., to 37 °C for one hour) to remove the excess water from the deposited striping solution. The membrane is then allowed to dry further by being kept in a controlled humidity environment of < 30 % RH to further fix the proteins to the nitrocellulose.

2.4.2. Antibody−particle conjugates

The main component of LFIA is the detector particles that are decorated with antibodies [64]. A common type of detector particles used in LFIA are gold nanoparticles and latex microparticles for visualization purposes, which appear as a colored line when bound at a specific location on the membrane [56, 65]. Because the optical properties of gold nanoparticles are dependent on size and shape, the sensitivity of LFIA is limited by the intensity of the signal from the small (typically 40 nm in diameter) reporter particles [66, 67]. If the clinically relevant range of the analyte cannot be reached, the lateral flow strip will not have a commercial market.

The particle size is the important factor that influences the wicking time. Capillary rise of larger gold nanoparticles (≈ 40 nm) through lateral flow membranes was slower than for smaller ones (≈ 20 nm) [16]. The latex microparticles size was 300 nm, and their mobility was sufficiently decreased. However, several studies showed that a decreased mobility of larger particles resulted in a better assay sensitivity [68]. Good mobility of the latex microparticles also depended on the wicking time of the membrane and its pore size [69, 70]. Antibodies are composed of amino acids, some with reactive side chains which can be utilized for covalent coupling with particles containing superficial functional groups that have been produced previously on the particles [71]. An alternative simple method for conjugation of proteins with particles is via passive absorption [72] which is based on three separate but dependent phenomena:

1) ionic attraction between the abundant positively charged sites on the antibody and the negatively charged gold nanoparticles
2) hydrophobic interaction between the antibody and the gold surface
3) dative binding between the gold conducting electrons and amino acid sulfur atoms of the antibody

According to Nardo et al. [73], covalent coupling of antibodies to gold nanoparticles has more benefits, such as low risk of aggregation during the coupling process, no dependency of the coupling efficiency on coupling conditions, that generally less antibody is required than for passive absorption, and the higher stability of the conjugate. However, passive absorption is a traditional method of conjugation, little chemistry is involved in contrast to covalent coupling that requires an additional activation step for the carboxyl group on the surface of the particles with EDC and NHS chemistry). Clearly, passive adsorption is performed at less cost [74]. Moreover, conjugating

proteins, for example, with gold nanoparticles can lead to diverse affinities for their antigens depending on how the antibodies are immobilized.

2.4.3. Variants of Lateral flow immunoassay format

2.4.3.1. Sandwich format

The sandwich format of LFIA is used for high molecular weight analytes with multiple antigenic sites [56, 75]. The best-known example of this format is the pregnancy test. It works by detecting human chorionic gonadotropin (hCG). To perform this assay, two analyte-specific antibodies are used separately as "capture" and "detecting" reagents [55, 56, 76, 77]. If there is target present in the sample, it will be sandwiched between the "detector" antibody−gold nanoparticle conjugate and the "capture" antibody on the test line, yielding a positive signal. A positive test is represented by the presence of a colored test (T-line) and control line (C-line) (**Figure 10 B**). The response is directly proportional to the amount of analyte in the sample. A negative test is represented by the absence of a T-line (**Figure 10 A**). The control line zone will always bind the surplus antibody-nanoparticle conjugate, yielding a strong control line signal that demonstrates that the assay is functioning correctly.

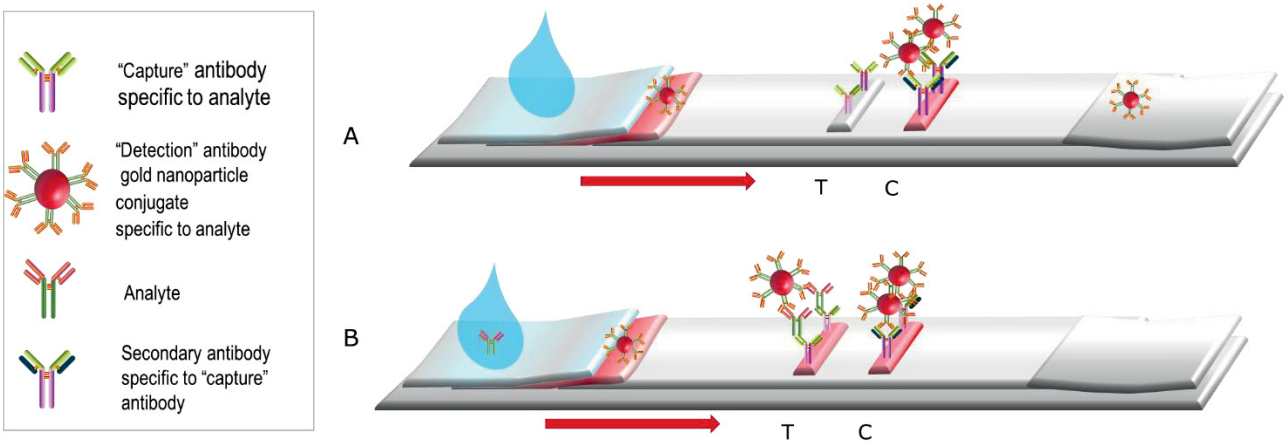

Figure 10. Schematic illustration of a sandwich LFIA. **A**. Negative result. **B**. Positive result

2.4.3.2. Competitive format

Competitive LFIA format used for low molecular weight analytes that have only one epitope, such as for the determination of bisphenol A [78, 79]. To perform this assay, an analyte–protein conjugate is applied at the T-line, and nanoparticle-conjugated analyte-specific antibody is applied at

the conjugate pad. In order to verify that the device does, indeed, function, a control line is often added to provide a control signal. Thus, when the solution does not contain any target analytes in the sample, the antibody gold nanoparticle conjugate will bind to the T-line and the C-line, yielding a strong signal intensity. If the analyte is present in the sample, the antibody–nanoparticle conjugate will bind the analyte in solution and will not be able to bind to the immobilized analyte-protein conjugate, thus diminishing the intensity of the test line signal (**Figure 11**).

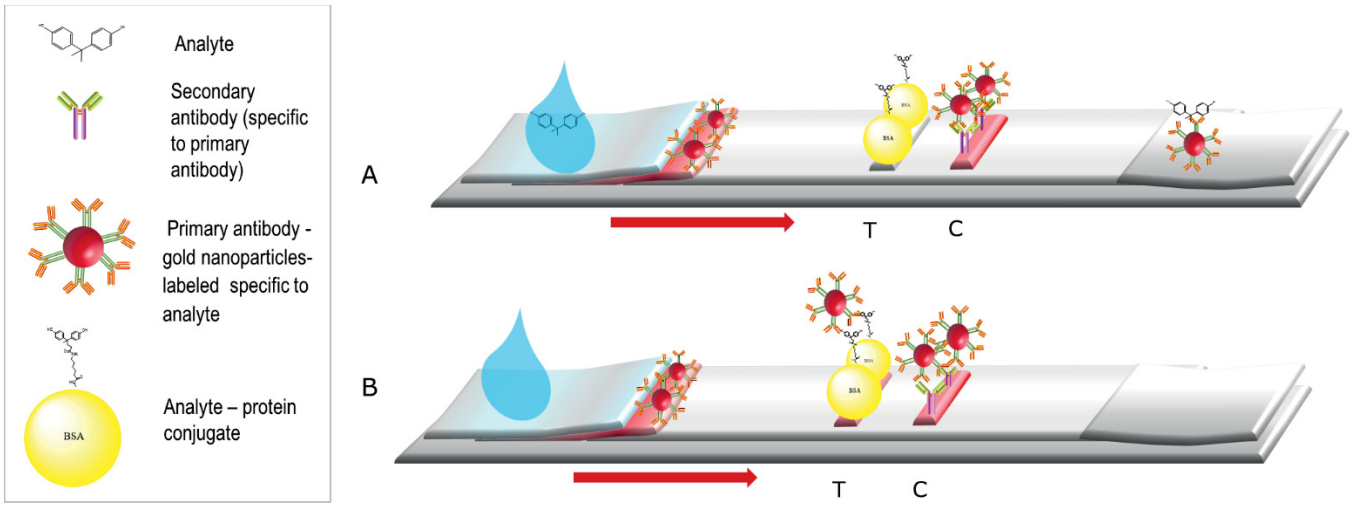

Figure 11. Schematic illustration of competitive LFIA. **A**. Positive result is seen when the analyte becomes bound to the analyte-specific antibody and therefore cannot bind to the analyte-protein conjugate which has been immobilized at the T(test) line. **B**. Negative result

2.5. ANALYTICAL PERFORMANCE DESCRIPTION OF IMMUNOASSAYS

Four-parameter sigmoidal fitting is the most commonly used with immunoassays. The calibration curves are fitted to the mean absorbance values (ELISA), intensities (LFIA) or FP values (FPIA) applying an equation proposed by Rodbard [80] (**Equation 1**):

$$S = \frac{A - D}{1 + \left(\frac{c}{C_o}\right)^B} + D \qquad (1)$$

Where S is the mean value of the signal, and c is the analyte concentration. The variables A to D were assigned to specific features of the curve: A (upper asymptote), B (slope at the inflection point), D (lower asymptote) and C_o (the inflection point, midpoint) (**Figure 12**) [81]. The C_o parameter is often equal to the 50 % inhibitory concentration (IC_{50}) of the calibration curve and indicates the concentration of analyte which induces a response halfway between the upper asymptote and lower asymptote after a specified exposure time. The concentration of 50 % inhibition is a measure of the sensitivity of immunoassays. The lower the IC_{50} the more sensitive is the immunoassay. Due to Weller et al., the computing of affinity constants can be accomplished when extrapolating the found midpoint (IC_{50}) of both enzyme conjugate and antibody approaching zero in a series of dilutions [82, 83]. The correlation coefficient (R^2) is one of the primary criteria for goodness of fit and must be at least 0.90 [84].

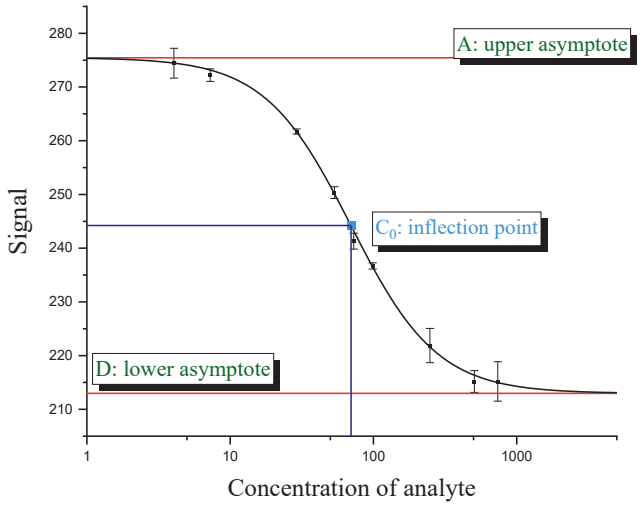

Figure 12. Example of calibration curve (gray solid line) used to correlate signal with analyte concentration

The measurement range was assessed applying the concept of the precision profile (a response error relationship) according to Ekins [85] by calculating the relative error for each calibrator concentration, using, for interpolation of the profile, the model by Hoffmann et al. [86] (**Equation 2**).

$$x = -100\frac{\sigma(s)}{B(D-A)}\left[\left(\frac{C_0}{c}\right)^B + 2 + \left(\frac{c}{C_o}\right)^B\right] \quad (2)$$

A function, $y = (ax^b) + c + \left(\frac{d}{x^e}\right)$, developed before [86], allows to fit a continuous line to the data points of the precision profile, with *a*, *b*, *c*, *d*, and *e* being variables, *x* being the concentration of the analyte. The precision profile of immunoassays shows a typical U shape (**Figure 13**). A relative error of the determined concentration of 30 % was considered allowable to mark the limit of detection (LOD).

The determination of the limit of detection (LOD) can be made in several ways and has therefore been subject for discussion [87]. For a linear calibration curve, it is assumed that the instrument response *y* is linearly related to the standard concentration *x* for a limited range of concentration $y = a + bx$. The model is used to compute the sensitivity *b* and the limit of detection (LOD) [88] (Equation 3).

$$\mathbf{LOD} = \mathbf{3,3} \times \frac{\boldsymbol{\sigma}}{\boldsymbol{m}} \quad (3)$$

where σ is the standard deviation of the response and *m* is the slope of the calibration curve.

In the immunoassays the limit of analyte detection (LOD) is, for simplicity, often set to 20 % of the inhibitory concentration value (IC_{20}), and the dynamic range of assay defined as IC_{20} …IC_{80}.

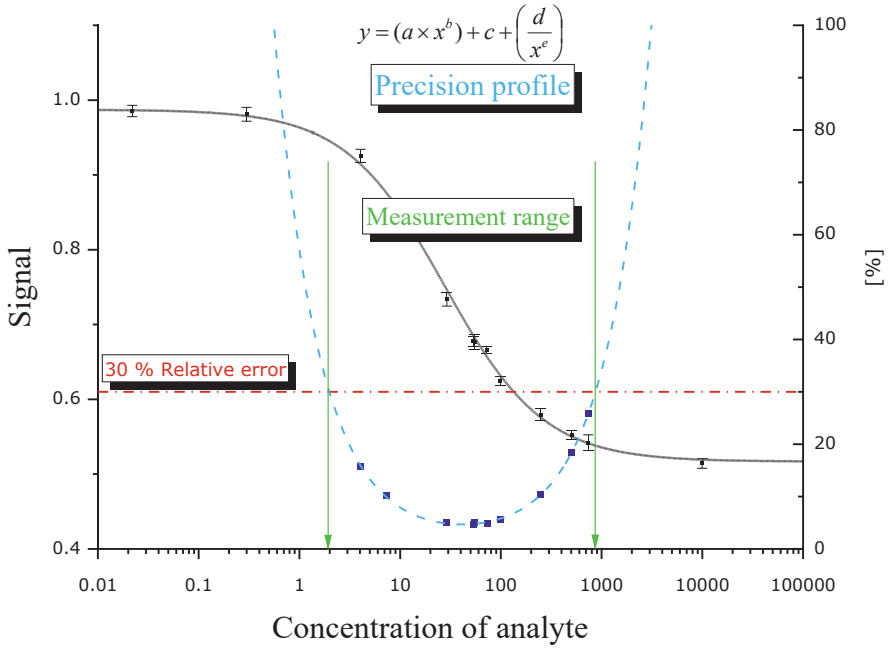

Figure 13. Example of calibration curve of and precision profile (dotted line shows moving average of three adjacent points) using three replicates per calibrator

The coefficient of variation (CV) between test replicates was determined using the following formula [89]:

$$CV = \frac{\text{STDev}}{\text{Mean}} * 100\ \%$$

Where, CV is coefficient of variation; STDev is standard deviation.

2.6. SELECTIVITY OF ANTIBODY

In addition to the actual target analyte, structurally similar compounds are also detected in an immunoassay. The reason for this is that these compounds also fit sterically and electronically into the binding site of the antibodies. Therefore, they can cross-react with similar epitopes of compounds structurally related to the target analyte, but usually with less affinity. In order to estimate how large the influence of cross-reactions on an assay is, different substances structurally related to the analyte itself are tested. Antibodies with a broad cross-reactivity (CR, in %) pattern can be used to simultaneously detect a group of structurally related compounds and for the development of broad-specificity screening immunoassays. This effect can often be observed in polyclonal antibodies, as different antibody fractions are present in the serum [90]. But for the accurate and precise determination of one analyte, only low or ideally no cross-reactivities are desired.

Immunoassay selectivity was tested by assaying several compounds structurally related to bisphenol A. The specificity of the monoclonal antibody and selectivity of the assay was evaluated [91] by determining their IC_{50} values (midpoints, parameter C in the 4-parametric sigmoidal fitting curve ~half maximum inhibitory concentration) and calculating their cross-reactivity (CR, in %) as follows:

$$CR_{\%} = \frac{IC_{50}(BPA)}{IC_{50}(test\ compound)} \times 100\ \%$$

When an antibody binds to unintended proteins, to particles or to sensor surfaces by simple adsorption, hydrophobic, and other types of interactions, we speak of “non-specific binding” (NSB). Although the causes of non-specific background immunostaining may differ, they all equally complicate the use of immunoassays. However, this is not an actual affine detection and the problem can be easily avoided by buffer additives [92] or optimized surface modification.

2.7. IMMUNOCHEMICAL METHODS FOR THE DETERMINATION OF BISPHENOL A

Immunoassays have been studied and used for the detection of BPA, and many research reports deal with antibody production and the development of heterogeneous immunoassay methods, such as the established ELISA and FLISA methods, which both need immobilization of one binding partner and several washing steps. Due to these time-consuming steps, they are not suitable for the demand of a fast, efficient, and high-throughput screening method. A homogeneous immunoassay, such as the Fluorescence polarization immunoassay (FPIA), does not require the immobilization of reagents, can be operated in a single phase, and does not need further washing steps which makes the entire procedure faster (**Table 2)** [106, 107].

Table 2 Immunochemical methods for the determination of bisphenol A.

Immunoassay	Substance	Sensitivity	Reference
ELISA	Canned food, water samples, plastic materials	LOD 15–0.05 ng/mL	[78, 93–97]
Gold nanoflower-enhanced ELISA		LOD 0.1–0.05 ng/mL	[98]
FPIA	Water samples Environmental water	LOD 5.60 ng/mL	[99, 100]
FLISA	Water samples:	LOD 13.1 ng/mL.	[101]
LFIA	Baby bottles	LOD 100 ng/mL	[78, 79]
Quantum-Dot-Based		LOD 10 ng/mL	[102]
LFIA	Water samples	LOD 4 µg/L	[103]
Other modifications of LFIA		LOD 0.4 ng/ml	[104, 105]

The use of membrane-based immunoassay tests for rapid on-site screening provides a simple and low-cost alternative to expensive, laborious and time-consuming instrumental methods and also to more sophisticated immunoassay formats [108–110]. The lateral-flow technique or immunochromatography is the most advanced and user-friendly format in terms of simplification and rapid on-site testing. The one-step lateral-flow method with the use of gold nanoparticles-labeled antibodies, based on the transportation of a reactant to its binding partner immobilized on the membrane surface, offers several advantages, including short assay time, visual interpretation of results, long-term stability and cost-effectiveness. Few studies were performed on the development of gold-based technique lateral flow immunoassays for BPA (**Table 2**), leaving room for optimization and improvement.

II. OBJECTIVES OF THE STUDY

The work presented in this thesis deals with the development of low-cost, flexible, rapid, and easy-to-use immunoassay techniques for determination of the endocrine disruptor bisphenol A.

To achieve the objectives of this study, the following work packages have been formulated:

(a) to synthesize the required hapten-protein conjugate and to develop a sensitive competitive lateral flow immunoassay (LFIA) device with colorimetric detection from these reagents, which can be evaluated visually and using program for a data visualization and image analysis or using a portable scanner.
(b) to examine the use of gold nanoparticles and latex microparticles as markers (as signal reporter) in LFIA, and to evaluate the potential of improving assay sensitivity and the capability to produce quantitative results.
(c) to examine different types of nitrocellulose membranes and glass fibers, which can be translated into an increase in sensitivity and an improved detection limit for this LFIA device. The influence of some critical parameters on the sensitivity of the device should also be thoroughly assessed.
(d) to synthesize new tracer molecules, linking the fluorescein fluorophore with and without a spacer to the bisphenol A moiety, and assess for performance in the fluorescence polarization immunoassay (FPIA).

III. MATERIALS AND METHODS

3.1. Materials and Equipment

Transparent microtitre plates with 96 flat-bottom wells possessing high protein binding capacity (MaxiSorpTM) were purchased from Nunc (Thermo Scientific). UV-transparent 96 wells micro-titre plates, UV-Star™, were purchased from Greiner bio-one (Frickenhausen, Germany). TLC plates used were silica gel 60 with/without concentration zone, with/without fluorescence indicator from Merck KGaA (Darmstadt, Germany). Filters syringes with a Teflon membrane with a pore size of 0.45 µm and 17 mm in diameter from Merck KGaA (Darmstadt, Germany). PD-10 columns containing Sephadex G-25 were obtained from GE Healthcare (Munich, Germany). The LFIA test strips were cut using cutter (Dahle 502, Novus Dahle GmbH Lingen, Germany).

Table 3 Absorbent pad, conjugate pad, sample pad used within this thesis (were purchased from Merck.

	Merck Millipore		**MDI Membrane Technologies**	
	Product name	**Material**	**Product name**	**Material**
Absorbent pad	SureWickR C048	Cellulose	AP045	Cellulose
	SureWickR C068	Cellulose	AP080	Cellulose,
	SureWickR C083	Cellulose	AP110	Cellulose
	SureWickR C248	Cellulose	AP120	Cellulose
Conjugate pad	SureWickR GFDX	glass fibre	PT-R1	Polyester
	SureWickR G027	glass fibre	PT-R5	Polyester
	SureWickR G041	glass fibre	PT-R6	Polyester
			PT-R7	Polyester
Sample pad	SureWickR C048	Cellulose	GFB-R4	glass fibre
	SureWickR C068	Cellulose	GFB-R7L	glass fibre
	SureWickR C083	Cellulose		
	SureWickR C248	Cellulose		

Table 4 Nitrocellulose membranes used within this thesis (were purchased from Merck KGaA (Darmstadt, Germany) and MDI Membrane Technologies (Ambala Cantonment, India).

Nitrocellulose membrane	Type *	Sub-Type			Capillary Flow Time Specification (sec/4cm)	Membrane Thickness (µm)	Sensitivity
Merck Millipore	Hi-Flow ™ Plus Cellulose Ester Membrane	HF 180	K15274	166 to 204 174 to 196	180 ± 45	135	Most sensitive ↓ Least sensitive
			K15383	216 to 254 56 to 94			
	Hi-Flow ™ Plus Cellulose Ester Membrane	HF 135	K15112	166 to 204 174 to 196	135 ± 34	135	
			K15102	216 to 254 56 to 94			
	Hi-Flow ™ Plus Cellulose Ester Membrane	HF 120	K15042	166 to 204 174 to 196	120 ± 30	135	
			RK14051	216 to 254 56 to 94			
	Hi-Flow ™ Plus Cellulose Ester Membrane	HF 90	K15102	166 to 204 174 to 196	90 ± 23	135	
			K15112	216 to 254 56 to 94			
	Hi-Flow ™ Plus Cellulose Ester Membrane	HF 75	K15113	166 to 204 174 to 196	75 ± 19	135	
			K15124	216 to 254 56 to 94			
MDI Membrane Technologies	CNPC	SS12			Pore size 15 µm	100	Lower
	CNPC	SS12			Pore size 12 µm	100	Medium
	CNPF	SN12			Pore size 10 µm	100	Medium
	CNPF	SN12			Pore size 8 µm	100	Highest
	200 CNPH-N	SS60			200	100	Most sensitive ↓ Least sensitive
	150 CNPH-N	SS40			150	100	
	90 CNPH-N	SS40			90	100	
	70 CNPH-N	SS40			70	100	

* **Type:** CNPF – Lower protein binding
CNPC – Higher protein binding
CNPH-N – Highest protein binding

Type: CNPF and CNPC are rated by pore size
CNPH-N is rated by Wicking Time

The anti-bisphenol A mouse monoclonal antibody was provided by the lab of Professor Chuanlai Xu (School of Food Science & Technology, State Key Lab of Food Science and Technology Jiangnan University, Wuxi, Jiangsu, China) buffered (7 mg/ml in 0,01 M PBS, pH 7.4, 1 % BSA, 1 % glycerol azide 0.02 %) [79, 100, 111]. Polyclonal goat anti-mouse HRP labeled antibody (clone A4416) (whole molecule, with 0.5–3 mg/ml in 0,01 M PBS, pH 7.4, 1 % BSA, azide 0.02 %) provided by Merck Millipore, (Darmstadt, Germany). HRP-conjugated sheep anti-mouse-IgG (R1256HRP) and sheep anti-mouse IgG (R1256P) provided by Acris Antibody GmbH (Herford, Germany).

All the reagents for buffer were purchased from Merck KGaA (Darmstadt, Germany). All buffers were prepared in Milli-Q water unless other solvent is mentioned.

Table 5. Buffers used within this thesis.

Solution name	Composition	pH
PBS buffer	10 mM sodium dihydrogen phosphate 70 mM disodium hydrogen phosphate 145 mM sodium chloride	7.6
TMB solution (Tetramethylbenzidine)	40 mM tetramethylbenzidine 8 mM tetrabutylammonium borohydride in N, N-dimethylacetamide	
Carbonate buffer	15 mM sodium carbonate 35 mM sodium bicarbonate	9.6
Tris buffer	10 mM tris-(hydroxylmethyl)-aminomethan 150 mM sodium chloride	8.5
Washing buffer	0.05% (*v/v*) tween™ 20 in PBS buffer	7.6
Borate Buffer	50 mM sodium tetraborate decahydrate 0.01 % sodium azide	8.5
MES buffer	0.5 M 2-(N-morpholino)ethanesulfonic acid	4.0
Citrate Buffer	220 mM trisodium citrate	4.0

N-Hydroxysuccinimide (NHS, Sulfo-NHS), *N*,*N*′-dicyclohexylcarbodiimide (DCC), 1-ethyl-3-(3-dimethylaminopropyl) carbodiimide * HCl (EDC), chlorotrimethylsilane (TMS-Cl), abs. *N*,*N*-dimethylformamide (DMF), ethyl acetate, chloroform, triethylamine, 6-aminohexanoic acid (Ahx), bovine serum albumin (BSA), D-(+)-trehalose dihydrate, sucrose, bisphenol A (BPA), bisphenol A-d16 (BPA-d16), bisphenol valeric acid (BVA), bisphenol B (BPB), bisphenol E (BPE), bisphenol F (BPF), bisphenol S (BPS), 4-cumylphenol (4-CP), 4-octylphenol (OCP), and 4-nonylphenol (4-NP) were purchased from Merck KGaA (Darmstadt, Germany).

4'-(Aminomethyl)fluorescein hydrochloride (AMF) was from Invitrogen (Carlsbad, CA, USA), methanol (MeOH) from J.T. Baker (Griesheim, Germany), ethanol from ChemSolute (Renningen, Germany). Carboxy-modified dyed latex microspheres (Estapor®, product K1-030 blue) and ethanolamine were provided by Merck Millipore, (Darmstadt, Germany). Gold nanoparticles (40 nm) were provided by nanocomposix Europe (Prague, Czech Republic).

General instrumentation:

MALDI-TOF mass spectra were acquired using a Bruker Reflex III MALDI mass spectrometer from Bruker-Daltonik (Bremen, Germany) operated with a nitrogen laser and at 20 kV acceleration voltage.

Spectrophotometer SpectraMax Plus384 from Molecular Devices (Ismaning, Germany) controlled by SoftMax® Pro software (v 5.2, Molecular Devices) at 450 nm and referenced to 620 nm.

Titramax 101 **plate shaker** (Heidolph, Schwabach, Germany). An automatic 96-channel **plate washer** (BioTek Instruments, ELx405 Select™, Bad Friedrichshall, Germany).

Fluorescence polarization was registered on a **Sentry 2000Si** (Ellie LLC, Wauwatosa, WI, USA). The Sentry 2000Si is a multi-well fluorescence polarization instrument. Reactions are read in black 8 or 12-well microplate strips. The instrument is equipped with a ceramic fluid metering systems pump, with high volume precision.

UV-Vis-Spectrophotometer Evolution™ 201/220 from Thermo Scientific™ (Waltham, Massachusetts, U.S.).

All proteins were deposited onto the membrane strips using a piezoelectric printer **sciFLEXARRAYER S3**, (Scienion AG, Berlin, Germany). Lateral flow readers **opTrilyzer® and Cube®** by Chembio Diagnostics (Berlin, Germany). **Software:** extra quantitative analysis of lateral flow immunoassay images were performed by **Gwyddion v2.19**. software (Czech Metrology Institute, http://gwyddion.net), **ImageJ**, 30 free image processing software (ImageJ, National Institute of Health; Bethesda, Maryland, USA). **Origin™** 8.0 Software (OriginLab, Northampton, USA) was used for most of the displayed graphs. **ChemBioDraw** Ultra (v 18.0.1) and ChemBio3D Ultra (v 11.0.1), from CambridgeSoft (Cambridge, United Kingdom) were used for drawing the chemical structures, the reaction mechanisms and 3D representations. **Canon EOS 750D (Canon, Japan)** camera and smartphone camera from the **iPhone Xs** (California, USA) with macro (20X) and super wide lens (Black Eye 3-in-1 Set, China).

BPA reference concentrations of samples were determined by LC-MS/MS using an Agilent 1260 Infinity LC system with a binary pump, degasser, autosampler, and column heater. The chromatographic separation was carried out on a Kinetex XBC18, 100 Å, 2.6 µm, 150 × 3 mm analytical LC column with an UHPLC C18, 3 mm guard column (both Phenomenex, Aschaffenburg, Germany). As mobile phases, Milli-Q water with 10 mM NH4Ac and 0.1 % (*v/v*) acetic acid (A) and MeOH with 10 mM NH4Ac and 0.1 % (*v/v*) AcOH (B) were used. The system was run at a flow rate of 350 µL min^{-1} and a column heater temperature of 30 °C. An elution gradient was applied, starting with 80 % A for the first 15 min. Within 5 min, A is decreased to 5 % (95 % B). Then, A is ramped up back to 80 % within 0.5 min and maintained at this level for 14.5 min to re-equilibrate the column. Fifteen microliters of sample were injected. Mass spectrometric detection was performed on an ABSciex 6500 Triple Quad mass spectrometer. Electrospray ionization (ESI) in positive ionization mode was employed.

Solid-phase extraction (SPE) was performed using an automatic SPE workstation, AutoTrace™, from Dionex (Idstein, Germany). Extracts evaporation was achieved by using a benchtop nitrogen stream evaporator, SLS 02 Evaporator from SLS-Labor (Bad Münstereifel, Germany).

3.2. Methods

3.2.1. Synthesis of the hapten-protein conjugate and tracer

3.2.1.1. Synthesis of the hapten-protein conjugate BVA-BSA

Bisphenol A is a “small molecule” with a molecular weight of 228.29 g/mol. To increase its immunogenicity, BPA was linked to bovine serum albumin (BSA). Since BPA does not have reactive functional groups, such as carboxylic or amino groups, a commercially available reagent, 4,4-bis(4-hydroxyphenyl) valeric acid (BVA), which is a structural analogue of BPA (**Figure 14**), was used as a mimotope. They have the same antigenic determinant which, coupled to a protein, can mimic the epitope that binds to certain anti-BPA antibodies. BVA contains a carboxyl group which was chosen for coupling it to amino groups on proteins, e.g., BSA [112].

Conjugation of BVA to BSA was carried out by a modified method of Montoya’s group [95, 96], with minor modification. The coupling reactions were performed at pH 6 according to the following procedure. NHS (2.6 mg in 200 µL DMSO) was mixed with EDC (4.3 µg in 200 µL DMSO) and BVA (5.2 µg in 200 µL DMSO). The mixture was incubated with continuous stirring for 2 h at room temperature. 22 mg of BSA were dissolved in 2 mL PBS pH 6. The activated BVA was added dropwise to the protein solution. After 4 h reaction time, the protein conjugate was purified

by size exclusion chromatography on Sephadex™ G-25 in a PD-10 desalting column (Healthcare Bio-Sciences, Freiburg), PBS/water (1: 10; *v:v*) being the eluent, collecting 96 fractions into a non-binding well plate. The efficiency of the conjugation reaction was verified by MALDI-ToF-MS (**Fig. S 1**).

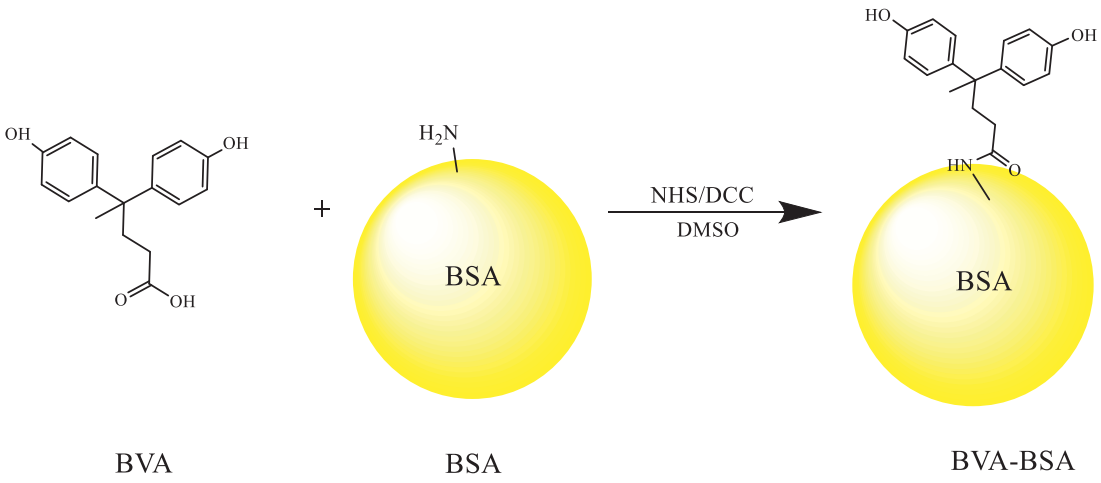

Figure 14. Reaction scheme for the synthesis of BVA-BSA

3.2.1.2. Synthesis of the hapten-protein conjugate BVA-Ahx-BSA

The chemical structure of the conjugated hapten will greatly determine the binding to the antibody, In 1969, Nobel Prize laureate Karl Landsteiner demonstrated specificity of antibodies is mainly directed to the distal moieties of the hapten [113]. According to Schmidt et al. [114], a linear six carbon aliphatic chain is considered to be the optimal spacer for enabling optimal binding. For all those reasons, the synthesis of functionalized derivatives of the target compound is a key to increase the sensitivity of the assay. For this purpose, aminohexanoic acid (Ahx) was coupled with 4,4-bis(4-hydroxyphenyl) valeric acid (BVA). Briefly, BVA (26.3 mg) and NHS (12.9 mg) were mixed with EDC (22.3 mg) in 3 mL DMSO dissolved and stirred in an amber glass vial and the mixture was incubated with continuous stirring for 2 h at room temperature under argon. Ahx (9.8 mg) was dissolved in 1.5 mL DMSO and was mixed with 1.5 mL PBS (pH 6). 2.5 mL of the reacted solution of BVA was added dropwise to the Ahx solution and incubated for 4 h at room temperature.

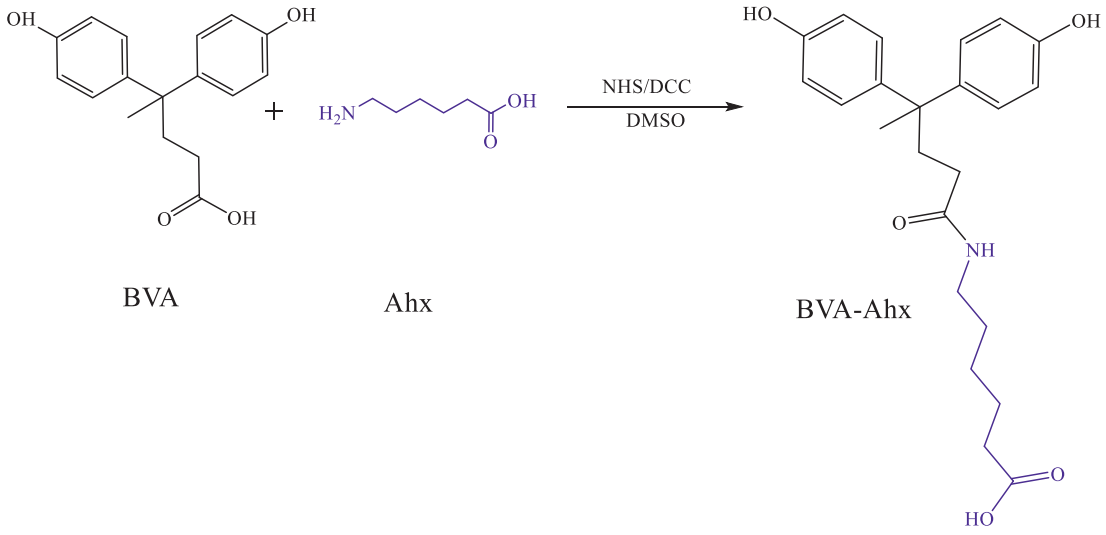

Figure 15. Reaction scheme for the synthesis of BVA-Ahx

BVA-Ahx (**Figure 15**) is not indefinitely stable and is probably (partially) decomposed during the long period of preparative HPLC (**Figure S 3).** So, the freshly prepared solution of BVA-Ahx was added to the appropriate protein solution and reacted at room temperature for 4 h with stirring.

22 mg of BSA were dissolved in 2 mL PBS pH 6. The activated BVA-Ahx were added dropwise to the protein solution. After 4 h reaction time, the protein conjugate was purified SEC on a PD-10 column and reaching a final protein concentration of BVA-BSA of 2.1 mg/mL and for BVA-Ahx-BSA (**Figure 16**) of 2.48 mg/mL, determined by Bradford assay [115]. The efficiency of the conjugation reaction was verified by MALDI-ToF-MS (**Figure S 2**).

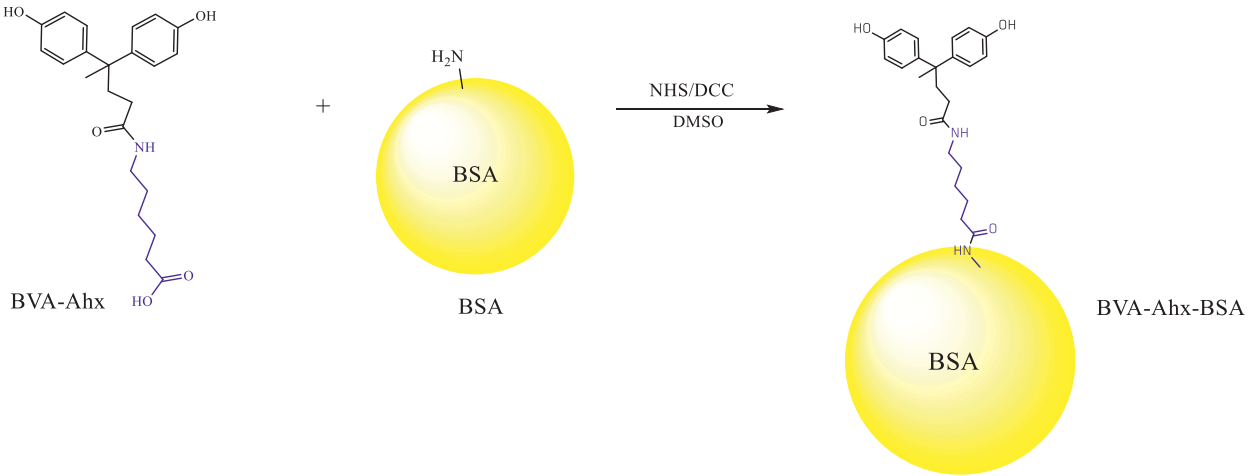

Figure 16. Reaction scheme for the synthesis of BVA-Ahx-BSA

The Bradford assay was used to determine the hapten-protein conjugate concentration. The Bradford method is a dye-based assay and is based on the ability of Coomassie blue to bind to proteins causing the dye color to shift from red to blue. Use of Coomassie G-250 dye as a colorimetric reagent for the detection and quantification of total protein was first described by Dr. Marion Bradford in 1976. The quantification is carried out by plotting a calibration curve (**Figure S 8**) of the respective protein and spectroscopic measurement (595 nm) [115]. It was founded that the concentration of BVA-BSA was 2.7 mg/mL, and that of BVA-Ahx-BSA was 2.8 mg/mL.

3.2.1.3. Synthesis of fluorescein-labeled tracers (BVA-AMF and BVA-Ahx-AMF)

The fluorescent tags were coupled to the haptens by the NHS activated ester method developed by Eremin and co-workers [46, 99, 116], with minor modifications. BVA and BVA-Ahx (**Figure 17, 18**) NHS activated esters were previously synthesized as described in chapter **2.4.2**, then added to 1.05 mg (2.6 µmol) AMF dissolved in 10 µL of triethylamine. All products formed a yellow-orange solution which was stirred for another 4 h before being purified by thin-layer chromatography (TLC).

TLC was performed on silica plates (2.5 x 7.5 cm; silica gel 60 with concentration zone, without fluorescence indicator, Merck). The mobile phase was $CHCl_3$:CH_3OH (4:1, *v/v*). For each tracer, the main yellow band, clearly visible under UV light (λ = 365 nm), was collected, dissolved in ethanol, stripped from silica via filtration through a Teflon membrane syringe filter with a pore size of 0.45 µm and 17 mm in diameter, and purified again by TLC (see retardation factors R_f in **Table S 1**). Ethanol as solvent was evaporated, the residue finally dissolved in 100 µL methanol, stored at 4 °C and later on directly used as tracer stock solution from which dilutions (Tracer Working Solutions) in borate buffer were prepared.

The success of the synthesis was confirmed by LC-MS/MS (see **Figures S 4, S 5, S 6, S 7**). Mass spectra were recorded at the retention time of the largest peak in the UV trace. m/z + 1 and $+Na^+$ adduct ions for each individual synthesis product could be identified. The chromatograms showed for some compounds not a high purity, but impurities.

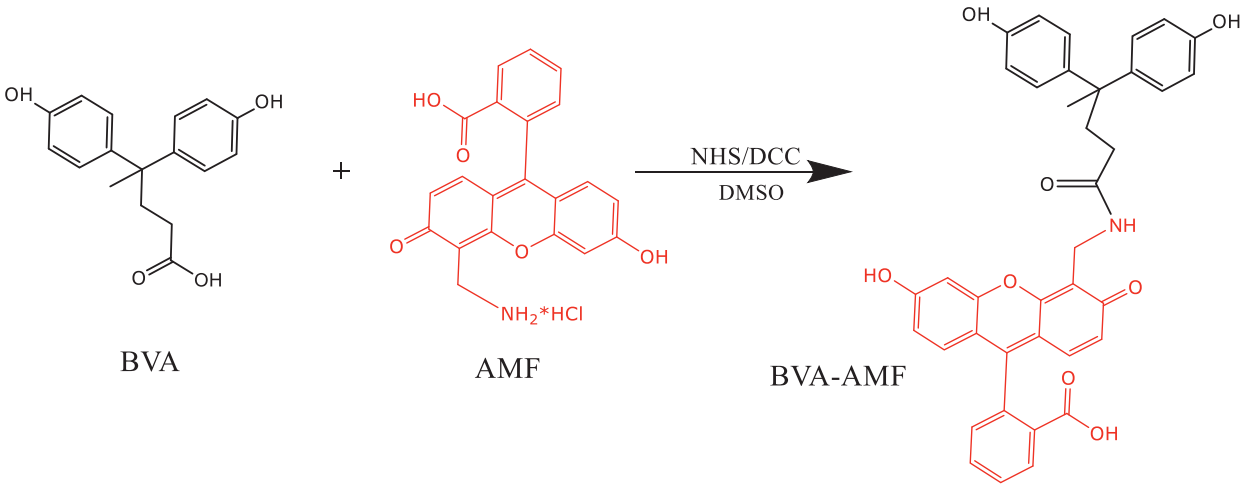

Figure 17. Reaction scheme for the synthesis of BVA-AMF

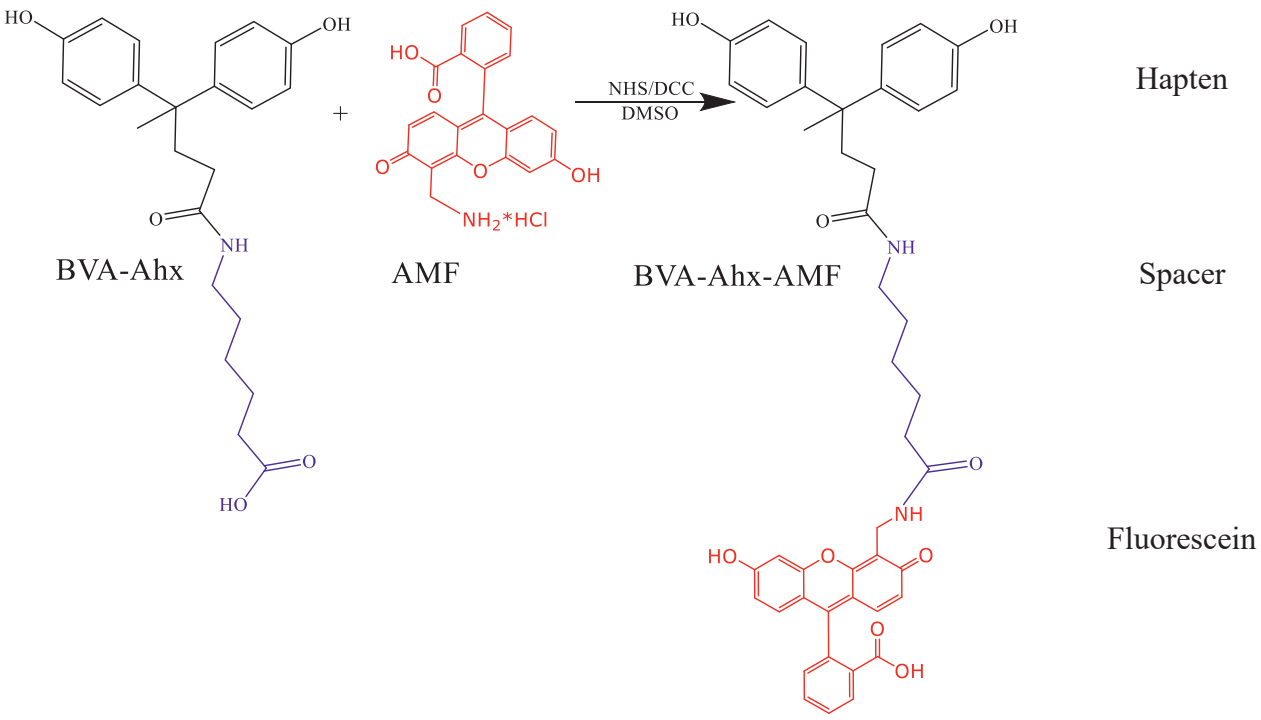

Figure 18. Reaction scheme for the synthesis of BVA-Ahx-AMF

3.2.2. Protocol of the indirect ELISA

Optimal dilutions of BVA-BSA or BVA-Ahx-BSA and anti-BPA mouse IgG, respectively, were determined by checkerboard titration. Transparent high-binding microtiter plates (96 flat-bottom wells) were coated with the respective conjugate in PBS pH 7.5, 200 µL per well, covered with Parafilm®, and incubated overnight (~18 h) on a plate shaker at 750 rpm. The plates were washed three times with the washing buffer. After the washing step, the plates were blocked using casein

in PBS (1 %, *w/v*, 200 µL per well) for 1 h. The plates were washed again, and 100 µL of sample or BPA standards and diluted anti-BPA monoclonal IgG were added and incubated for 60 min. After a three-cycle washing step, 100 µL HRP-conjugated goat anti-mouse-IgG (R1256HRP) (Acris Antibody GmbH, Herford, Germany) diluted 1 : 20 000 in PBS buffer was added in each well and incubated for 1 h. After another washing step, 200 µL substrate solution (TMB) was added. For one plate, 22 mL citrate buffer (220 mM potassium dihydrogen citrate, 0.5 mM sorbic acid potassium salt, pH 4.0) with 8.5 µL H_2O_2 (30 %) and 550 µL TMB solution (40 mM TMB, 8 mM tetrabutylammonium borohydride, in *N*,*N*′-dimethylacetamide) were mixed and 200 µL was added to each well. Following a 20 min incubation step, the reaction was stopped by adding 100 µL H_2SO_4 (1 M). Absorbance was measured photometrically by spectrophotometer SpectraMax Plus384 from Molecular Devices (Ismaning, Germany) controlled by SoftMax® Pro software (v 5.2, Molecular Devices) at 450 nm and referenced to 620 nm.

All incubation steps were performed at room temperature on a Titramax 101 plate shaker (Heidolph, Schwabach, Germany) at 750 rpm. Between individual incubation steps, the plates were washed with an automatic 96-channel plate washer (BioTek Instruments, ELx405 Select™, Bad Friedrichshall, Germany). Three-cycle washing steps were carried out with a PBS-based washing buffer (0.75 mM potassium dihydrogen phosphate, 6.25 mM dipotassium hydrogen phosphate, 0.025 mM sorbic acid potassium salt, 0.05 % (*v/v*) Tween™ 20, pH 7.6).

3.2.3. Protocol of the sandwich ELISA

Each well of transparent high-binding microtiter plates was coated with 100 µL of 2 mg/L sheep anti-mouse IgG in carbonate buffer and incubated for 18 h on a plate shaker. The plates were sealed to prevent evaporation. Following a three-cycle washing step, the remaining binding sites on the MTP were blocked with gelatin solution (0.1 %) in PBS buffer. After incubating for 1.30 h, the plates were washed again. Standards (100 µL mouse anti-BPA IgG) diluted in a range of 1 µg/mL – 0.05 ng/mL in TRIS buffer were incubated for 45 min. After a three-cycle washing step, 100 µL HRP-conjugated goat anti-mouse-IgG (R1256HRP) diluted 1 : 20 000 in PBS buffer was added to each well and incubated for 1 h. After another washing step, 200 µl substrate solution (TMB) was added. For one plate, 22 ml citrate buffer with 8.5 µL H_2O_2 (30 %) and 550 µL TMB solution were mixed and 200 µL were added to each well. Following a 25 min incubation step, the reaction was stopped by adding 100 µL of H_2SO_4 (1 M). Absorbance was measured at 450 nm and referenced to the absorbance at 620 nm.

3.2.4. Protocol of the FPIA

Running the assay. 120 µL of borate buffer, 40 µL of Milli-Q water (blank) or sample, and 30 µL of an appropriate dilution of the tracer stock (tracer working solution, TWS) are pipetted into each microwell of an 8-well strip and the blank value (mP_0) read after a certain tracer incubation time (see below). 30 µL of an optimal antibody dilution is added to this mix. After shaking for the optimal antibody incubation time (see below), mP is determined.

Optimization of sensitivity. To find the optimum ratio between antibody and tracer (i.e., dilution and volume) to obtain maximum sensitivity at a reasonable signal/noise ratio, to result in a low variance.

This was achieved in 3 steps: 1) First, the amount of tracer was initially set as low as possible with a still acceptable signal fluctuation. Intensity and mP is observed over time to select an appropriate time.

2) Next, antibody titration was performed by running the assay with 40 µL Milli-Q water to mimic a sample. 30 µL of different antibody dilutions were added to this solution to analyse for tracer binding. From the antibody dilution curve the optimal dilution of antibody and tracer were chosen.

3) Finally, FPIA calibration curves were recorded. Again, 120 µL BB, 40 µL of analyte (standard), and 30 µL of the TWS were mixed before 30 µL of the selected antibody dilution was added.

FPIA is a kinetic assay in which the degree of polarization changes over time, equilibrium is not completely reached during the desired short incubation times. Therefore, the time for the tracer to equilibrate with the system (tracer incubation time) and the time allowed for competition of the tracer and the analyte to bind to the antibody (antibody incubation time) had to be individually evaluated and mixing and shaking is very important for the assay reproducibility.

Initial to all measurements, the mP of the blank (mP_0) was determined and later on all mP values read divided by mP_0. For calibration, the results were plotted against the logarithm of the BPA concentrations and to the data points a sigmoidal curve described by a logistic, four-parameter equation, was fitted, using Origin 8G Software (OriginLab, Northampton, MA, USA).

3.2.5. Lateral flow immunoassay development

3.2.5.1. Conjugation of antibody with gold nanoparticles by passive absorption

The antibody gold nanoparticles (IgG−GNP) was prepared according to a previously described protocol [60, 117]. Purified protein, 80 µL (20 µg) was incubated with 20 ml of gold nanoparticles (40 nm) solution (pH 8.5) provided by nanoComposix Europe (Prague, Czech Republic) with stirring for 18 h. After the mixture was stirred for 30 min at room temperature, 1 mL of 10 % bovine serum albumin (BSA) solution was added to the stirred solution and stirred for another 60 min at room temperature (**Figure 19**). The resulting suspension was centrifuged (3800 rpm) at 4 °C for 10 min. Finally, the IgG−GNPs were resuspended with 1 mL of 1 mM sodium borate buffer (containing 1 % BSA, 1 % sucrose,), and stored at 4 °C.

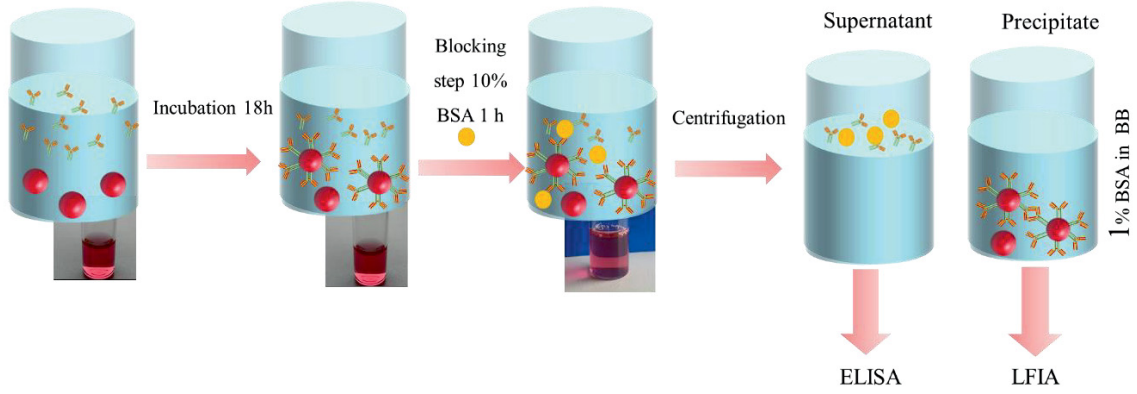

Figure 19. Schematic illustration of conjugation of GNP with IgG by passive absorption

3.2.5.2. Conjugation of antibody with gold nanoparticles by covalent coupling

The antibody was covalently linked with carboxylated gold nanoparticles by the activated ester reaction [72, 118]. One mL of GNP 40 nm was added to 200 mM EDC and 400 mM Sulfo-NHS dissolved in 1 mL 5 mM PBS, pH 6.0, and stirred and incubated for 90 min at room temperature. The activated GNP were isolated from the mixture by centrifugation at 10 °C for 10 min at 3800 rpm. The pellet was then dissolved in 1 mL of reaction buffer (1 mM BB pH 8.5) and 20 µg of IgG per milliliter of solution was added. The mixture was reacted for 2.5 h on a rotary wheel at room temperature, and the reaction was quenched by addition of 30 µL of ethanolamine per 1 mL of 1 % microspheres for 30 min to deactivate any remaining active NHS esters. The mixture was centrifugated at 10 °C for 10 min at 3800 rpm. The supernatant was tested by sandwich ELISA to quantify unbound IgG. Then precipitate was resuspended in the blocking buffer (1 mM BB, pH 8.0 with 0.5 % BSA).

3.2.5.3. Preparation of latex particles labelled with antibody by covalent coupling

The antibody was covalently linked with carboxylated latex microparticles (LMP) by the active ester reaction [72, 119, 120]. For this, 100 µL of latex microparticles were added to 1 mL of activation/coupling buffer (50 mM MES, pH 6.0), then 24 µL of 200 mM EDC and 240 µL of 200 mM Sulfo-NHS dissolved in latex microparticles solution were added while stirring for 30 min. The activated latex microparticles were isolated from the mixture by centrifugation at 10 °C for 7 min at 14 000 rpm. The pellet was then dissolved in 1 mL of activation buffer and sonicated for 2 min, followed by the addition of 20 µg of IgG per milliliter of solution. The mixture was reacted for 2.5 h on a rotary wheel at room temperature, and the reaction was quenched by addition of 30 µL of ethanolamine per 1 mL of 1 % latex microparticles for 30 min. The mixture was centrifugated at 10 °C for 7 min at 14 000 rpm. The supernatant was tested by sandwich ELISA to quantify unbound mouse IgG in the supernatant. Then the microspheres were centrifugated and resuspended in the blocking buffer (50 mM Tris, pH 8.0 with 0.5 % BSA).

3.2.5.4. Fabrication of lateral flow test strips

The nitrocellulose membrane is one of the essential parts of a lateral flow device. The reagents were deposited onto the nitrocellulose membrane strips using an XYZ piezoelectric printer (sciFLEXARRAYER S3, Scienion AG, Berlin, Germany) [121, 122]. The coating hapten-protein conjugate BVA-Ahx-BSA was adsorbed on the test line (T) and sheep anti-mouse IgG was adsorbed on the control line (C) (**Figure 20**).

According to the literature, the optimum width of testing zones should be around 0.5–1.0 mm [32, 56]. The lines were made up of several rows of spots spaced at a distance of 250 microns from each other. Each spot was formed as a result of the deposition of a number of droplets (each of 0.35 nL). The number of rows, number of spots per row, and number of droplets per spot varied to reach optimal load of reagents in test and control lines. After spotting, the membranes were dried at 37 °C for 1 h.

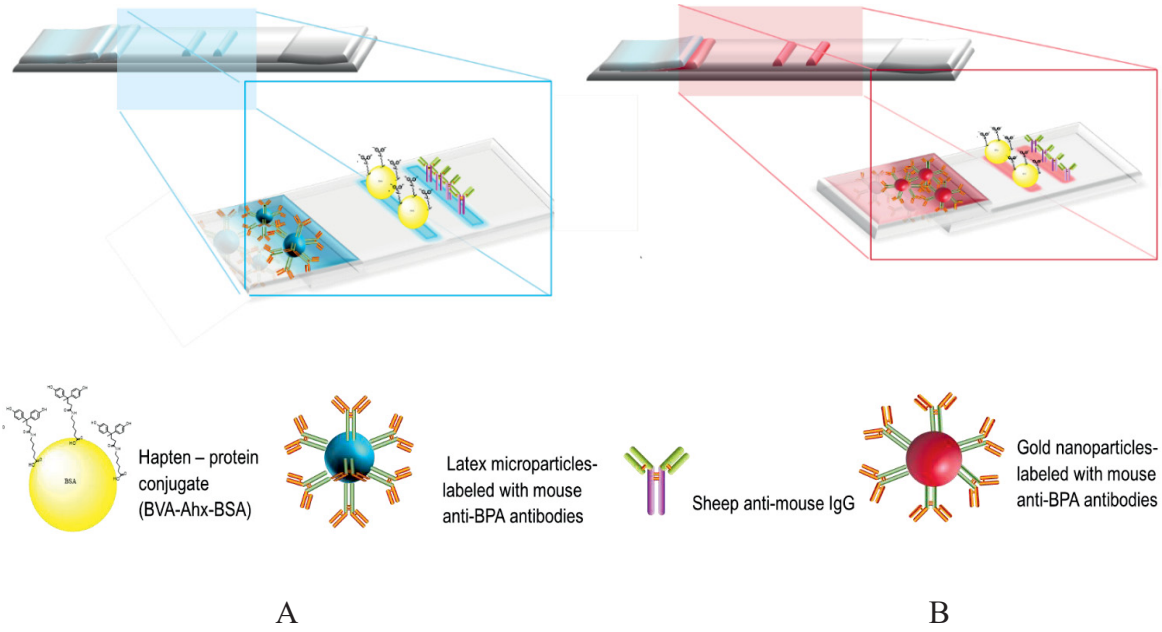

A B

Figure 20. Schematic of the set-up of the developed lateral flow immunoassay for BPA **A**. The LFIA test strip with IgG−LMP **B**. The LFIA test strip with IgG−GNP

The card with membranes was blocked with 1 % casein in PBS for 10 minutes, then washed twice for 10 seconds in Milli-Q, and dried 1 h at 37 °C. The card was cut into 3-mm wide individual test strips using a cutter Dahle 502 (Novus Dahle GmbH Lingen, Germany). During the experiment, several blocking methods and drying conditions were tried, and they will be discussed in **section 4.5**. The conjugate pad was treated with 20 mM borate buffer (BB, pH 8.2) containing 1 % casein and 1 % sucrose and dried at 37 ºC for 30 min. The latex microparticles labeled with anti-BPA antibodies (IgG−LMP) or gold nanoparticles labeled with anti-BPA antibodies (IgG−GNP) probe taken in optimal volume and concentration were added on the conjugate pad. During the experiment, several buffers for treatment of the conjugate pad were tried out and will be discussed in **section 4.5**. All of the above four parts were assembled on a plastic adhesive backing card: firstly, the NC membrane was pasted on the center of the backing pad (PVC plate). Then, sample and absorbent pads were glued to the bottom and upper section of the adhesive backing pad with a 2-mm overlap of the NC membrane as shown in **Figure 20**.

3.2.6. Measurements and data interpretation of the LFIA

Standard solutions of bisphenol A were prepared from corresponding stock solutions (1 mg/mL) in ethanol by serial dilutions in Milli-Q. The test strip was vertically inserted into the wells of a microtiter plate with 100 µL of standard solution of BPA or sample. After incubation at room temperature for 10 min, the result can already be assessed by the naked eye. A visual assessment is convenient for on-site diagnostics since it does not require a special reader device. The disadvantage, however, is that this method only provides a qualitative yes/no response.

The quantitative performance was done by using portable readers and analytical image processing software to calculate the average signal (intensity) of both the test and control lines (**Figure 21.1).**

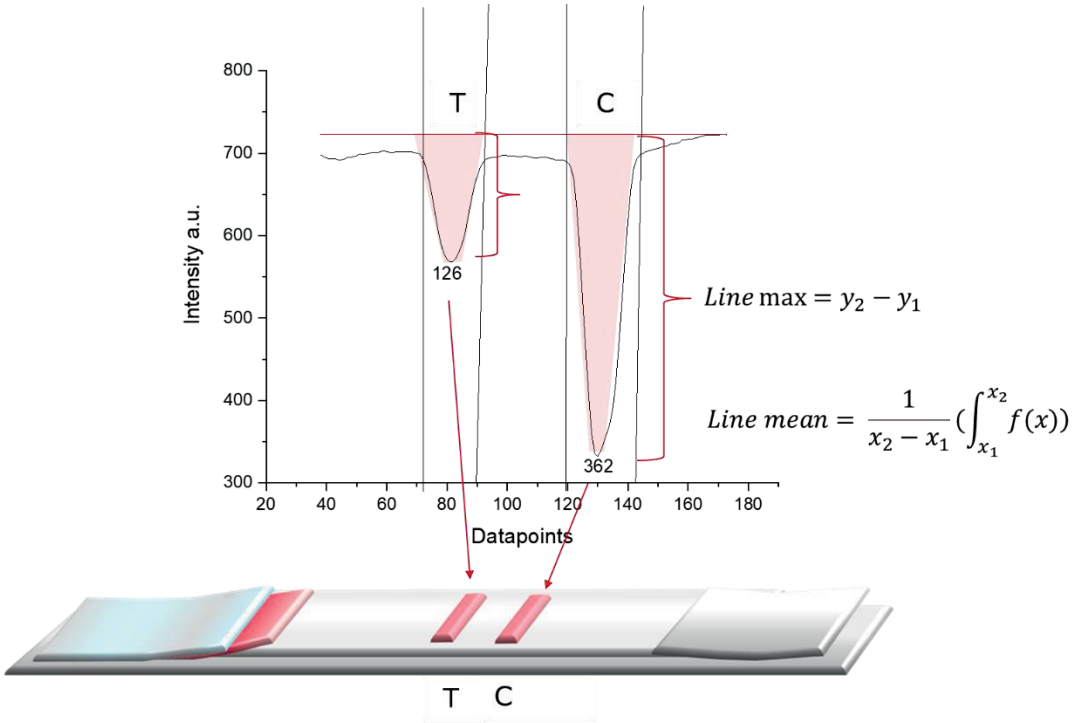

Figure 21.1. Schematic illustration of the peak integration of the test and control line signals. The total area of the peak is integrated from the 1.2 mm scanning area. "Line mean" integrates the pink area bordered by the line width (black vertical lines) and the red curve dip and the black horizontal line whereas "Line max" shows the maximal intensity of the test line at the darkest (deepest) part of the line. The red vertical line is a baseline correction.

The instrumental limit of detection (LOD) was calculated as the concentration yielding a signal reduction of three times the standard deviation (SD) of the signal for the sample without analyte ("blank"); B_0 (sample without analyte) minus a value of three times the standard deviation of that blank signal ($B = B_0 - 3 \times \mathrm{SD}$). The dependence of the color intensity on the concentration of BPA

(**Figure 21.2 A, B**) was plotted as calibration curve (**Figure 21.2 C**). The equation for the calibration curve approximation (4-parametric sigmoidal fitting) was as in **section 2.5**.

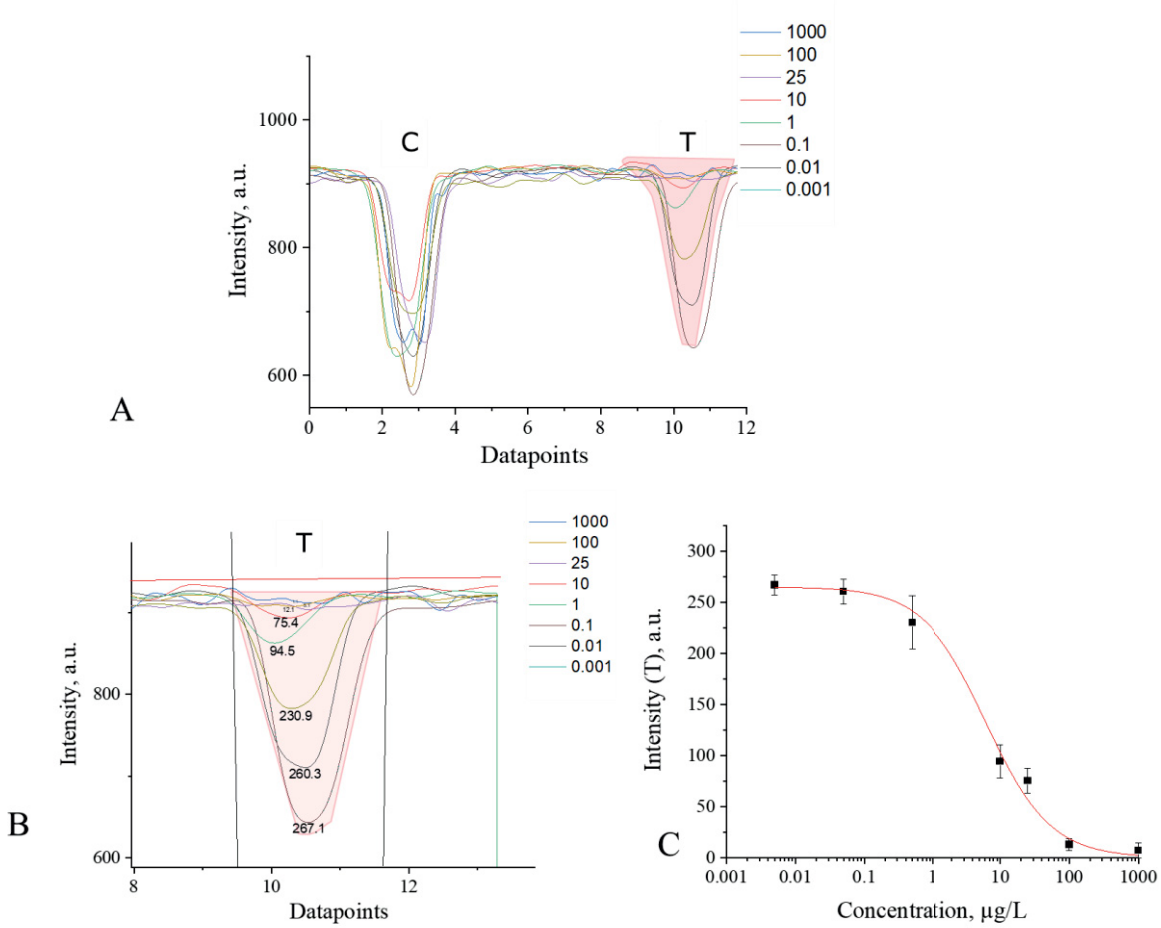

Figure 21.2. A. Intensity profile of a test and control line and different concentrations of BPA spiked as samples. **B.** Evaluation of different test line signals and baseline correction. **C.** A calibration curve obtained by plotting the measured values of the test line intensity versus BPA standard concentration. The mean and standard deviation (SD) were calculated using results from multiple experiments.

The visual limit of detection (vLOD) of the assay was interpreted as the minimal BPA concentration that caused visible absence of coloration in the test zone in comparison with the nearest lower concentration that already shows a colored test line.

Both the opTrilyzer® and the Cube® microreader were employed as detecting devices in the LFIA experiments for registration and quantification of the color intensity of the control and test lines. The Cube® microreader has a cubic shape with an edge length of approx. 41 mm and weighs 40 g.

Both devices are based on the optical analysis of the LFIA test strips. The preset instrument mode of measurement is a colorimetric readout at a wavelength of 525 nm.

The general elements of the opTrilyzer® and Cube® microreader are: (1) a simple LED serves as the light source, (2) the device registers the light reflected by the test surface, and (3) a lens-based optical focusing system is employed. The registered image is further processed using software tools. The software calculates the analyte content based on the control line and test line intensity and gives this information as the result of the measurement. The digital optical registration represents an image of a test strip as raw data for an array of points arranged in horizontal and vertical rows. Each pixel is characterized by three numerical parameters that corresponds to three channels of image formation red, green, and blue (RGB) [123]. The registration results for each of the three channels are integers that increase as staining intensity increases.

In the opTrilyzer the signal value ranges from 0 to 800 a.u. with high-resolution imaging capability (**Figure 22 A)**. The high-end imaging system (**Figure 22 B**) can enhance the detection sensitivity and the signal can be quantified (i.e., the amount of label) using reader systems because the signal intensity is generally proportional to the number of particles captured in the test line (**Figure 22 B, C**), which also correlates with the amount of BPA. The results are shown on a display and a calibration curve can be obtained by plotting the measured test line intensity versus the concentration of BPA (**Figure 22 E**).

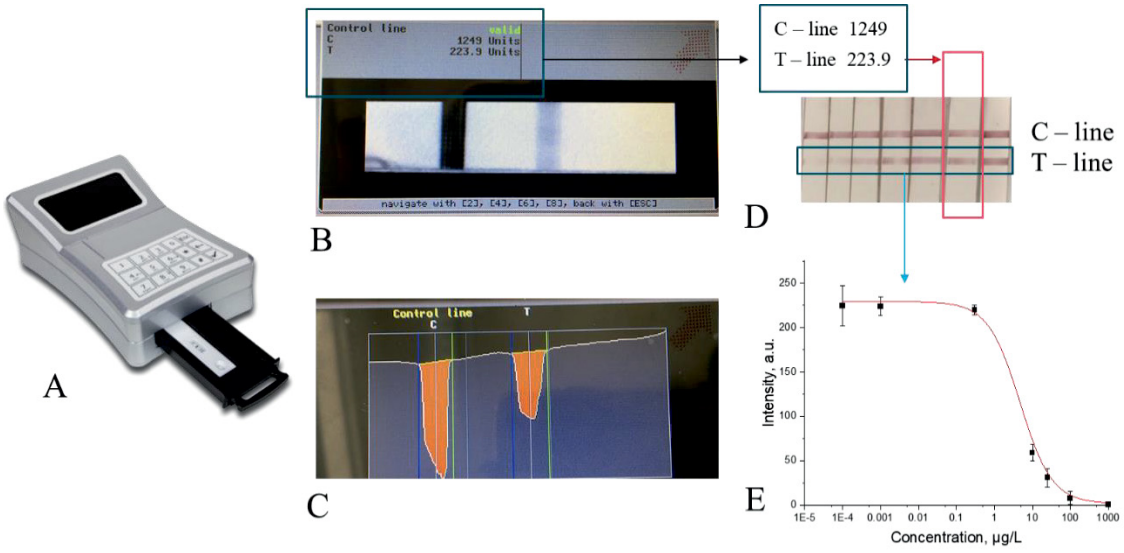

Figure 22 A. opTrilyzer® reader; **B**. Working window with image of test strip; **C**. Working window in the opTrilyzer® with optical density profile of the C-line and T-line; **D**. Test strips

with different concentration of BPA; **E**. Calibration curve (n = 3) for LFIA determination of BPA in aqueous samples was obtained by plotting the measured test line intensity versus the BPA concentration.

With the Cube® microreader the signal value ranges from 0 to 300 a.u. [123]. The imaging quality of the Cube® microreader is slightly inferior to that of the opTrilyzer®, however, it provides the intensity profile (optical density (OD) profile) of a test and control line and digitalized results of data processing can be accessed through a computer (**Figure 23**).

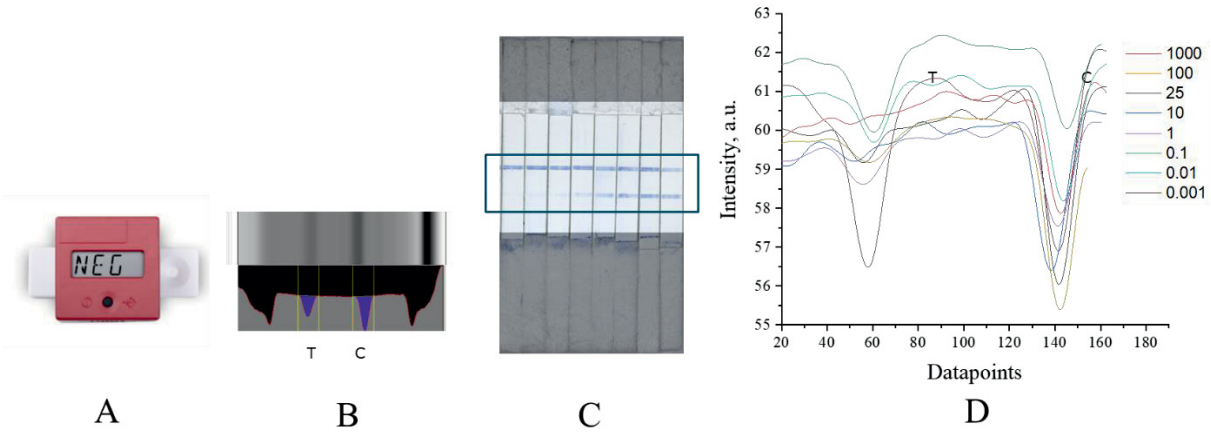

Figure 23 A. Cube® microreader. **B**. working window in the Cube® microreader software with image of test strip and optical density profile of the C-line and T-line. **C**. LFIA test strips with different concentration of BPA. **D**. Converted raw data of optical density of the profiles of T-lines and C-lines, respectively, into a plot created by Origin software.

It should be noted that the disadvantage of dealing with those test strip images inserted into readers may result in low reproducibility of the results. The reasons causing this effect is firstly the positioning error which comes from the relative positions of the test inside the reader that affects the control bands during printing of capture molecules (control and test line) onto the strip membrane. The second positioning error (**Figure 23 C**) is cutting of the membranes that can result in slightly different lengths. The third positioning error is that the strips can be positioned a little bit to the right or to the left relative to the reading window and the cassette housing. The uncertainty of the positioning of the strip in the reader results in an unstable baseline. For statistically reliable results based on a large amount of samples, this simple reader is unsuitable due the large resulting standard deviation.

An alternative approach for quantification of the color intensity of test and control lines is image processing software. The digital imaging of LFIA strips were processed with the image analysis software Gwyddion v2.19 (**Figure 24**) [124, 125]. It works with 48-bit images – from 0 to 65,535 range of intensity values (shades of grey) – and automatically calculates the value in area under study which ensures an automated quantitative analysis of the images and is therefore user-friendly. A gray scale optical analysis was performed from photographed images by Canon EOS 750D (Canon, Japan) under an LED ring lamp (AIXPI, China), where an area of the size 8 × 1.2 mm was selected for the analysis of each image (**Figure 24 A**). The program has a function of automatically smoothing the data (**Figure 24 B, C**). The data can directly be transferred as one file to Origin.

In contrast to the ImageJ® free image processing software (ImageJ, National Institute of Health; Bethesda, Maryland, USA), the software Gwyddion allows for a quick processing of large amounts of test strips because of the implemented algorithms for data analysis. ImageJ does not provide these functions and data processing can only be done manually by using, for example, the software Origin.

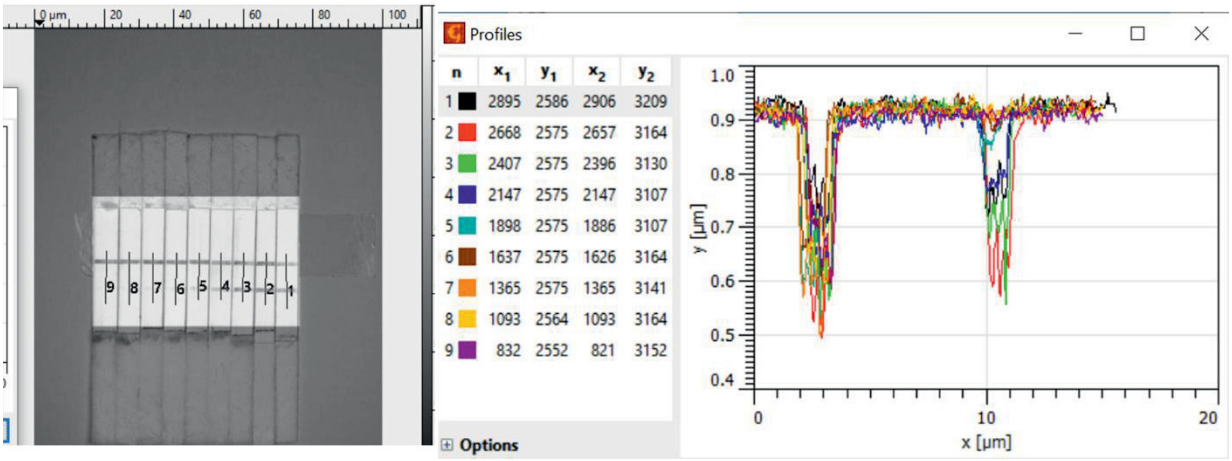

A B

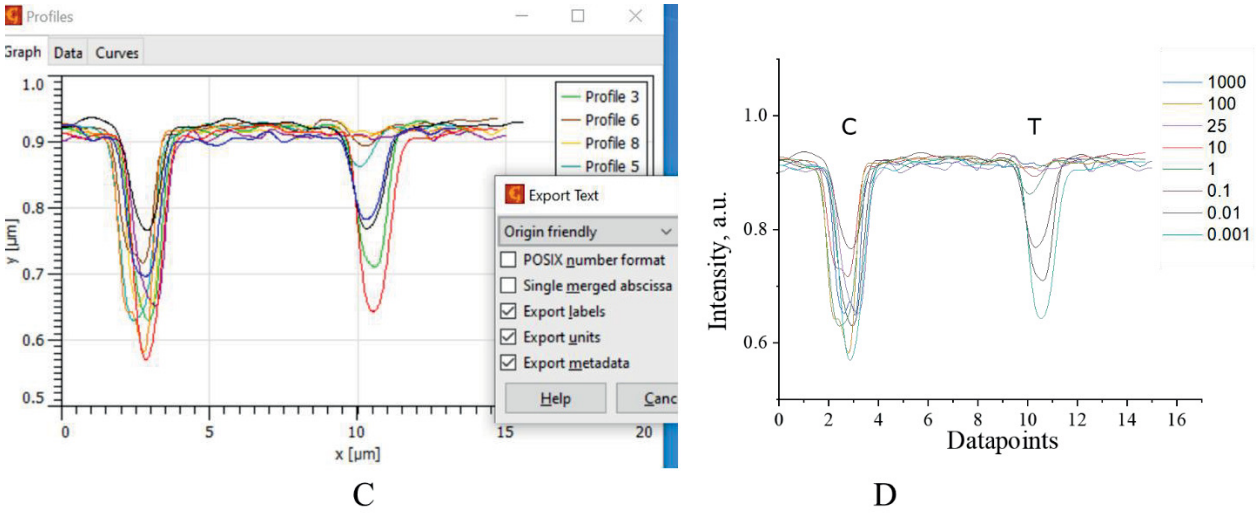

Figure 24. Screenshot from the Gwyddion software and its use for the quantitative assessment of LFIA results. **A**. Test strips with different concentration of BPA. **B.** Raw identification data of the control and test lines and assessment of its optical density profiles. **C**. Normalized identification data by the software of the control and test lines and assessment of its optical density profiles. **D**. Converted Gwyddion raw data of optical density of the test lines and control lines profiles transferred into a template of the data analysis software Origin™.

IV. RESULTS AND DISCUSSION

4.1. CHARACTERIZATION OF THE HAPTEN-PROTEIN-CONJUGATES

Indirect immunoassays for small molecules require as competitor a hapten-protein conjugate that is immobilized on the solid phase and acts as competitor in this competitive immunoassay format. Protein conjugates often use bovine serum albumin (BSA) as the protein part since it is inexpensively available in high purity and can be coated directly to microtiter plate well surfaces.

For the development of highly sensitive and specific immunoassays, it is important to design a proper hapten structure. Two basic approaches were used for design and synthesis of BPA haptens. One strategy of these approaches was aimed to preserve the two phenolic groups as the potential immunodominant epitope in a homologous approach. The other, heterologous, approach is based on the fact that in a competitive format it would be expected that assay sensitivity can be improved by increasing antibody affinity towards the analyte over the hapten-protein conjugate competitor that here differs more in structure than in the homologous format [94].

In the first approach, the commercial bisphenol valeric acid (BVA) was used as a hapten, protein, i.e., BSA, conjugation was achieved – as in the immunogen – via the carboxyl group of BVA, leaving the two phenol groups free for the immunorecognition. The antibodies that were raised against this hapten [126] were expected to recognize the two phenolic groups. In the second approach, 6-aminohexanoic acid (Ahx), a linker with six carbons as a spacer, was used for the first time in the synthesis of a BVA hapten-protein conjugate. It was introduced to give more flexibility and to give rise to greater affinity differentiation between the analyte and a competing hapten by the antibody. The results indicated that the coupling of the haptens to BSA was successful.

4.2. DEVELOPMENT AND OPTIMIZATION OF THE INDIRECT ELISA

After preparation of the conjugate, the indirect competitive ELISA was optimized by checkerboard titrations. The optimal concentration of the primary antibody for BVA-BSA was 9 ng/mL, and for BVA-Ahx-BSA 7 ng/mL, the dilution of BVA-BSA was 1: 550 000 and of BVA-Ahx-BSA 1: 600 000 and the optimal dilution of goat-anti-mouse HRP was 1: 20 000. **Figure 25** shows that the lower IC_{50} value was obtained with the BVA-Ahx-BSA conjugate. The results revealed that the hapten-protein conjugate including a C_6 spacer displayed satisfactory precision and sensitivity with an IC_{50} of 0.2 µg/L. The lower the value of IC_{50} the more sensitive measurements are possible.

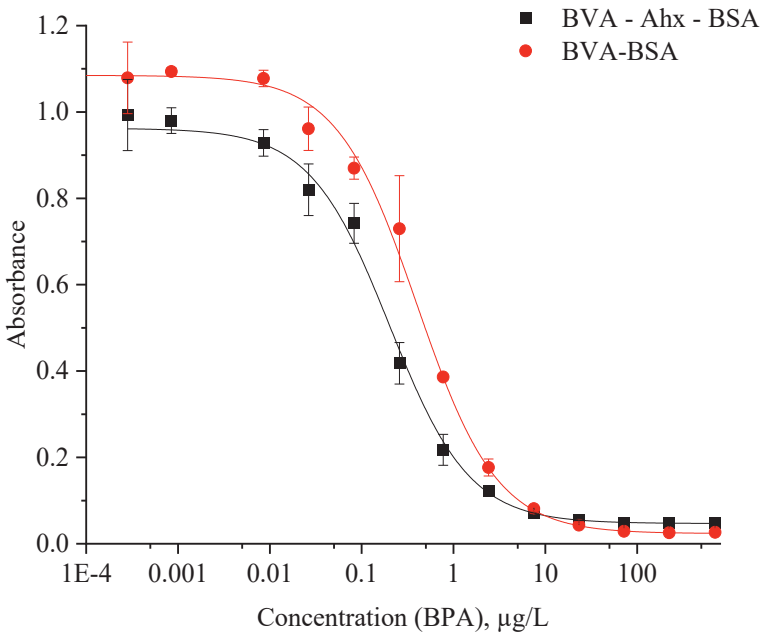

Figure 25. Calibration curves obtained for optimized conditions with the two conjugates (BVA-BSA, BVA-Ahx-BSA). Parameters of the 4-parameter fitting are shown in **Table 5.**

Table 5 Parameters of the 4-parameter fitting of the calibration curves of **Figure 25.**

	A1	**A2**	**IC_{50} µg/L**	**R^2**	**LOD µg/L**
BVA-BSA	1.09	0.02	0.4	0.99	0.08
BSA-Ahx-BSA	0.97	0.04	0.2	0.99	0.05

In our study, the pair IgG with BVA-Ahx-BSA yield better sensitivity than with BVA-BSA system (**Table 5**) (**Figure 25**). BVA-Ahx-BSA was chosen for future characterization and validation of assay performance. The "precision profile" [85] was plotted for the assay with BVA-Ahx-BSA conjugate, which provides information to reliably calculate the value of the LOD and the limits of the measurement range. The precision profile is shown in **Figure 26**.

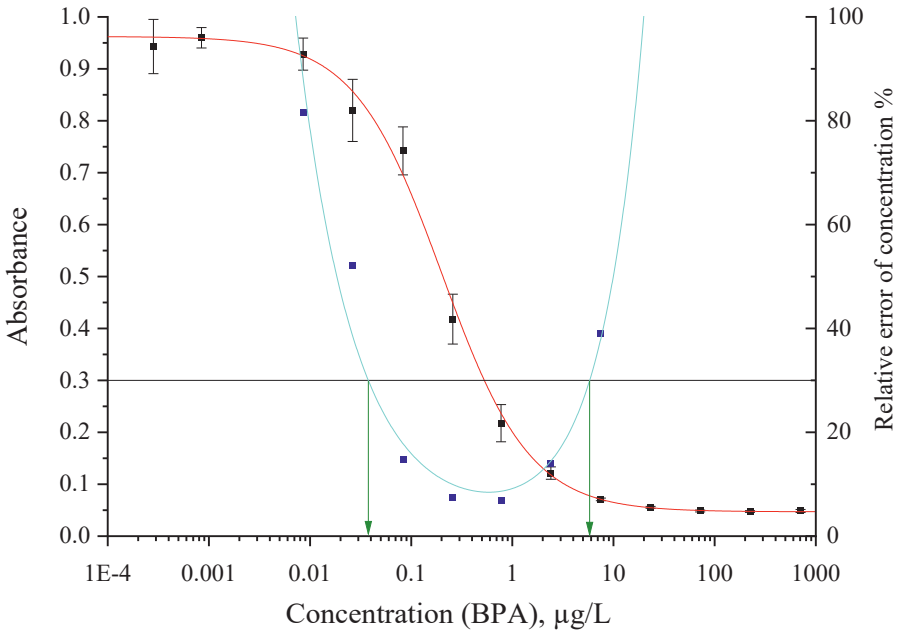

Figure 26. ELISA calibration curve with conjugate BVA-Ahx-BSA (red solid line), precision profile (blue squares and cyan line), and measurement range (indicated by green arrows) from 0.05 to 8 µg/L (intersection points at 30 % relative error of concentration, solid black lines).

A relative error of the determined concentration of 30 % was considered acceptable to mark the limits of detection (LOD). A lower limit of detection of 0.05 µg/L and an upper limit of detection of 8 µg/L was determined, the measurement range spanning over more than 2 decades.

4.3. FPIA: Selection of optimal tracer-antibody combination and characterization

The combination of tracer and antibody has a significant influence on sensitivity, selectivity, and reliability of an FPIA, and should always be carefully studied. In this work, new tracers were synthesized. The strategy for tracer synthesis, namely to use the amino group in AMF and coupling BVA via its carboxylic acid group, especially compared to using, in two cases, 6-aminohexanoic acid (6-Ahx) as spacer, was to study the influence of tracer structure on the assay sensitivity in FPIA [127, 128].

Fluorescence polarization was determined on a Sentry 2000Si, a multi-well fluorescence polarization instrument equipped with a ceramic fluid metering system pump for automated reagent

dosage. The light source is an LED with 485/535 nm filter set and a 510 nm dichroic mirror. Reactions are read in black medium-binding 8-microwell Fluorotrac strips.

The intensity of the blank (borate buffer) on the instrument was about 37 000 in both orientations ($I_{\parallel}$ and $I_{\perp}$). FP is close to zero (0 mP). When a tracer dilution of 1: 10 000 is added, intensity reading rises to ca. 200 000. This approx. 5-fold increase is a prerequisite for stable readings with the instrument and can be achieved by increasing the tracer concentrations. In any case, signal development must be observed and the optimal tracer incubation time, before the addition of the antibody, determined. This resulted in waiting times of 2.5 to 6 min. Tracers are stable on storage and benefit from the ability of fluorescein to fluoresce with high quantum yield while retaining the immunoreactivity of the antigen. But, since the tracer working solution is a dilution of the tracer in the buffer, it is not very stable to elevated temperatures, pH and it is light sensitive [129]. It was found that tracer working dilutions must be freshly prepared every day.

When the antibody is added and mP determined, a tracer that effectively binds to the antibody, leads to a strong decrease in mP with increasing dilution of the antibody (antibody titration) in a sigmoidal course (**Figure 27**). When the tracer cannot bind to the antibody, no change with antibody concentration is observed. According to the antibody dilution curves in **Figure 27,** the two tracers synthesized bind to the antibody. The optimum dilution of the antibody can be obtained from the antibody dilution curves in **Figure 27**; it corresponds to approximately 50 % of the maximum signal (**Table 6**). Higher dilutions result in too small signal changes, lower dilutions waste antibody. Optimum dilutions were in the range of 1: 100 to 1: 20 000.

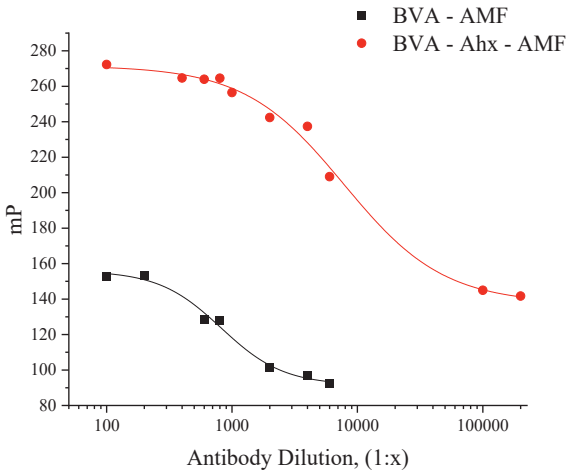

Figure 27. Antibody titration curves in the FPIA with the two tracers

In FPIA, antibody binding is kinetically controlled, thus the time until measurement after adding the antibody must be optimized individually (**Table 6**).

Table 6. Characteristics of the binding of the two tracers to the monoclonal anti-BPA antibody (diluted accordingly in borate buffer; tracer dilution: 1: 10 000).

Tracer	Optimal tracer dilution	Optimal Antibody dilution	Concentration of Antibody [g/mL]	mP value of free tracer [mP]	Optimal tracer incubation time [s]	Optimal antibody incubation time [s]
BVA-AMF	1:4000	1:800	8.75	114	120	90
BVA-Ahx-AMF	1:6500	1:4000	1.75	221	200	90

The tracer structure could significantly influence the immunoassay performance. As shown in **Table 7**, the spacer Ahx (C_6) plays an important role in the binding reaction, higher sensitivity was observed by using the BVA-Ahx-AMF tracer (IC_{50}, 7.5 µg/L) and BVA-AMF (IC_{50}, 33.4 µg/L). The selection of the optimal tracer was based on the parameters of assay IC_{50} and LOD. This phenomenon has been confirmed in other studies [40, 130, 131]. Therefore, the tracer BVA-Ahx-AMF was finally selected for further studies (**Figure 28**).

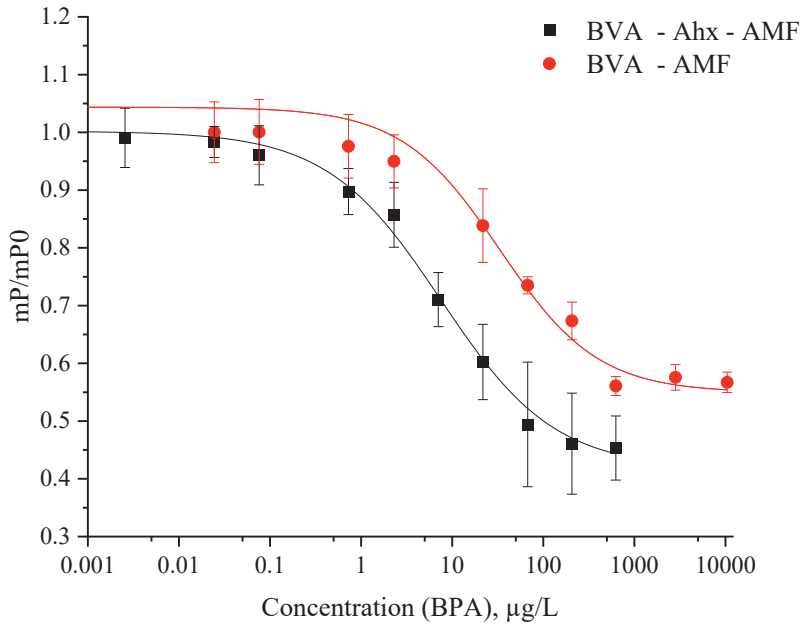

Figure 28. Calibration curves obtained for optimized conditions with the two tracers (BVA-AMF, BVA-Ahx-AMF). Parameters of the 4-parameter fitting are shown in **Table 8**.

Table 7. Parameters of the 4-parameter fitting in the developed FPIAs using different tracers.

	A1	A2	IC_{50} µg/L	R^2	LOD µg/L
BVA-AMF	1.0	0.4	33	0.99	11
BSA-Ahx-AMF	1.0	0.5	7.5	0.99	1.0

Calibration curves with precision profiles for the FPIA with BVA-Ahx-AMF was determined under optimized conditions and is shown in **Figure 29**.

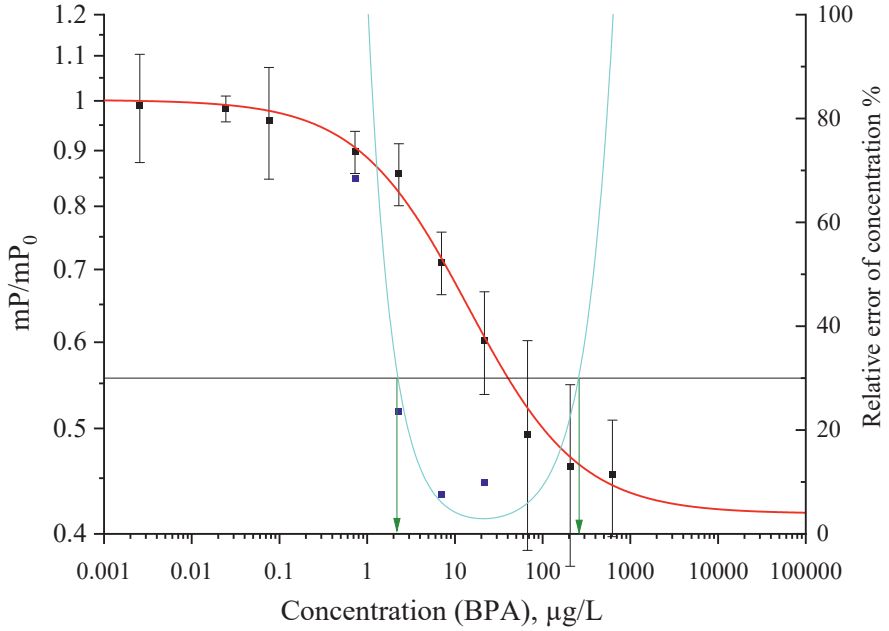

Figure 29. FPIA calibration curve with conjugate BVA-Ahx-AMF (red solid line), precision profile (blue squares and cyan line), and measurement range (indicated by green arrows) from 2 to 155 µg/L, determined via intersection points at 30 % allowed relative error allowed relative error of the determined concentration (black line).

4.4. Investigation of matrix effects in ELISA and FPIA

One of the important parameters for the optimization of immunoassays is the evaluation of the influence of matrix components, which can interact in a variety of ways with the components of an immunoassay. Matrix compounds are mainly dissolved salts, organic solvents (from

extraction), and endogenous disturbances, e.g., humic acids or proteins, which vary in different samples. This “matrix effect” is a common problem for the immunoassay, which could reduce the sensitivity and reliability of the competitive immunoassay. Usually, interferences are quantified by comparing a standard curve produced in a blank matrix (e.g., ultrapure water) with a calibration curve generated in the sample matrix. If the two curves are coinciding when superimposed, the effect of the matrix is not significant, hence, the samples can be analyzed using the standard curve prepared in the matrix blank [132].

In this study, the effect of 5 % acetone, 5 % methanol, 10 % methanol, 3.5 % sodium chloride and hard water with 7 degrees of German hardness (°dH), 14 °dH and 21 °dH were investigated (1 °dH corresponds to a quantity of 10 mg of calcium oxide per liter of water). The spiked solutions were analyzed by ELISA and by FPIA. As shown in the **Table 8** and **Figure 30**, an ELISA in the presence of methanol, sodium chloride, and acetone, still showed high sensitivity (low IC_{50}), but the signal (A1) was lower than that of the standard curve without matrix. It is possible to dilute the samples multiple times by which it could be possible to lower the matrix effect.

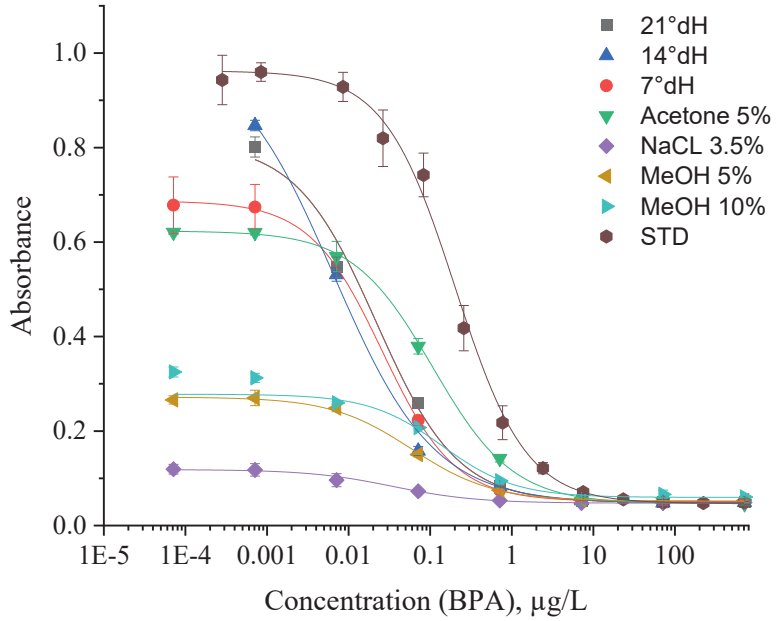

Figure 30. ELISA standard curves for BPA detection using different matrices (n = 3)

It was also interesting to observe that the ELISA signal (A1) and sensitivity (IC_{50}) were considerably enhanced when the Ca^{2+} concentration was increased (data shown **Table 8** and **Figure 30**). To lower the matrix effect of calcium a high-salinity buffer is preferably used.

Table 8 Parameters of ELISA for BPA in different matrices

	A1	**A2**	**IC_{50}**	***B* (Slope)**	**R^2**
Reference curve (STD)	0.96	0.05	0.2	0.99	0.99
Ca^{2+} 21 °dH	0.8	0.04	0.02	0.87	0.98
Ca^{2+} 14 °dH	1.01	0.04	0.06	0.7	0.99
Ca^{2+} 7 °dH	0.68	0.05	0.02	0.97	0.99
NaCl 3.5 %	0.11	0.04	0.03	0.84	0.99
Acetone 5 %	0.6	0.04	0.1	0.88	0.98
MeOH 5 %	0.3	0.05	0.05	0.87	0.99
MeOH 10 %	0.3	0.05	0.14	0.97	0.98

Compared with ELISA, it was interesting to observe that with the FPIA, as shown in **Figure 31** and **Table 9**, the value A1 and the sensitivity (IC_{50}) were considerably enhanced with the matrix present, which is very likely a result of the quite high buffering capacity of BB used as working buffer. However, to prevent false negative results due to matrix interferences, in the case of the FPIA it was possible to dilute the samples multiple times by which it was possible to lower the matrix effect.

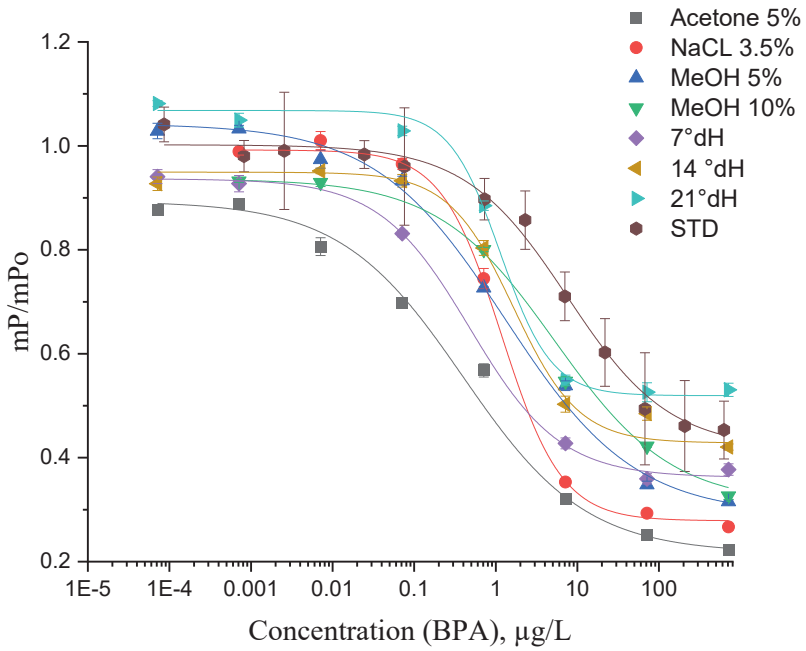

Figure 31. FPIA standard curves for BPA detection using different matrices (n = 3)

Table 9. Parameters of FPIA detection of BPA in different matrix.

	A1	**A2**	**IC_{50}**	***B* (Slope)**	**R^2**
Reference curve (STD)	1.0	0.4	7.52	0.69	0.99
Ca^{2+} 7 °dH	0.93	0.4	0.48	0.78	0.99
Ca^{2+} 14 °dH	0.94	0.4	1.6	1.1	0.99
Ca^{2+} 21 °dH	1.1	0.5	1.1	1.1	0.99
NaCl 3.5 %	0.9	0.2	1.1	1.2	0.99
Acetone 5 %	0.8	0.2	0.4	0.57	0.99
MeOH 5 %	1.0	0.3	1.3	0.54	0.99
MeOH 10 %	0.93	0.3	5.3	0.6	0.99

4.5. Optimization of analytical parameters of LFIA

4.5.1. Determining optimal concentration and pH for antibody conjugation

The central reagent in lateral-flow immunoassays (LFIA) are antibodies that "carry" particles that upon their deposition in dedicated zone form "lines" (T and C lines) that are visible to the naked eye. To establish such an assay, the particles, e.g., gold nanoparticles (GNP) have to be "decorated" with the analyte-selective antibody (IgG). Several methods have been studied.

For conjugation of gold nanoparticles and antibody by passive absorption, the optimal pH and a minimum amount of antibody for a stable GNP reagent [133, 134] had to be found. To determine the minimum amount of IgG and the most appropriate buffer for conjugation of gold nanoparticles, the electrolyte 10 % sodium chloride, added to several buffers with ionic strength 1 mM containing different amounts of IgG, was chosen. If no antibody is present, the addition of NaCl would cause gold particle coagulation. The titration was executed in a flat-bottom 96-well non-binding micro-plate. Firstly, the same amount (200 µL) of 40 nm gold nanoparticles was added into the wells. Then 20 µL of different concentrations of IgG was added in order to obtain concentrations of 300 µg/L – 3 µg/L, respectively, in different buffers: Milli-Q water (from row A_{1-3} to H_{1-3}) pH 7 , PBS pH 7.5 (A_{4-6}-H_{4-6}), borate buffer (BB) pH 8.5 (A_{7-9}-H_{7-9}), carbonate buffer (CB) (A_{10-12} – H_{10-12}) pH 9.6, and incubated for 1 h on a plate shaker at 750 rpm. After incubation, 20 µL of 10 % NaCl solution (in Milli-Q water) was added to every well and incubated for 10 min, then $OD_{280;520;800}$ was measured for each mixture in different wells after the color change was completed. The well positions which remained red demonstrated successful formation of a gold-antibody conjugate, where the antibodies protect the gold nanoparticles from the salt and hence from aggregation. The positions that turned blue have aggregated gold particles in them and those mixtures do not have enough antibody to protect the gold nanoparticles from aggregation salt. This is shown in **Figure 32 A, B**.

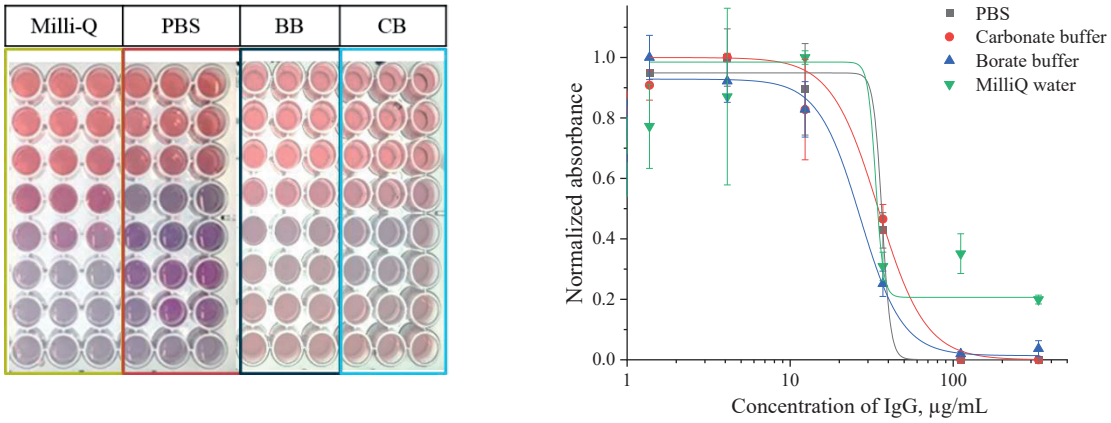

A B

Figure 32 A. The wells of an MTP turned blue when aggregated gold particles formed in it. Upon successful conjugation, the wells remained red. **B**. Concentration dependence of GNP (optical density at 580 nm) after adding different concentrations of anti-BPA IgG in different buffers.

In the experiment, according to the calibration curve (**Figure 32 B**), 7 µg of IgG in carbonate and borate buffer were found to be the minimum amount of IgG and suitable buffers for stabilization of the gold. However, we selected 20 µg and borate buffer for conjugation, because, in this study, 7 µg of IgG and carbonate buffer often caused coagulation of GNP during the conjugation.

After a successful conjugation of gold nanoparticles with 20 µg of anti-BPA IgG in different buffers (PBS, BB, CB), the stability was confirmed by UV-Vis spectroscopy**. Figure 33 A, B** show pictures and UV-Vis absorption spectra.

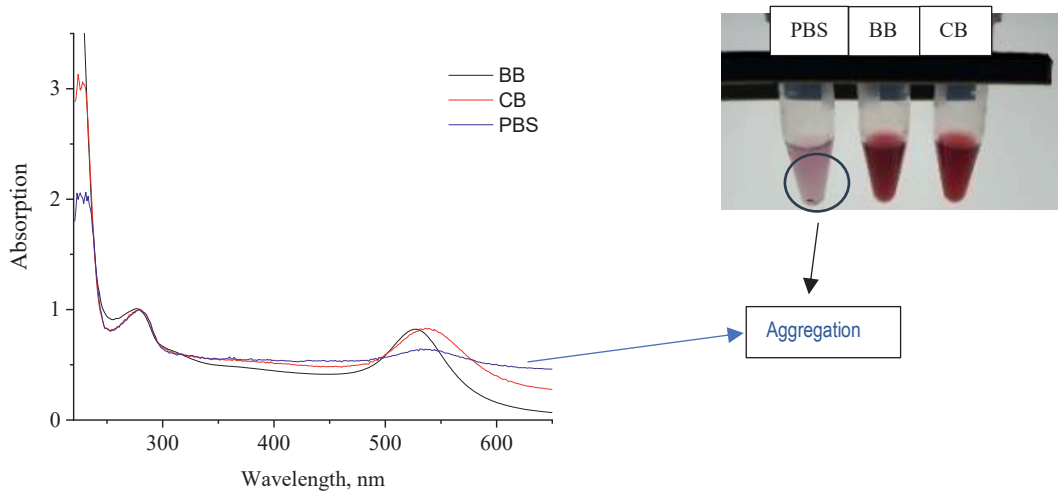

Figure 33. UV-Vis spectra and photograph of GNP conjugates. **A**. The UV-Vis spectra from the conjugates in borate buffer, carbonate buffer and PBS coupled with 20 µg of antibody. The blue line represents aggregation of the conjugate. **B**. Plastic tubes with GNP turned to blue having aggregated gold particles in it. Succeeded conjugation is in the tube remaining red.

It was confirmed that PBS buffer is not a suitable buffer for conjugation. The PBS buffer used contained approximately 0.14 M NaCl, which is higher than the biological salt concentration of about 0.10 M. Borate and carbonate buffers do not contain sodium chloride and have optimum pH, which provides the net charge of the protein is zero or slightly negative. This prevents the aggregation of the protein owing to electrostatic attraction while maintaining the hydrophobic interactions and facilitates the conjugation of the antibody to the gold.

4.5.2. Determination of coupling ratio of particles with antibody by sandwich ELISA

The coupling ratio of gold nanoparticles (and the later used latex microparticles) to antibody (IgG) is an important factor that can influence assay sensitivity. Too many antibodies would reduce the sensitivity of the LFIA, and too few IgG would cause incomplete coupling, leading to a weak intensity band of the T-line, which would be adverse to the detection limit. Numerous studies have used various methods to measure the amount of protein attached to a nanoparticle surface [135–137].

In this study, a sandwich ELISA to quantify mouse IgG in the supernatant was developed. The absolute concentration of antibody adsorbed onto the GNP and latex was inferred to be the mass

difference between the antibody added to the gold nanoparticles (GNP) and latex microparticles (LMP) and the antibody remaining in the supernatant.

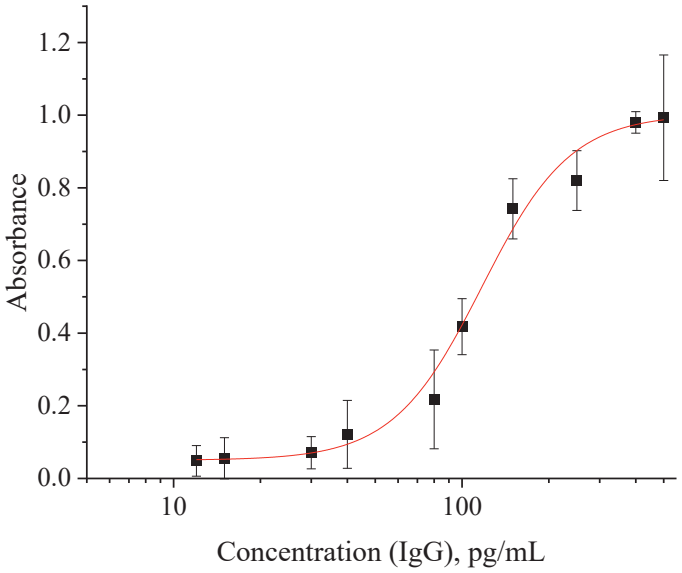

Figure 34. Calibration curve of the sandwich ELISA for determination of mouse anti-BPA IgG in supernatant.

From the ELISA calibration curves (**Figure 34**), it was found that 56 % of IgG was coupled with GNP by covalent coupling. It was also found that 49 % of IgG was adsorbed onto GNP by passive absorption when using borate buffer. By using carbonate buffer, only 40 % of IgG was attached to the GNP. By using PBS, the amount of IgG attached to the GNP was reduced to just 25 %. It appears that the convenient and highly affordable method of coupling GNP with IgG by passive adsorption using borate buffer works sufficiently well. A study of incubation times showed that for passive absorption an optimal incubation time with IgG was 18 hours.

4.5.3. Membrane selection for LFIA

The individual type of nitrocellulose membrane chosen is one of the most significant factors that influence the protein binding level, mobility of reagents, testing time and sensitivity of a LFIA test [121, 138]. The combination of the type of membrane and the immobilized reagent should be appropriate to ensure optimal loading of hapten-protein conjugate (test line) and secondary antibody (control line) on the surface of the membrane, available for specific interaction with the antibody-particle probe. Moreover, the particle size is another important factor that influences the flow rate. Capillary rise of larger gold nanoparticles (≈ 40 nm) through lateral flow membranes

was slower than for smaller ones (≈ 20 nm) [73, 139]. The 300 nm latex microparticles is 20 times brighter in visibility per particle than traditional 40 nm gold in LFIA [32]. It provides greater contrast against the white background of a lateral flow membrane than colloidal gold [31]. It is important that for any OD per volume, there are about twenty times less particles, so conjugate volumes will need to be adjusted. As a starting point, increasing OD or conjugate volume per strip two-fold will give a boost in sensitivity, because they are of blue color (good visibility for eyes and devices) and 300 nm in size and their mobility was sufficiently decreased. Several studies[55, 70, 74, 119, 140, 141] had shown that decreased mobility of larger particles resulted in better assay sensitivity, because it leads to longer incubation times of the reagents.

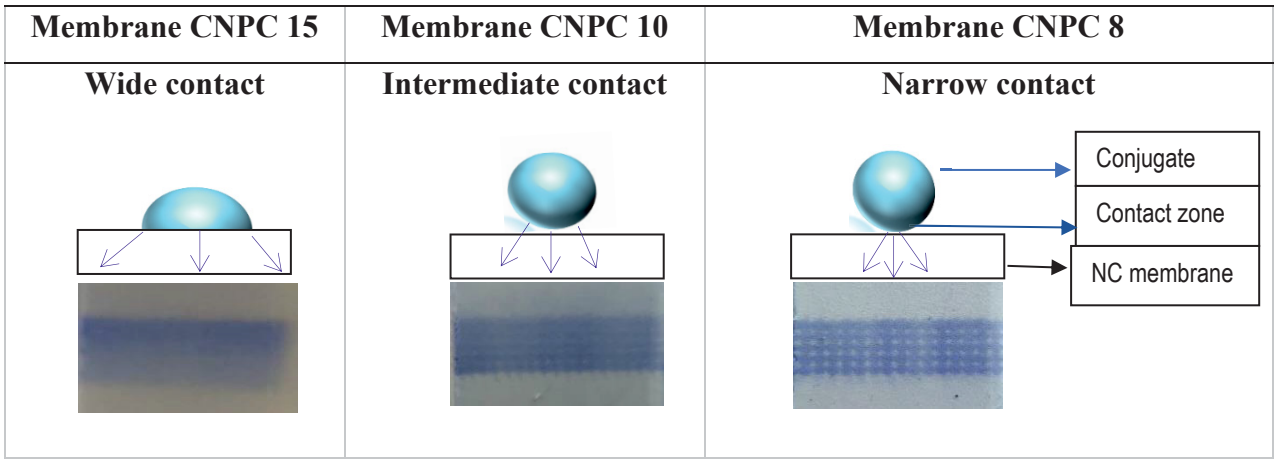

Figure 35. Conjugate band width as a function of liquid contact zone and photographs of different nitrocellulose membranes with latex microparticles spotted equidistantly onto the membrane.

The mobility of microparticles on a membrane also depends on its pore size and its so-called "wicking" times. The available NC membranes are characterized by different pore sizes (8 – 15 µm), protein binding capacity (low-medium-high) and by the wicking time (100 – 200 sec), see **Table S 2**. All these characteristics may influence the response time, intensity and sharpness of the signal, and resultant sensitivity and reproducibility of the test. **Figure 35,** Supplementary material **Figure S 9, S 10,** and Supplementary material **Table S 2** summarize the experiments performed on the interaction of the IgG−LMP and IgG−GNP probes with the coating conjugate BVA-Ahx-BSA, deposited in the test zone of various types of membranes. The photographs show that the most contrasting and brightest reaction zone depends on both the pore size/flow rate of the

membrane and the molecular weight of the protein conjugate (IgG: 150 kDa, BVA-Ahx-BSA: 72 kDa) **(Table 10, Table S 2)**.

Table 10. The specific interaction of the antibody-latex probe on different types of membranes.

Membrane characteristics*				**Microphoto images of interaction with anti-mouse IgG and coating conjugate**		
Membrane type	Pore size, µm	Binding capacity	Wicking time, sec	Anti-mouse IgG C –line IgG−LMP	BVA-Ahx-BSA T- line	
					IgG−LMP	IgG−GNP
CNPF	8	low	170 ± 25		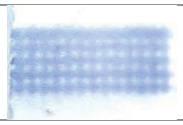	
CNPF	10	low	125 ± 25	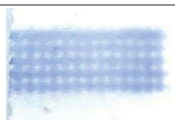	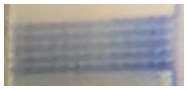	
CNPC	12	medium	120 + 28	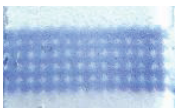		
CNPC	15	medium	100 ± 25	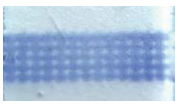		
CNPH-N	ND	high	70 ± 20		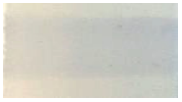	
CNPH-N	ND	high	90 ± 35	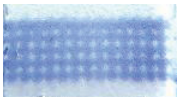		

* Characteristics are provided by manufacturer. ND – not disclosed

It may be summarized that binding capacity was not a critical factor for the quality of visibility of the test line, whereas little pore size 8 and 10 µm and the larger molecular weight of IgG (150 kDa) in comparison with BVA-Ahx-BSA (72 kDa) (**Table 10** and **Table S 2**) appeared to be sufficient for better surface fixation and availability for binding with the relatively large latex probe (Ø = 300 nm) and gold nanoparticles (Ø = 40 nm). It is likely that high pore size promotes deeper and more widespread penetration and fixation of coating antigen.

In this regard, the latter was not available for the IgG−LMP and IgG−GNP probe. This effect became more critical for the conjugates with smaller molecular weight, for example with OVA (ovalbumin, MW 42.8 kDa). Consequently, a better visual effect was achieved when a larger molecular weight conjugate, such as BVA-Ahx-BSA (72 kDa), was coated on NC membranes with a

smaller pore size (8−10 μm). Additionally, the size of the particles has an influence on migration speed through the NC. It was found that NC membranes with a pore size of 8−10 μm are suitable for 40 nm IgG−GNP. NC membranes with pore size 10 μm are suitable for 300 nm IgG−LMP. The NC membrane with 10 μm provides an optimal visibility of the test line and ideal migration speed of the particles (IgG−GNP and IgG−LMP).

4.5.4. Membrane blocking and test duration

The migration of sample and IgG−LMP/IgG−GNP probe through a membrane is affected by their non-specific interactions with NC membrane due to its sorption capacity. To prevent unwanted interactions of test reagents, a membrane blocking was evaluated [142]. Several blocking solutions, such as Milli-Q water or PBS buffer containing or 1 % Casein, 1 % BSA, or 0.1 % gelatin, were examined in the study (**Table 11**, **Table 12**). The optimal blocking solution appeared to be 1 % casein, the speed of signal development was rather fast, then 1 % BSA/PBS. It was found that blocking of the NC membrane with 1 % casein and 0.1 % gelatin provided comparable migration speed unlike to 1 % BSA blocking which resulted in slower mobility of antibody−latex microparticles and antibody–gold nanoparticles. Interference from anti-carrier antibody interaction with BSA could result in such an effect, so BSA was excluded from blocking agents. It is noteworthy that a 1.5-fold increase in membrane pore size (from 8 to 12 μm) accelerated the test by 1.5 times, regardless of the blocking formulation.

Table 11. Influence of blocking agents on migration speeds of IgG−GNP.

N	Membrane type	Pore size, μm	Flow time (sec) in 2.5 cm-membranes blocked with			Wicking time
			1 % Casein	1 % BSA	0.1 % Gelatin	
1	CNPF	8	400	500	480	Slow ↓
2	CNPF	10	240	360	270	
3	CNPC	12	200	430	250	
4	CNPC	15	150	330	200	Fast

Table 12. Influence of blocking agents on migration speeds of IgG−LMP.

N	Membrane type	Pore size, μm	Flow time, sec, in 2.5 cm-membranes blocked with			Wicking time
			1 % Casein	1 % BSA	0.1 % Gelatin	
1	CNPF	8	600	1100	660	Slow ↓
2	CNPF	10	440	800	470	
3	CNPC	12	400	730	440	
4	CNPC	15	350	630	400	Fast

Thus, the blocking of membrane surface with 1 % casein solution was optimal to avoid non-specific binding and control the flow rate as well as to stabilize reagents in the test and control lines but decreased the mobility of reagents through the membranes.
The compensating acceleration was achieved by choosing membranes with 10 μm pores for IgG−LMP and 8 μm pores for IgG−GNP.

4.5.5. Composition of the detection reagent mixture on the conjugate pad

In order to improve solubilization of IgG−GNP or IgG−LMP, prevent aggregation, and to provide an appropriate test line formation with an adequate migration rate, different reagents are often used as additives on the conjugate pad. Those additives are used for protein stabilization on a dry matrix. It should be emphasized that the choice and concentration of a surfactant was an important factor influencing assay performance [60, 75, 141, 143].

Seven kinds of conjugate pad (SureWick® GFDX, SureWick® G027, SureWick® G041, PT-R1, PT-R5, PT-R6, PT-R7) (**Table 3**) were tested.

Moreover, in combination, several blocking solutions were tested:
(A) 25 mM BB, 0.5 % BSA, 0.5 % Tween 20, pH 8, 10 % sucrose, 5 % trehalose
(B) 25 mM BB, 1 % BSA, 10 % sucrose
(C) 25 mM BB, 1 % BSA, 10 % sucrose, 5 % trehalose
Five μL of blocking solution was pipetted onto the conjugate pad and dried at 37 °C for 60 min. Then GNP-IgG or latex-IgG was pipetted onto the conjugate pad with the pipette, 5 μL per strip, and again dried at 37 °C for 60 min.

Using BB without any additives resulted in low sensitivity and weak color (**Table 13**). The optimal conjugate pads were previously blocked with solution C (25 mM BB, 1 % BSA, 10 % sucrose, 5 % trehalose) (**Table 13**).

Application of this mixture resulted in improved color intensity, optimal flow rate and enhanced test sensitivity. There was also a good solubilization of the detector reagent from the conjugate pad and a better protection of IgG−GNP or IgG−LMP. Application of this mixture resulted in improved signal intensity, and it markedly increased flow rate and test sensitivity.

Table 13. Influence of blocking agents on the intensity of the test line.

	Without treatment	A	B	C		Without treatment	A	B	C
IgG−GNP on the conjugate pad					IgG−LMP on the conjugate pad				
T -line (IgG−GNP)					T-line (IgG−LMP)				
Intensity of the T-line /a.u.	80	100	145	240	Intensity of the T-line /a.u.	98	120	320	500

A conjugate pad with a good hydrophilicity and release efficiency promises the favorably fast release of the gold nanoparticles conjugate and latex microparticles conjugate. The best performance according to the color intensity of the test line was found for the gold conjugate pad PT-5. For the latex conjugate, the pad SureWick® G027 was chosen for the following experiments. It was found that conjugate pads with treatment provided better stability of the particles, and the repeated experiment with 2-year-old strips provided comparable results (**Figure 36**).

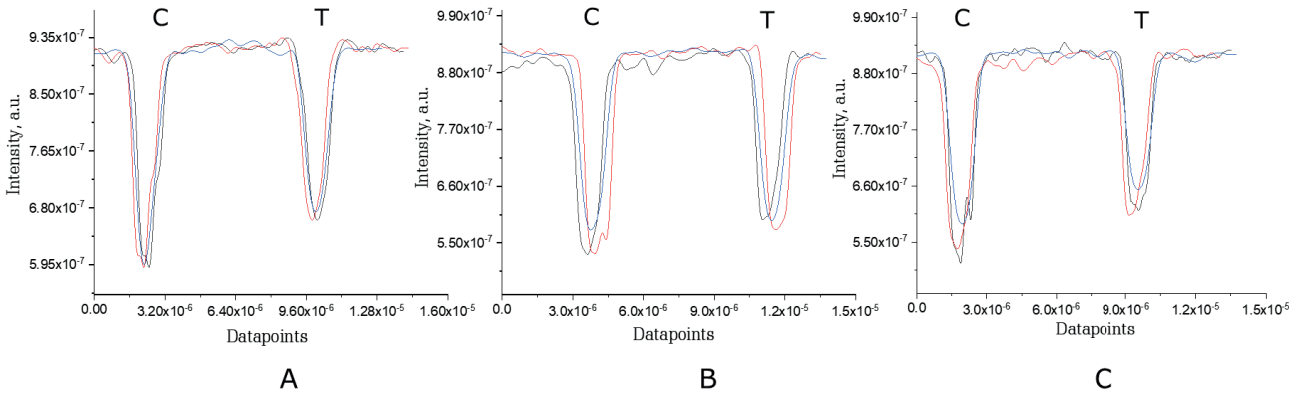

Figure 36. Reproducibility study: a sample spiked with 0.01 µg/L BPA was applied to the LFIA strips with IgG−GNPs. **A**. freshly prepared strips (n = 3). **B**. 12 months old strips (n = 3). **C**. 24 months old strips (n = 3) processed using the Gwyddion software combined with a fit using Origin™. The standard deviation is in the range of 0.5 – 0.80 %

4.5.6. Optimization of spotting conditions and reagent application

Appropriate amounts of detector reagent, antibody-particle probe, and coating reagent, BVA-Ahx-BSA, had to be concurrently optimized to get the highest sensitivity of detection. Moreover, an optimal concentration of capture control reagent (anti-mouse IgG antibody) had to be found for the formation of adequate color intensity in the control zone.

As known from the principles of competitive assays, higher concentrations of the reagents promote a high signal but decrease the sensitivity of the assay [144]. Thus, the task of optimization for development of a sensitive competitive assay means possible minimization of reagent amounts keeping well-visible reaction zones. The resultant color intensity of the test line was registered as a maximal peak value of summarized optical density and depended on multiple factors.

In order to create lines using a non-contact spotter, solutions were arrayed with 350 µm and 250 µm spot to spot pitch (**Table 14**). It was found that the distance between the spots with 350 µm spacing is too wide and this may lead to inaccurate results during interpretation of results with the cassette readers opTrilyzer® and Cube®.

Table 14 Influence of spot pitch on the image of the test line.

Spot pitch 350 µm	Spot pitch 250 µm
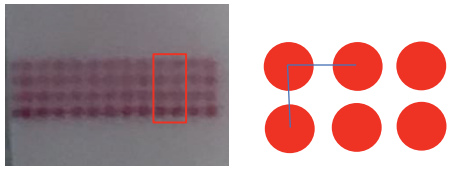	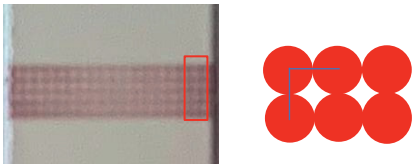

The loading of the coating conjugate per strip could be regulated by the concentration of the coating conjugate solution to be applied, by solution volume calculated in microdroplets, and the application area. The loading of antibody per strip varied during IgG–LMP or IgG–GNP probe preparation and depended on the amount of probe deposited in the sample pad.

In the study, the overall loadings of coating antigen as well as antibody loading were decreased by a factor of 5, so the resultant maximal value of optical signal became 2.5-fold lower, from 500 to 100 units. However, due to the reduction in the working area of test zone from 75 to 30 spots, the mean color intensity of an individual spot remained the same (2.65 units). This allowed for improving the limit of BPA detection 100-fold without loss of visual quality. However, for visual evaluation, the strips with latex look brighter (**Table 15, Figure 37**).

Table 15. Optimization of reagent load and test strip characteristics for BPA detection.

Coating antigen application			Antibody load		Assay characteristics		
Number of droplets / / spotted volume	T-line area, lines x spots	Load per strip, µg	IgG, µL* per LMP, mL	IgG–LMP, µL per strip	Max. intensity a.u.	Intensity per spot	Visual LOD, µg/L
40 // 14 nL	5 × 15	0.96	40	5.0	500	6.7	1000
40 // 14 nL	5 × 15	0.96	40	2.5	400	5.4	250
20 // 7 nL	5 × 10	0.44	20	2.5	350	11	25
25 // 8.75nL	3 × 10	0.2	20	2.0	250	8.3	10

Coating antigen application			Antibody load		Assay characteristics		
Number of droplets / / spotted volume	T-line area, lines x spots	Load per strip, µg	IgG, µL* per GNP, mL	IgG–GNP, µL per strip	Intensity max, a.u.	Intensity per spot	Visual LOD, µg/L
40 // 14 nL	5 × 15	0.96	40	5.0	450	6	1000
40 // 14 nL	5 × 15	0.96	40	2.5	220	3.0	250
20 // 7 nL	5 × 10	0.44	20	2.5	160	5.0	25
25 // 8.75nL	3 × 10	0.2	20	2.0	100	2.65	10

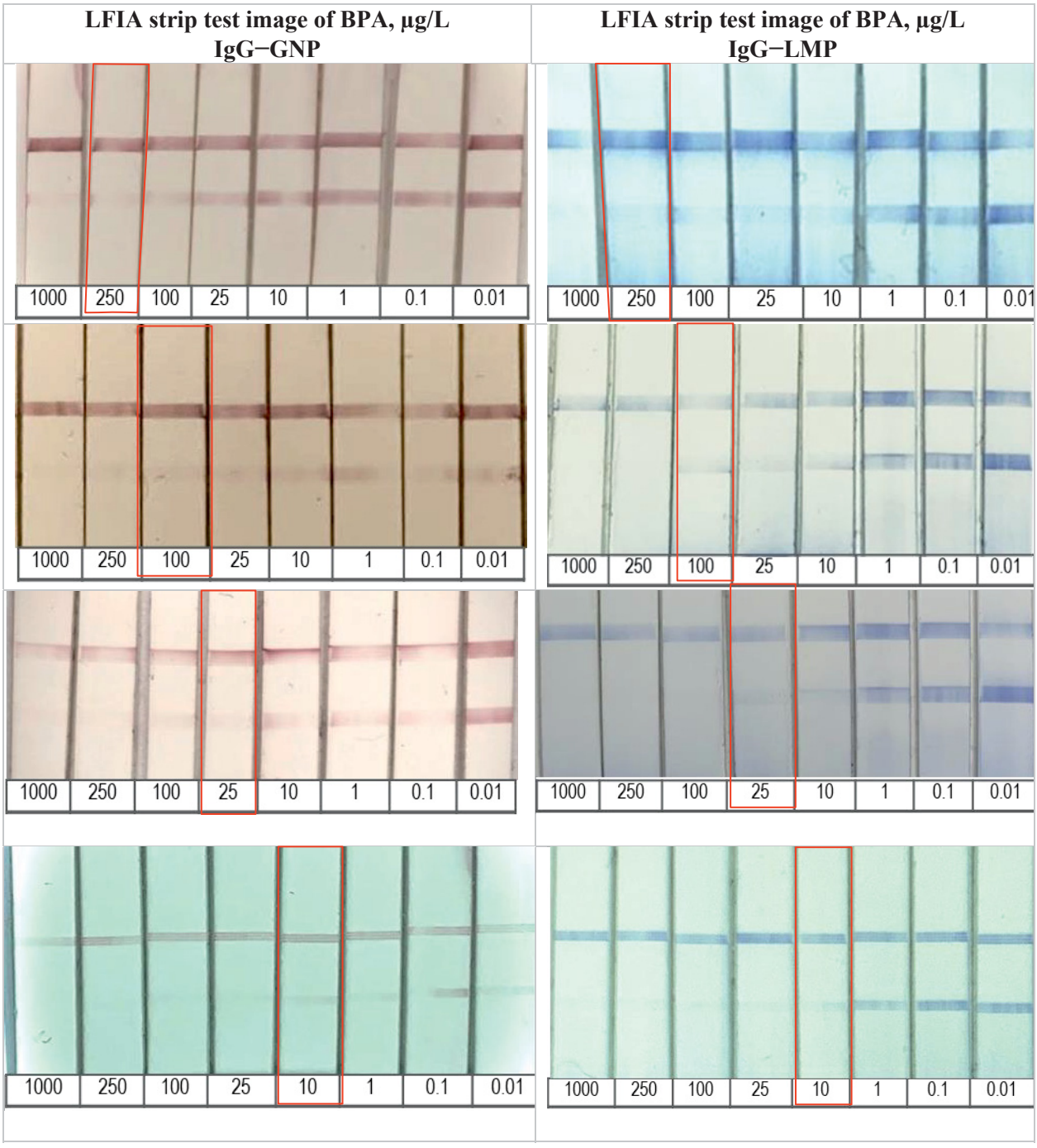

Figure 37. Determination of BPA in LFIA strip test, visual LOD (in red)

4.5.7. Analytical characteristics of the of LFIA

The results of the LFIA test strip can be evaluated both visually and with a device that scans the test zone and registers its color intensity. Digitization of the color intensity in the test zone using a strip reader allows quantifying the reaction by pre-calibration. Moreover, the limit of detection determined by instrumental readout is much lower than the cut-off estimated by naked eye. The LOD is calculated from the standard curve and defined as the concentration that corresponds to the mean intensity of the blank test line value minus 3×SD of the blank [145−147]. Alternatively, for convenience, LOD is taken as IC_{20}, and the measurement range is taken as $IC_{20} – IC_{80}$ (**Figure 38, Table 16**).

The intensity of test line color was converted into digital units by a strip-scan reader and used for plotting of the standard curves. The corresponding BPA standard curves are shown in **Figure 38.**

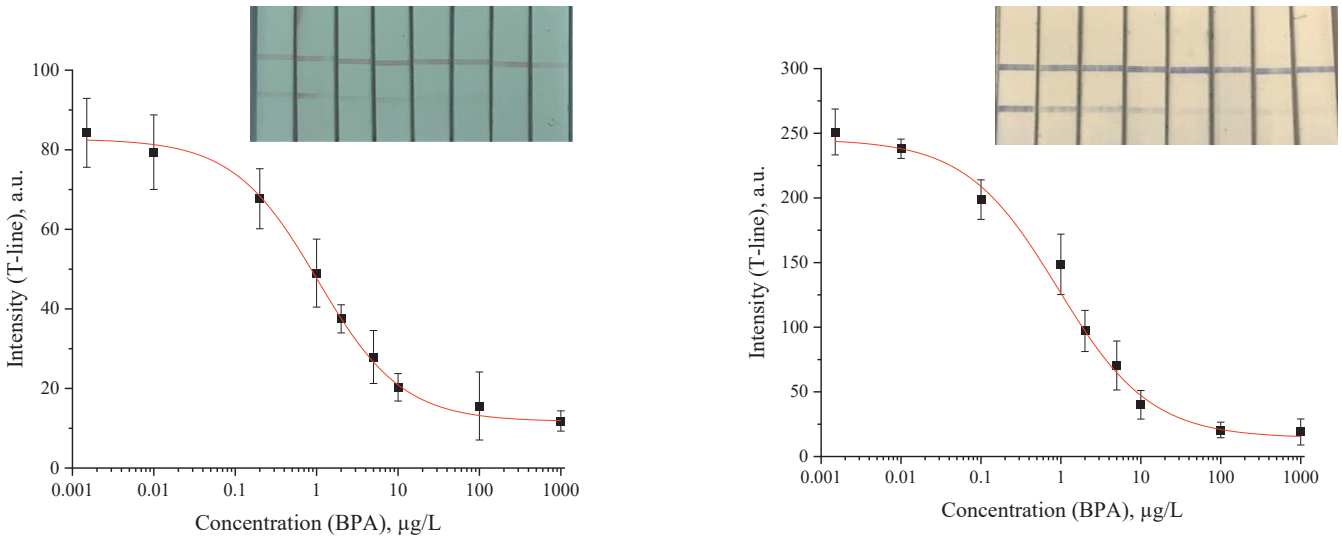

Figure 38. BPA standard curves (**A.** IgG−GNP and **B.** IgG−LMP). Parameters of visual and instrumental detection of BPA in the developed LFIA of BPA. Test and control lines are visible and scanned using the opTrilyze® reader, a handheld device, and number plotted with Origin™.

Table 16. Parameters of visual and instrumental detection of BPA in the developed LFIA.

Particles	Visual cut-off, µg/L	IC_{50}, µg/L	IC_{20} (LOD), µg/L
GNP	10	1.2	0.2
Latex	10	0.9	0.14

4.5.8. Influence of matrix interference on the sensitivity of the LFIA

In this study, the influence of organic solvents on the standard BPA curve was tested with Milli-Q containing 0 %, 10 %, 30 %, 50 %, and 80 % of methanol, or 5 % of acetone. The influence of water mineralization was tested by assaying water with 3.5 % sodium chloride (simulating marine water) and Ca^{2+}/Mg^{2+} levels simulating hard water with 7 °dH ("Grad deutscher Härte", degrees of German hardness), 14° dH and 21° dH. It was demonstrated that 5 % acetone, 3.5 % sodium chloride and hard water with 7 °dH, 14° dH and 21° dH did not affect the assay performance.

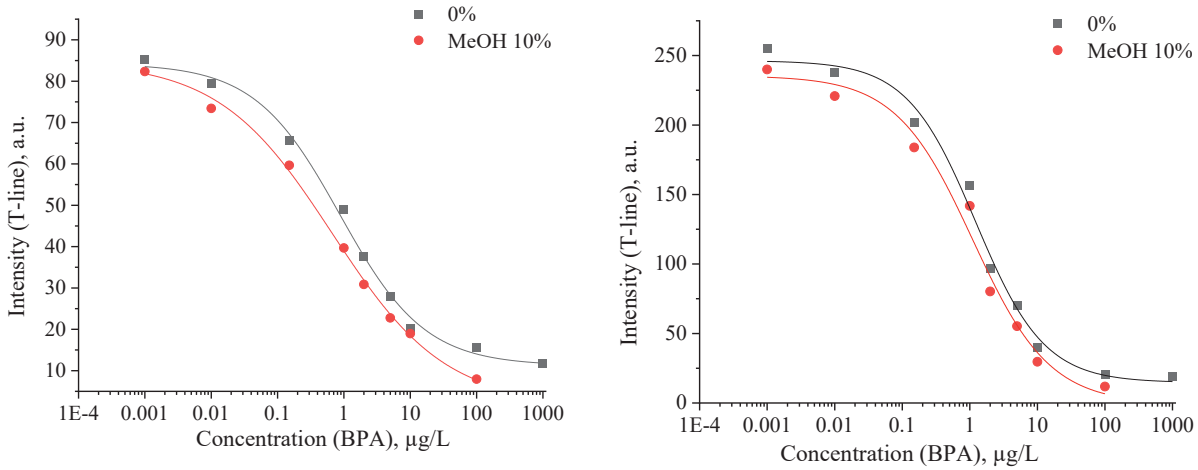

Figure 39. The influence of methanol concentration of 10 % compared to the standard curve obtained from calibrators in Milli-Q with **A**. IgG−GNP and **B**. IgG−LMP conjugates for BPA determination by LFIA.

The action of methanol resulted in a decrease of color intensity due to the deterioration of probe release from the conjugate pad and inhibition of antibody binding in an organic solvent medium. Thus, staining in the test and control zones of the membrane at 80 % methanol was not observed at all. At 50 % methanol, the IgG−LMP color development remained rather weak compared to the Milli-Q reference. With IgG−GNP the test and control zones of the membrane was not observed at all. At 30 % methanol, the color development was weaker compared to the test performed with BPA standards in Milli-Q due to the IgG−GNP probe not being released completely. Full dose-response curves were obtained at 30 % share of methanol, however, an acceptable level of color intensity was only reached when methanol content was decreased to 10 %. The methanol content in pretreated samples was adjusted to 10 %. A slight left-shift of the calibration curve of calibrators in 10 % MeOH was observed in comparison with the curve generated in Milli-Q (**Figure 39**).

4.5.9. Cross-reactivity of the antibody

Cross-reactivity in aqueous solutions of various structural analogues of BPA was evaluated. Some compounds that are, apart from bisphenol A, present in food contact materials, plastics, or thermo paper, display structural similarities to bisphenol A. These compounds were therefore studied for cross-reactivity behavior. The results for different compounds are summarized in **Table 17.**

Compounds with a similar structure as bisphenol A showed cross-reactivity that varied according to the used method (FPIA, ELISA, and LFIA). Removal of central methyl groups and of the hydroxyl groups of the bisphenol A molecule resulted in a strong reduction in cross-reactivity, while the extension of the methyl group by an additional carbon in the case of bisphenol B (BPB) resulted in a cross-reactivity of about 200 %. This remarkably high cross-reactivity for this particular compound can be explained by the higher similarity of the compound to the antigen used for immunization. That antibody was probably produced from BVA directly coupled to a carrier protein to obtain an immunogen. However, more complex bisphenol A analogues, such as bisphenol S (BPS), were not recognized (CR < 0.1%). When structurally simpler phenolic compounds, such as 4-octylphenol (OCP) and 4-nonylphenol (4-NP) were detected, the color of the test line in the LFIA strip appeared to be of the same intensity as that of the negative control sample. Therefore, the test was specific for BPA and showed “no” (< 0.1%) cross-reactivity to OCP and 4-NP and no significant cross-reactivity was observed by ELISA and FPIA.

There was some disagreement between cross-reactivity of structural analogues determined by FPIA and indirect ELISA. This was previously reported. Xu et al. [148] and Kolosova et al. [149] also found different CRs using FPIA and indirect ELISA. We assume that this behavior is determined by binding kinetics.

Table 17. Cross-reactivity (CR, in %) of the antibody, determined by ELISA, FPIA, LFIA.

Abbr.	Chemical structure	ELISA	FPIA	LFIA	Abbr.	Chemical structure	ELISA	FPIA	LFIA
BPA	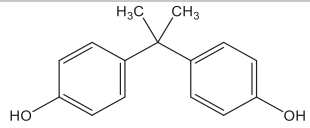	100	100	100	**BPF**	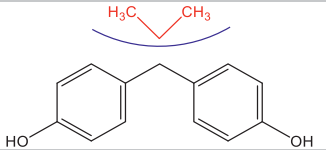	1.0	< 0.1	< 0.1
BPA-d16	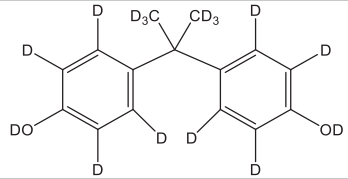	60	252	52	**BPS**	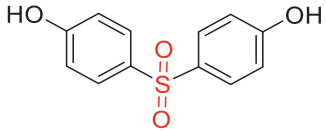	0.13	< 0.1	< 0.1
BVA	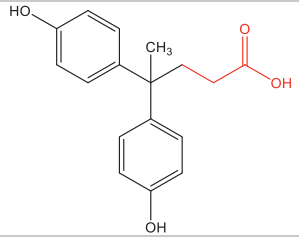	13.3	106	17	**BPB**	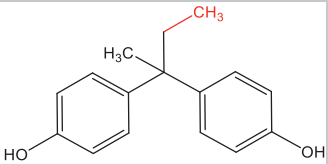	217	243	105
4-CP	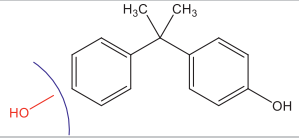	1.6	27.2	3.7	**OCP**	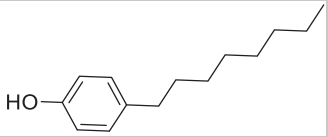	0.01	< 0.1	< 0.1
BPE	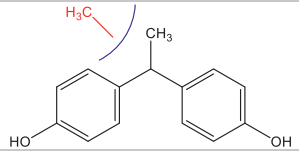	1.0	11.6	7.5	**4-NP**	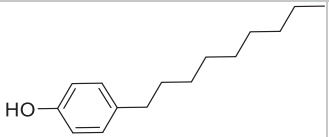	0.02	< 0.1	< 0.1

4.6. DETERMINATION OF BPA IN POLYMER MATERIALS AND PRODUCTS

After assay development, the test systems of LFIA, FPIA and ELISA have been optimized to the extent in which the analytical methods are also suitable for real samples.

Bisphenol A affects us in everyday life through contact with polymer products, for example, by wearing sunglasses made of plastic through dermal contact, using CDs, using phones with glass screen protector, transport tickets, etc. Children (and some adults as well) like to share the bath tub with a rubber duck, a very popular bath toy. But warm water at bath time can cause BPAs to leak into the water [137]. From paper used in thermal printers, used in cashier receipts, BPA can be transferred to other products or absorbed through the skin of consumers' hands or the hands of those who operate with the paper [144–147]. That's why in this work bisphenol A release from various different plastic samples was analysed by the optimized and improved test systems FPIA, LFIA and ELISA.

Taking into account that BPA is a ubiquitous environmental contaminant [150], six wastewater samples were obtained from three different wastewater treatment plants from Berlin (Ruhleben) and Brandenburg (Schönerlinde, Waßmannsdorf). The samples were first filtered through folded paper filters and then through glass-fibre syringe filters. Influent samples were diluted 1:100 with Milli-Q water before analysis, and effluent samples 1:10. None of them tested positive for BPA by any of the immunoassays and LC-MS.

Thermal paper samples (n = 3) were collected from local supermarkets of different countries, Germany (Berlin), Belgium (Brussels), and Russia (Moscow). Other paper products (n = 9) were collected mainly in Berlin in 2018. These samples were grouped into 3 categories: flyers (e.g., advertisement brochures from local restaurants), tickets (e.g., train tickets), food contact papers.

The analyzed samples were representative of various brands of rubber duck toys, CDs, sun glasses, phone glass screen protector available in a local EuroShop in Berlin, Germany.

4.6.1. Sample preparation

In order to obtain the best analytical methods for the examination of plastic samples, polycarbonate cubes were tested. Since polycarbonate is synthesized from bisphenol A, it could have gone for sure that the examined polycarbonate cubes contained bisphenol A. Eight different methods have been tested to extract bisphenol A from the polycarbonate cubes (**Table S 3**). The method that had

the highest yield of bisphenol A was subsequently used to determine the concentration of real plastic samples [30, 78, 95, 153–158]. The execution of this extraction is shown in **Figure 40**.

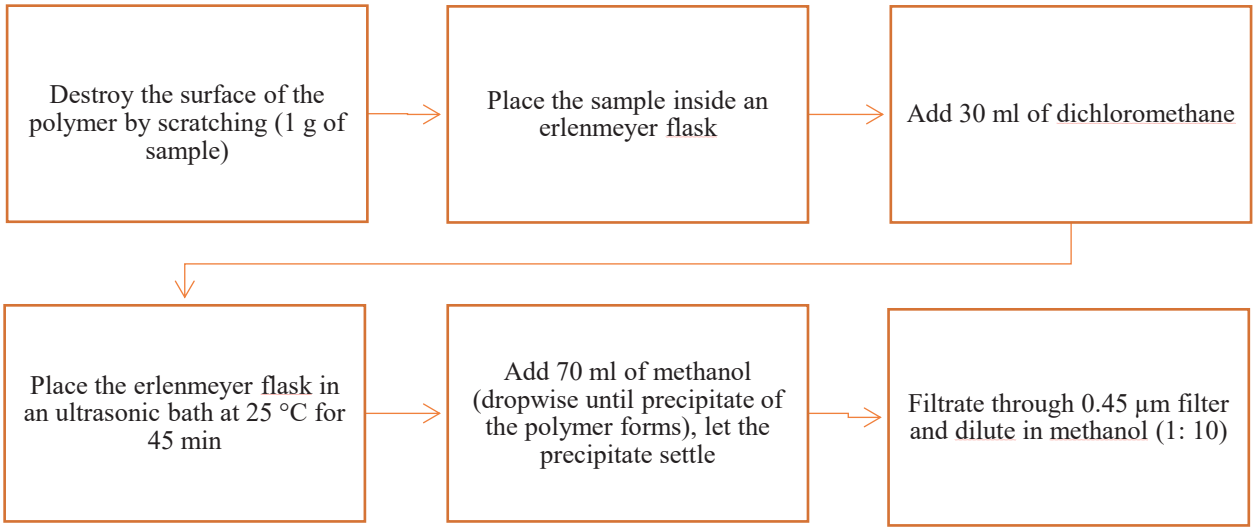

Figure 40. Scheme of sample preparation

The entire polymer was dissolved in dichloromethane and partially decomposed into the monomers. Other substances contained in the solution were precipitated by the addition of methanol. The measured concentrations of BPA are shown in **Table 18.** Before analysis the pretreated samples were serially diluted in Milli-Q water to eliminate impact of methanol.

The extraction of bisphenol A from other samples (not polycarbonate) was carried out by two methods. In the first method, used for the thermal receipt paper, 0.2 g of the thermal paper was inserted into 20 ml of ethanol and stirred for one hour at 35 °C [159]. The second method (taken from [160]) was used for flyers and magazines: 0.1 g of the sample was inserted into 2 ml of methanol and extracted in an ultrasonic bath at 35 °C for ten minutes. The samples were first filtered to remove the resulting dye coagulation and then cleaned with SPE as described below for LC-MS analysis. For the immunoassay, the solutions were filtrated and diluted in Milli-Q water.

Solid-phase extraction (SPE)

Real-world plastic samples represent a complex matrix which may contaminate or even clog instrumental analytical systems. For chromatographic analysis, a pre-treatment step had to be inserted after the extraction of bisphenol A, else the presence of interferences in the sample could result in instrument downtime due to a buildup of contamination with each injection into the LC-MS. It was important to perform solid-phase extraction (SPE) of the samples. During this clean-up, many disturbing substances that have a different polarity than bisphenol A, are removed from

the extract and thus cannot influence the measurement. The protocol of this SPE has been previously described [161, 162].

As said, clean-up by SPE is indispensable for LC-MS and it is an expensive and extremely time-consuming process. Immunoassays (LFIA, FPIA and ELISA) do not require SPE, which makes these assays especially cost-effective and fast.

4.6.2. Analysis of polymer materials and products

Samples were processed to obtain crude and purified extracts, then were analysed by LFIA, FPIA, ELISA, and LC-MS, respectively. The results are shown in **Table 18.**

Table 18. Analytical result of selected samples (n = 3 replicates). The values of BPA found with LC-MS/MS, FPIA, ELISA, and LFIA are shown. Information in brackets indicates the recovery rate (BPA in relation to LC-MS/MS) of the immunoassays.

Probe	***c* (BPA) ± SD (µg/L)**						
	LC-MS [µg/L]	**LFIA [µg/L]**	**CV%**	**FPIA [µg/L]**	**CV%**	**ELISA [µg/L]**	**CV%**
Compact Disc (CD)	49.5±4	51±10 (103)	9	60±3.2 (121)	6	56±3 (113)	5
Sun glass frame	144±11	158±11 (109)	13	121±6 (84)	5	132±12 (91)	9
Sun glass lenses	36.2±2	42±16 (116)	6	36±2.4 (99)	8	32±2 (88)	11
Rubber duck toy	1.6±0.2	<LOD	–	<LOD	–	1.5±0.2 (93)	17
iPhone screen protector	1±0.3	<LOD	–	<LOD	–	1.1±0.3 (106)	15
Thermal receipt paper BE [163]	0.7±0.03	<LOD	–	<LOD	–	0.76±0.5 (108)	18
Thermal receipt paper RU (Perekrestok)	<LOD	<LOD	–	<LOD	–	<LOD	–

Thermal receipt paper DE (Kaufland)	<LOD	<LOD	–	<LOD	–	<LOD	–
Tickets DE (S-Bahn)	13.5±1.2	15±10 (109)	6	16±1.2 (121)	9	17±2.1 (125)	12
Tickets RU (Metro)	34.1±2.3	29±10 (83)	8	36±6 (104)	16	43±1.6 (126)	9
Flyers DE	46.9±3	50±7 (105)	10	59±5 (126)	10	52±4.4 (110)	11
Food contact papers	<LOD	<LOD	–	<LOD	–	<LOD	–
Ruhleben, influent	<LOD	<LOD	–	<LOD	–	<LOD	–
Schönerlinde, influent	<LOD	<LOD	–	<LOD	–	<LOD	–
Waßmannsdorf, influent	<LOD	<LOD	–	<LOD	–	<LOD	–
Ruhleben, effluent	<LOD	<LOD	–	<LOD	–	<LOD	–
Schönerlinde, effluent	<LOD	<LOD	–	<LOD	–	<LOD	–
Waßmannsdorf, effluent	<LOD	<LOD	–	<LOD	–	<LOD	–

The FPIA, ELISA, LFIA results are in close agreement with each other. The satisfactory accuracy and precision of these methods suggests them to be sufficiently sensitive and reliable for the analysis of BPA in different type of samples.

It was found by the LC-MS analysis, that the thermal paper samples contain high concentrations of BPS (270–779 µg/L) (**Figure S 11**). Considering the toxic potential of BPS and due to the lack of data on transfer rates of BPS from paper to skin, it is needed to investigate further the effects of this compound in the environment and on human health [25, 164].

V. CONCLUSIONS

Three different techniques for the determination of the endocrine-disrupting compound bisphenol A in polymer materials were developed and compared, namely an easy-to-use Lateral Flow Immunoassay (LFIA), a mix-and-read Fluorescence Polarization Immunoassay (FPIA) and the high-throughput indirect ELISA as reference method, which possess different advantages in terms of efficacity and convenience to be used on-site.

An indirect competitive ELISA was developed and optimized, conjugates (BVA-BSA and BVA-Ahx-BSA, derived from BVA, a linkable BPA mimic) were synthesized, one including a C_6 spacer (Ahx). MALDI-TOF measurements showed the conjugation of BVA (bisphenol valeric acid) molecules to the BSA (bovine serum albumin) carrier protein and a spacer derivate of it (BSA-Ahx). Determined from the precision profile of the BPA calibration curve, the assay showed an LOD of 0.05 µg/L and an IC_{50} of 0.2 µg/L. ELISAs are suitable tools for quick and sensitive analysis with high sample throughput. However, such techniques often require long reaction times and involve multiple washing steps and incubations, thus ELISA was the most time-consuming among the three formats.

FPIA is a homogeneous mix-and-read method which does not require the immobilization of reagents. Structurally different tracers (including one with a C_6 spacer) to establish a fluorescence polarization immunoassay for BPA were synthesized and tested for the first time, and a rapid method was developed. The tracer molecules were assessed for performance and the FPIA for sensitivity. Full optimization of the assays was performed, studying the influence of the tracer structure on assay sensitivity, and the comparative assessment of performance was studied. FPIA displayed satisfactory precision and sensitivity with an IC_{50} of 7.5 µg/L and an LOD of 1.0 µg/L, which is sensitive compared to previously reported LODs. The FPIA method showed significant advantage in assay time, a sample measurement can be executed within 20 to 30 minutes. The satisfactory accuracy proved that the newly developed method is suitable to work as a rapid and inexpensive method for the detection of BPA.

Lateral Flow Immunoassay (LFIA) is an assay without the need for expensive equipment, washing, and/or separation steps, used in clinical laboratories or at the point-of-care with minimal training. It has obtained a high degree of familiarity in the 2020/2021 COVID-19 pandemic and proved its invaluable meaning in on-site analysis. In this work, gold nanoparticles and latex microparticles were functionalized with an antibody. Two different conjugation procedures were investigated,

direct physisorption and covalent attachment of the antibodies to the particles. Activity of bound antibodies was confirmed in both cases by a developed sandwich ELISA. Two solutions, one with latex microparticles and one with gold particles, with the same concentration results and the same surface coverage with antibody were obtained. The conjugate pad was selected from a huge variety of commercially available commodities and a blocking step was conceived and optimized.

An important base, the nitrocellulose membrane, was selected from a large choice, each nitrocellulose membrane having unique capillary flow characteristics based on the physical attributes of the membrane and the manufacturing process that impacts flow dynamics, sensitivity, specificity, and consistency of the assay. Non-contact spotting conditions, load of reagents per strip on the membrane (number of drops per spot, number of spots per line and number of lines), particle-antibody conjugate loads as well as membrane stabilizing solutions influencing the assay performance were investigated and optimized for the best color intensity. An additional membrane blocking step was selected and optimized.

Under the optimal conditions, the latex-based LFIA allowed BPA to be visually detected at 10 µg/L. Scanner-based quantification resulted in an LOD of 0.14 µg/L, respectively. To our knowledge, this is the first work reporting the development of a lateral-flow latex-based technique for the detection of BPA. Based on the results of this study, the described technique could be used for the fast and cost-effective determination of BPA.
Cross-reactivity studies involving structurally related compounds like BVA, 4-CP, BPE, BPF, OCP, BPS, 4-NP showed high selectivity of the antibody to BPA, except for BPB which resembles much BVA the supposedly used hapten to obtain these antibodies.

The quantification limits of LFIA, ELISA, and FPIA were far below the current Specific Migration Limit set for bisphenol A by the EU Commission (600 µg/L). Furthermore, the simplicity of all three immunoassays are clearly evidenced by their high sample throughput, since dozens of samples can be simultaneously analysed. So, they all are a promising technique for monitoring bisphenol A levels in aqueous food samples.

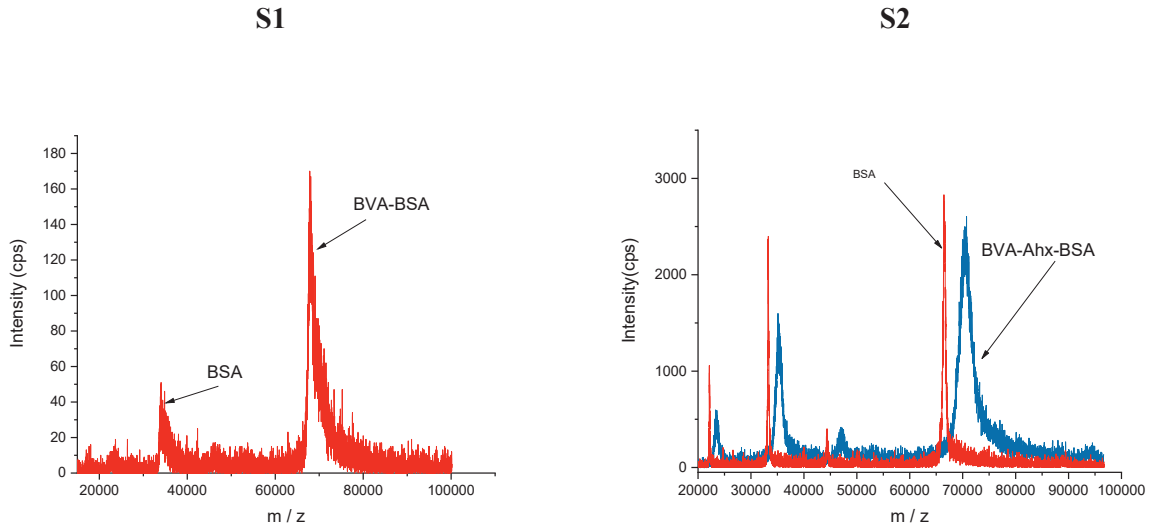

Figure S 1. MALDI-TOF/MS spectra of unconjugated BSA (present in the product) and BSA conjugated with BVA. It can be seen that the mean in the mass signal distribution of the conjugate has increased significantly compared to BSA. The spectrum represents the average of three measurement (n = 3).

Figure S 2. Overlay of MALDI-TOF/MS spectra of unconjugated BSA [167] and BSA conjugated with BVA-Ahx (blue). It can be seen that the mean in the mass signal distribution of the conjugate has increased significantly compared to BSA. The spectrum represents the average of three measurements (n = 3).

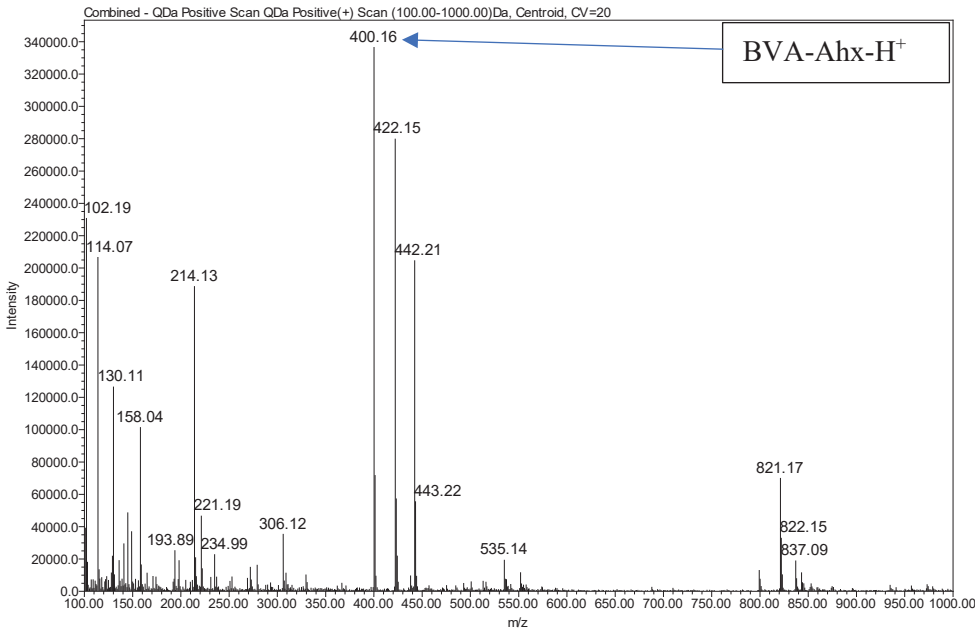

Figure S 3. Chromatographic peak: verification of the reaction of BVA with Ahx with the largest signal at m/z (BVA-Ahx-H^+) = 400.2. This reflects the mass of the desired product (399 g/mol) plus the mass of a proton (+1).

Table S 1. R_f values of the collected bands of the tracers during purification by TLC (each tracer was cleaned up for 3 times by TLC).

Tracer	**BVA-AMF**	**BVA-Ahx-AMF**
TLC retardation factor R_f	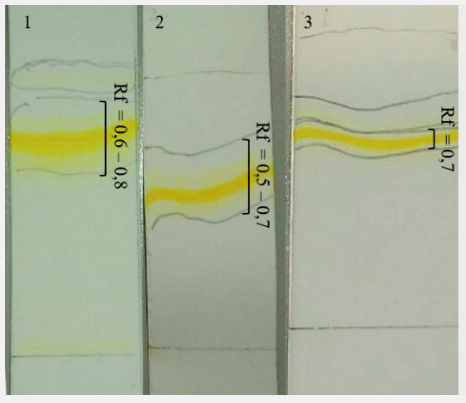	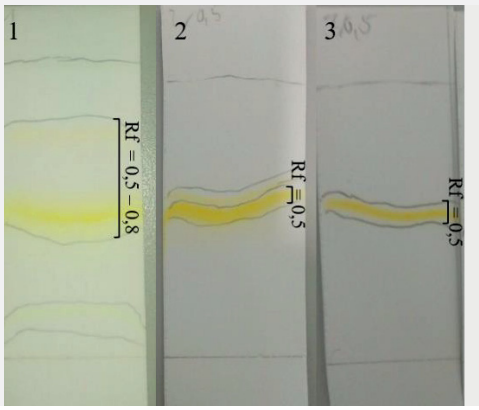

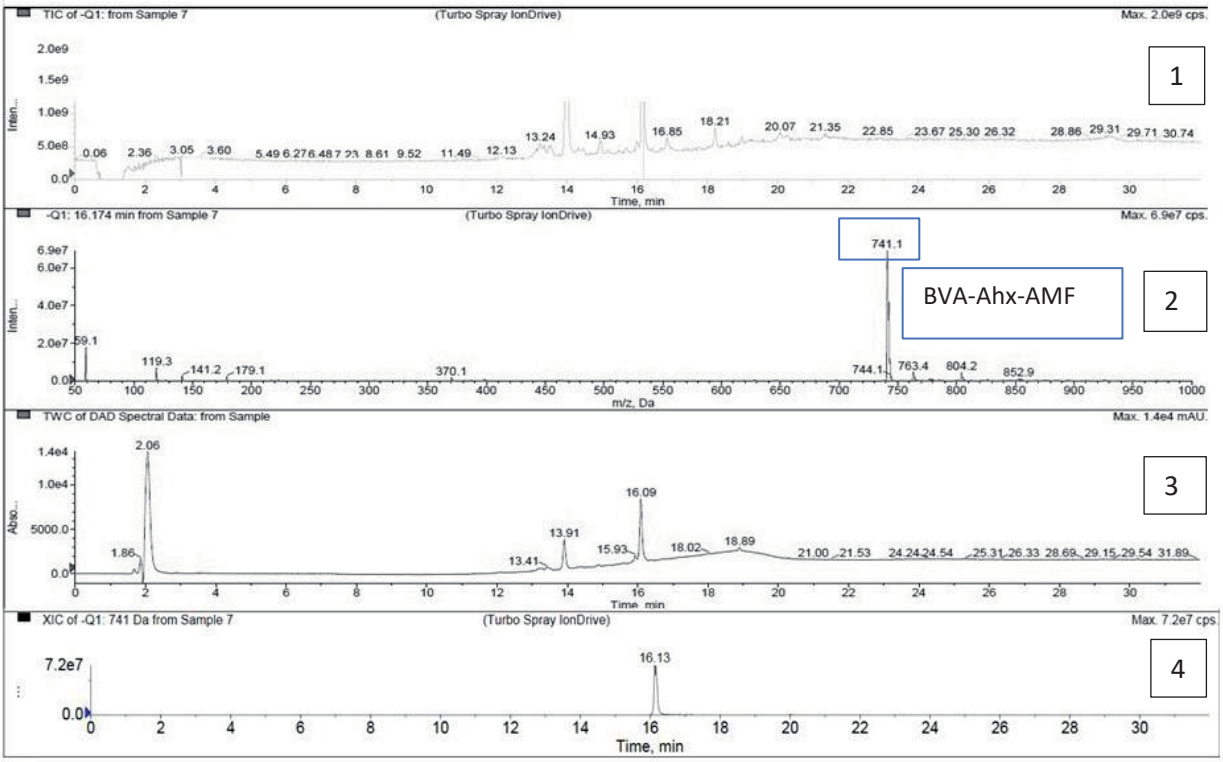

Figure S 4. Synthesis of BVA-Ahx-AMF before TLC purification: 1. Total ion chromatogram [168] showing the same peaks as the diode array detector (DAD) chromatogram (chromatogram 3) plus a major peak at RT = 16.2 min. 2. Mass spectrum of chromatographic peak at RT = 16.174 min, with the largest signal at m/z = 741.1 Da. This reflects the mass of the desired product (742.3 g/mol) minus the mass of a proton (–1). 3. HPLC chromatogram, DAD trace, showing two larger signals at RT = 16.174 min and RT = 16.13 min. 4. Extracted Ion Chromatogram (XIC, m/z = 741) showing the peak of the desired product at 16.13 min.

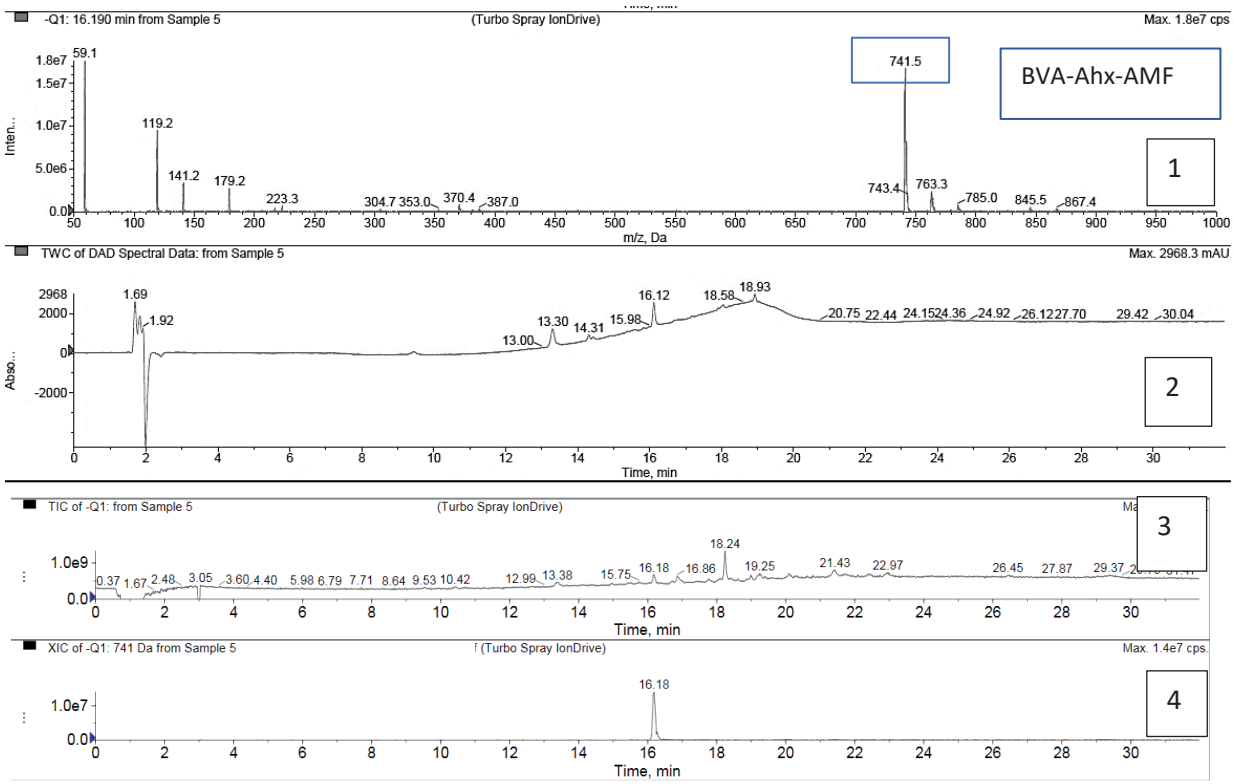

Figure S 5. Synthesis of BVA-Ahx-AMF after TLC purification: 1. Mass spectrum of chromatographic peak at RT = 16.190 min, with the largest signal at m/z = 741.5 Da. This reflects the mass of the desired product (742.3 g/mol) minus the mass of a proton (–1). 2. HPLC chromatogram, DAD trace, showing larger signals at RT = 16.12 min. 3. TIC (total ion chromatogram) showing the same peaks as the DAD plus a major peak at RT = 18.24 min. 4. Extracted Ion Chromatogram (XIC, m/z = 741) showing the peak of the desired product at 16.18 min.

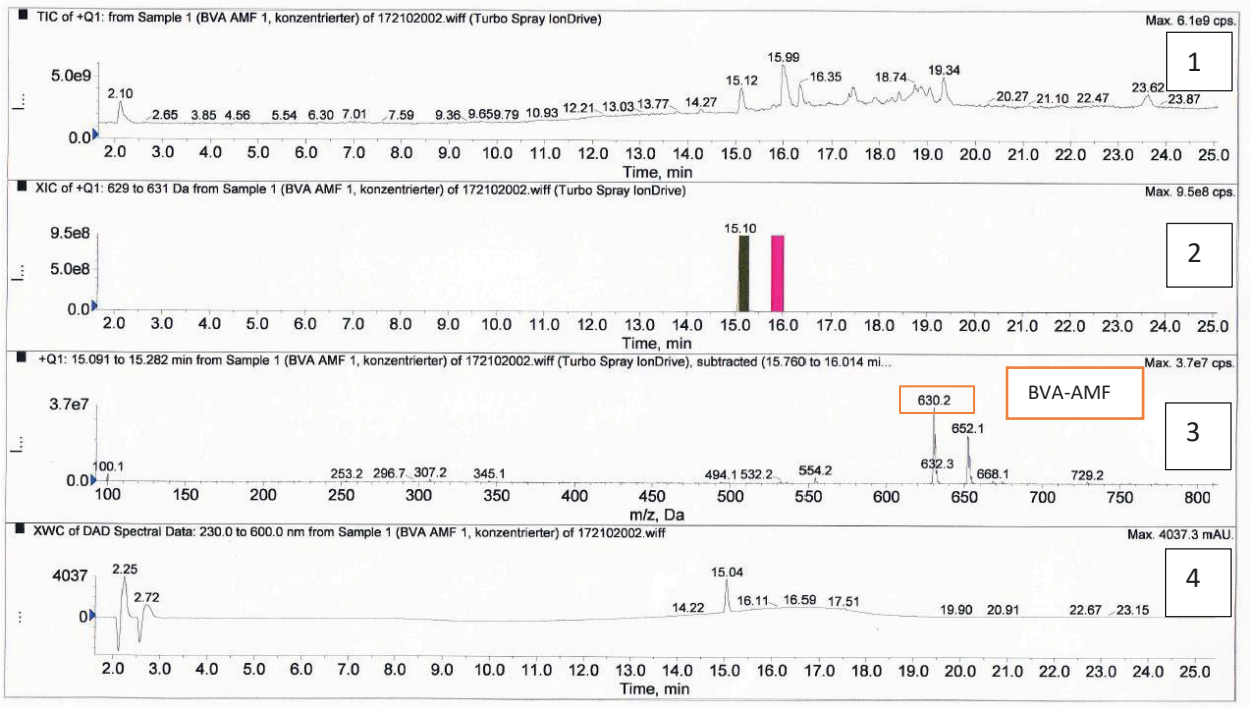

Figure S 6. Synthesis of BVA-AMF. Characterization of the product before TLC purification: 1. TIC (total ion chromatogram) showing the same peaks as the DAD (trace 4) plus a major peak at RT = 15.12 min. 2. Extracted Ion Chromatogram (XIC, m/z = from 629 to 631) showing the peak of the desired product at 15.10 min. 3. Mass spectrum of the chromatographic peak at RT from 15.091 to 15.282 min, with the largest signal at m/z = 630.2 Da. This reflects the mass of the desired product (629.3 g/mol) plus the mass of a proton (+1). 4. HPLC chromatogram, DAD trace, showing the largest signal at RT = 15.04.

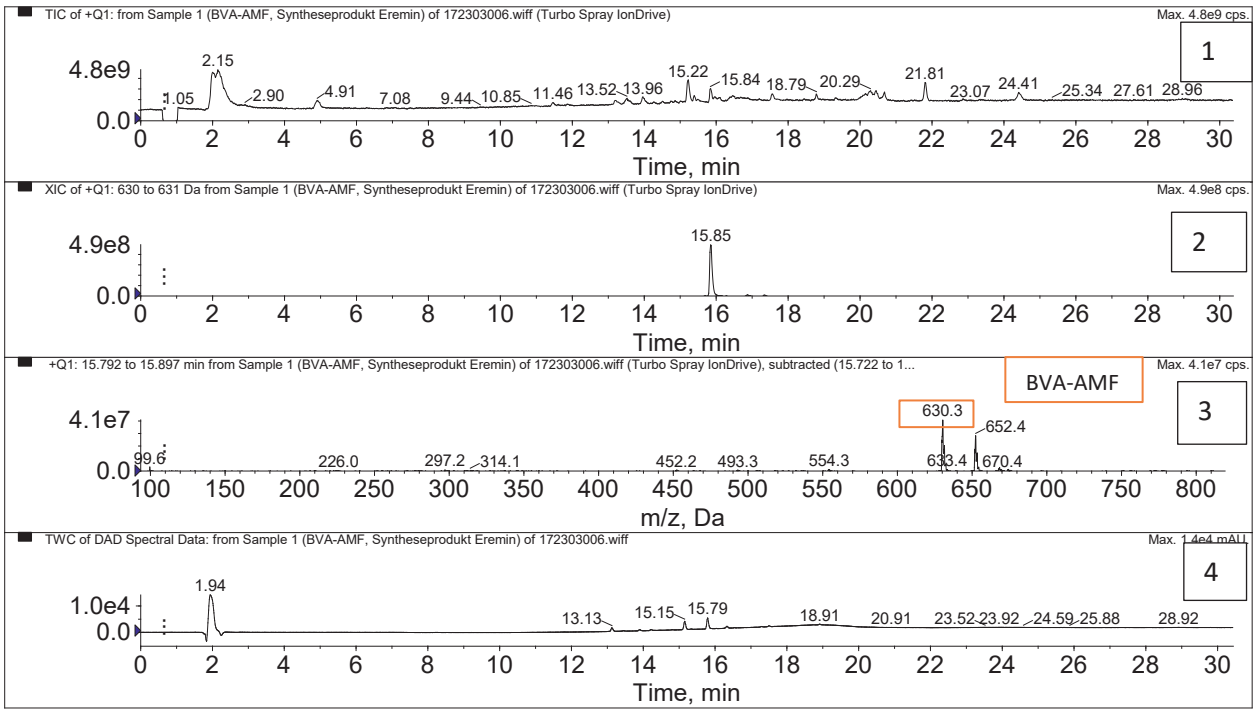

Figure S 7. Synthesis of BVA-AMF. Characterization of the product after TLC purification: 1. TIC (total ion chromatogram) showing the same peaks as the DAD (trace 4) plus a major peak at RT = 15.22 min. 2. Extracted Ion Chromatogram (XIC, m/z = from 630 to 631) showing the peak of the desired product at 15.85 min. 3. Mass spectrum of chromatographic peak at RT from 15.792 to 15.897 min, with the largest signal at m/z = 630.3 Da. This reflects the mass of the desired product (629.3 g/mol) plus the mass of a proton (+1). 4. HPLC chromatogram, DAD trace, showing a signal at RT = 15.15.

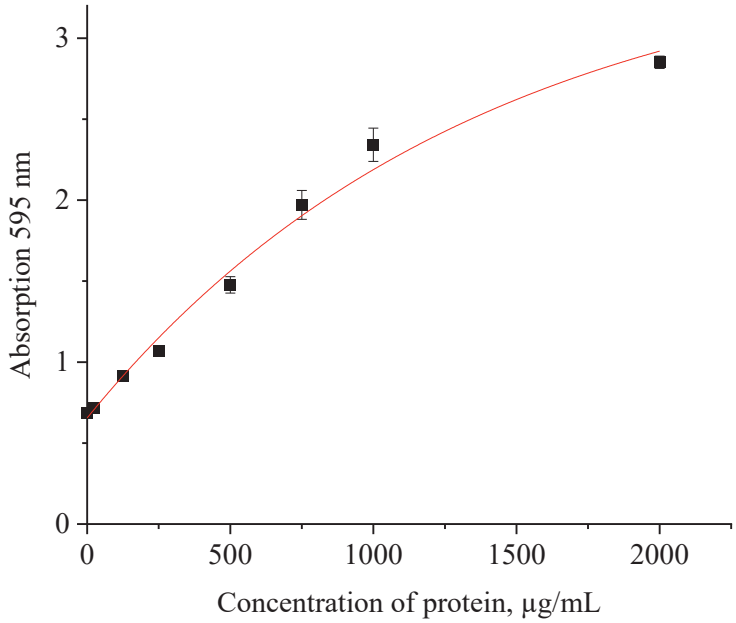

Figure S 8. Bradford assay standard curve of absorbance against protein concentration.

S.2 Dot-Lateral Flow Immunoassay

A Dot-LFIA is a simple and rapid technique for the determination of antibody-GNP and analyte conjugate binding [143, 169]. A schematic illustration of the one-dot LFIA is shown in **Figure S 9.** The key of the assay is using a pipette to apply the conjugate (T-spot) and a secondary antibody (C-spot) onto the NC membrane and identify the binding of the antibody-GNP in the test and control spot area. Once bound, the antibody and conjugate are visualized. A Dot-LFIA is able to provide information about the minimum concentration of conjugate needed for following the spotting on an NC membrane by a non-contact spotter. This information will conveniently help to reduce the time needed for spotting optimization. Secondly, it will visualize the difference of NC membranes by measuring the optical density of the signal (**Figure S 9**) dependent on the concentration of GNP.

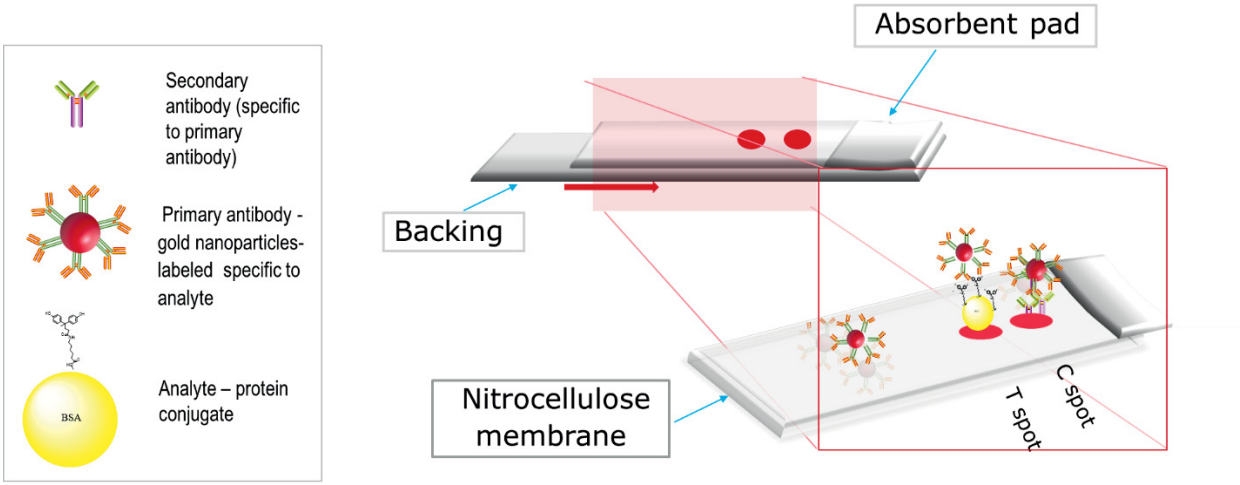

Figure S 9. Schematic of the Dot-LFIA

Protocol of the Dot-LFIA

First, one µL of the sheep anti-mouse-IgG (1 µg/mL) was applied on the NC membrane with a pipette as a control spot. Next, one µL of BVA-Ahx-BSA solution with different concentration (5 µg/mL, 10 µg/mL, 15 µg/mL) was applied as a test spot, then the membrane was dried for 25 min at room temperature. The NC membrane was blocked by immersion in 2 % Casein in PBS for 15 minutes under continuous shaking at 150 rpm and subsequently washed three times with Milli-Q water (**Figure S 9**). Ultimately, the NC membrane was soaked with anti-BPA-IgG-GNP with 2 OD. The concentration of 10 µg/mL BVA-Ahx-BSA was chosen for further optimization and the spotting step.

Afterwards, different types of nitrocellulose membranes (NC) were tested and soaked with anti-BPA-IgG-GNP with different optical densities (1, 2, 10, 20 OD) (**Figure S 10**) for 20 min and then washed in Milli-Q water. The intensity of the spot signals was determined by ImageJ. The NC with the most intensive signal was chosen for future optimization steps.

To calculate the dilutions of anti-BPA-IgG-GNP, the following equation (**a**) was used, entering the initial OD (OD_1 = OD provided on the certificate of analysis or measured by UV-Vis spectroscopy), the final OD_2 , and the desired final volume (V_2):

$$OD_1 V_1 = OD_2 V_2 \quad \text{(a)}$$

where OD corresponds to the optical density and V to the volume, respectively.

The specific binding reaction between the secondary antibody and GNP-primary antibody and conjugate caused the appearance of a red dot on the NC membrane (**Figure S 9**).

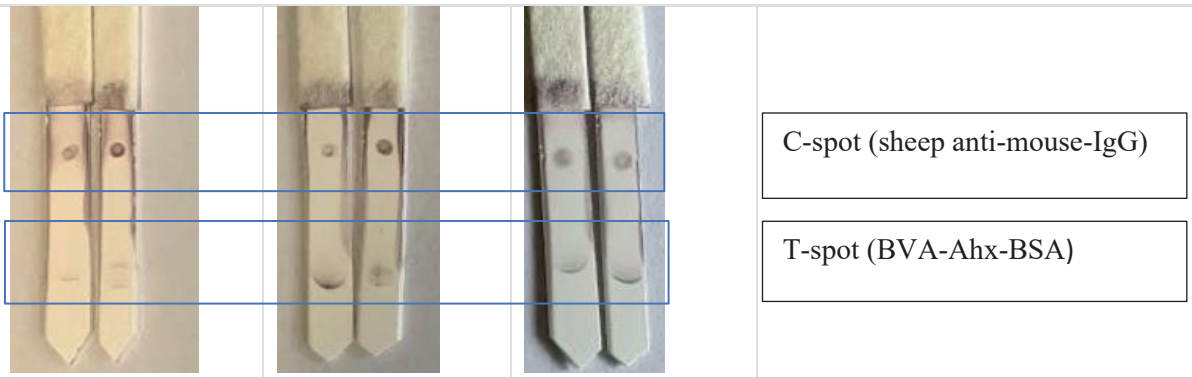

Figure S 9. Typical photograph of the Dot-LFIA strips

In this way, the color signal of GNPs can be enhanced since the most suitable nitrocellulose membrane is chosen for the following spotting process. The membrane assay provided an intense signal even with 1 OD GNP concentration, as demonstrated in **Table S 10.**

NC membrane Merck Millipore	Images of single spots	IgG–GNP with OD 20 10 2 1	NC membrane Merck Millipore	Images of single spots	IgG–GNP with OD 20 10 2 1
K15261	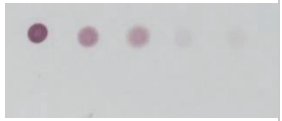	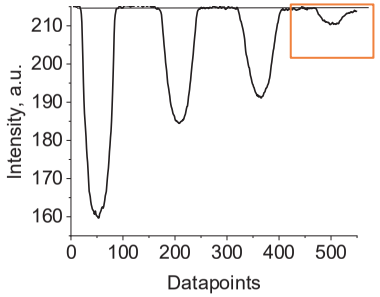	K15383		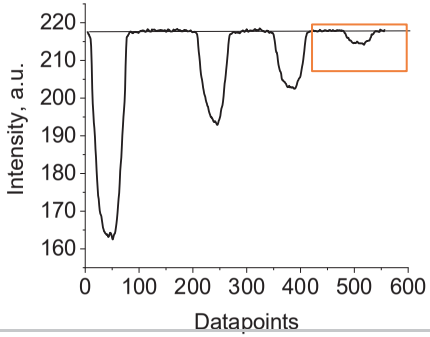
K15112		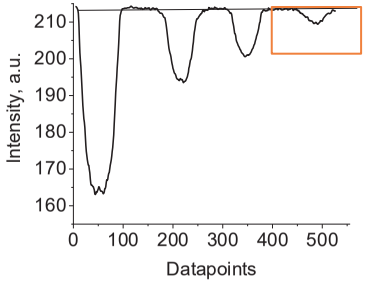	K15331		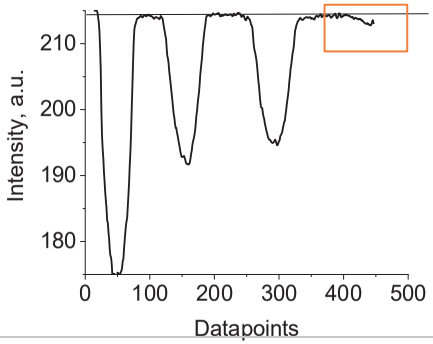

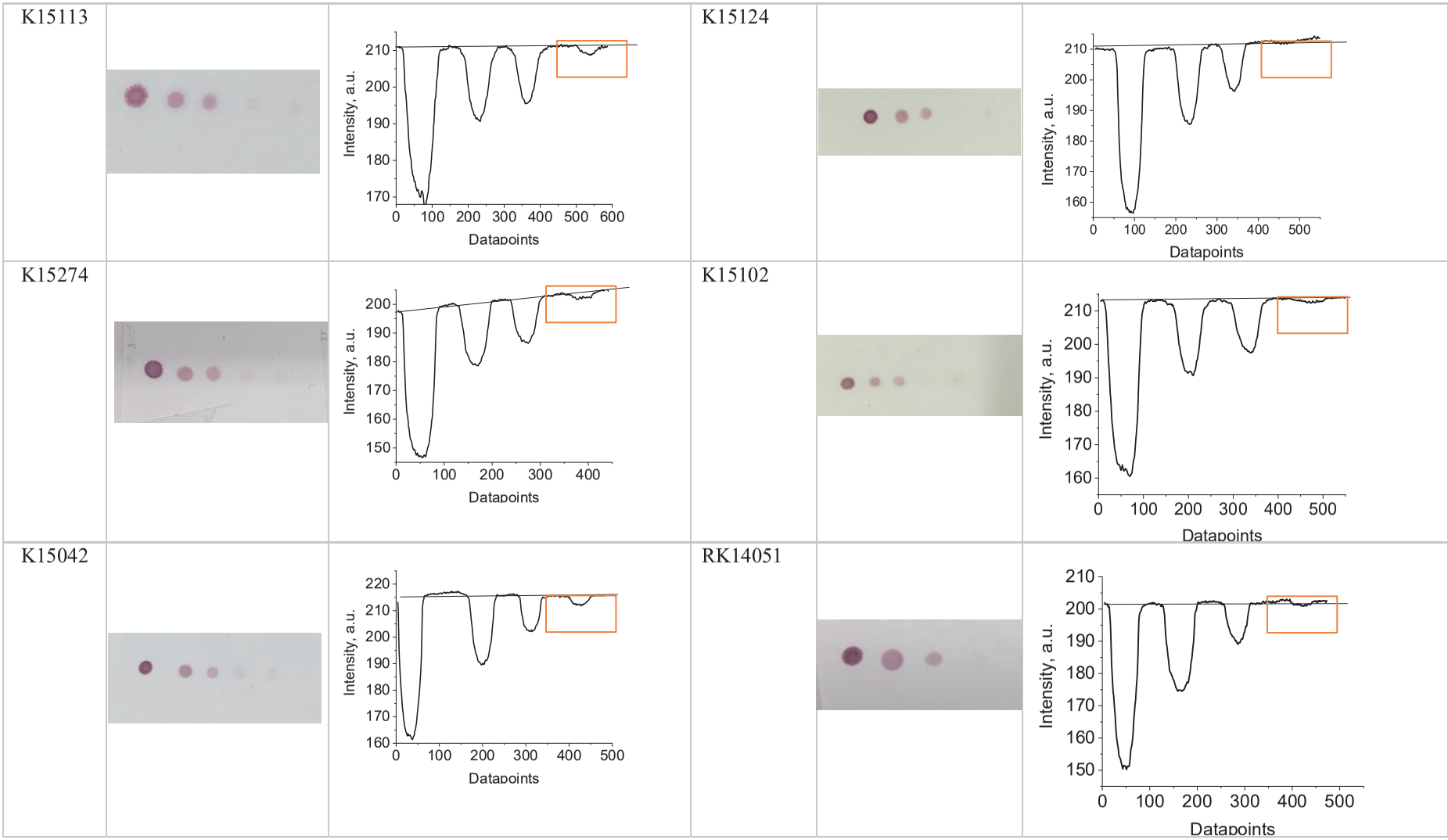

Figure S 10. Typical photographic image and reflective density profile of the detection area. Visible test bands were scanned and transformed into a densitogram using ImageJ free image processing software (ImageJ, National Institute of Health; Bethesda, Maryland, USA) [170, 171].

Table S 2. The specific interaction of the antibody-latex microparticles (IgG-LMP) and antibody-gold nanoparticles (IgG-GNP) probe on different types of membranes.

Membrane type	**Microphoto images of interaction with anti-BPA mouse IgG – particles and coating conjugate BVA-Ahx-BSA**	
Merck Millipore	**Microphoto images of single spot (IgG-GNP)**	**Microphoto images of line created by spotting several spots (IgG-GNP)**
K15261		
K15112	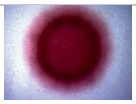	
K15113	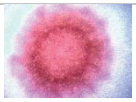	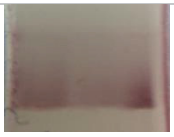
K15274		
K15042	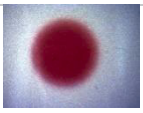	
RK14051	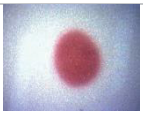	
K15383	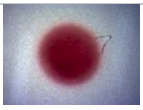	
K15331	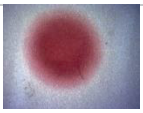	
K15124		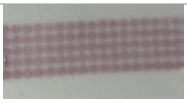
K15102	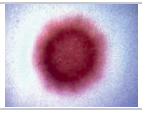	

MDI Membrane Technologies	Single spot IgG-GNP	IgG-GNP	IgG-LMP
15 µm CNPC-SS12-L2-P25	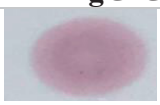		
12 µm CNPF-SN12-L2-P25	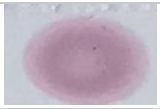		
10 µm CNPC-SS12-L2-P25	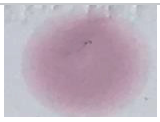		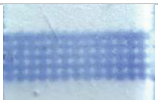
8 µm CNPF-SN12-L2-P25	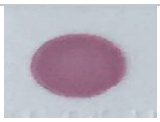		
200 CNPH-N-SS60-L2-P25	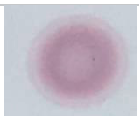		
150 CNPH-N-SS40-L2-P25	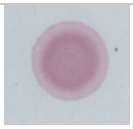	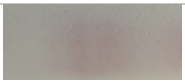	
90 CNPH-N-SS40-L2-P25	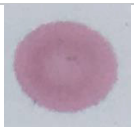		
70 CNPH-N-SS40-L2-P25	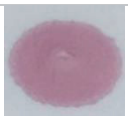		

Table S 3. Eight different methods tested to extract bisphenol A from the polycarbonate cube.

Method	Reference	Mass of the PC cube, g	Surface area of the PC cube, cm²	Measured concentration BPA, ng/ml (LC-MS)	Mass of BPA, ng	Mass of BPA per g of PC cube, ng/g	Mass of BPA per surface area, ng/cm²
1	[95]	1.5	7.68	1.6	79	50.5	10.2
2	[153]	1.7	7.58	0.4	20	11.3	2.6
3	[154]	1.4	6.38	1.0	1000	696.6	156.7
4	[155]	1.4	6.4	10.1	10.12	7.1	1.5
5	[156]	1.6	6.74	1.6	160	98.2	23.7
6	[157]	1.4	5.98	1.1	112	78.4	18.7
7	[158]	1.8	8.96	1.5	151	80.5	16.8
8	[159]	1.3	6.38	6.4	129	93.6	20.2

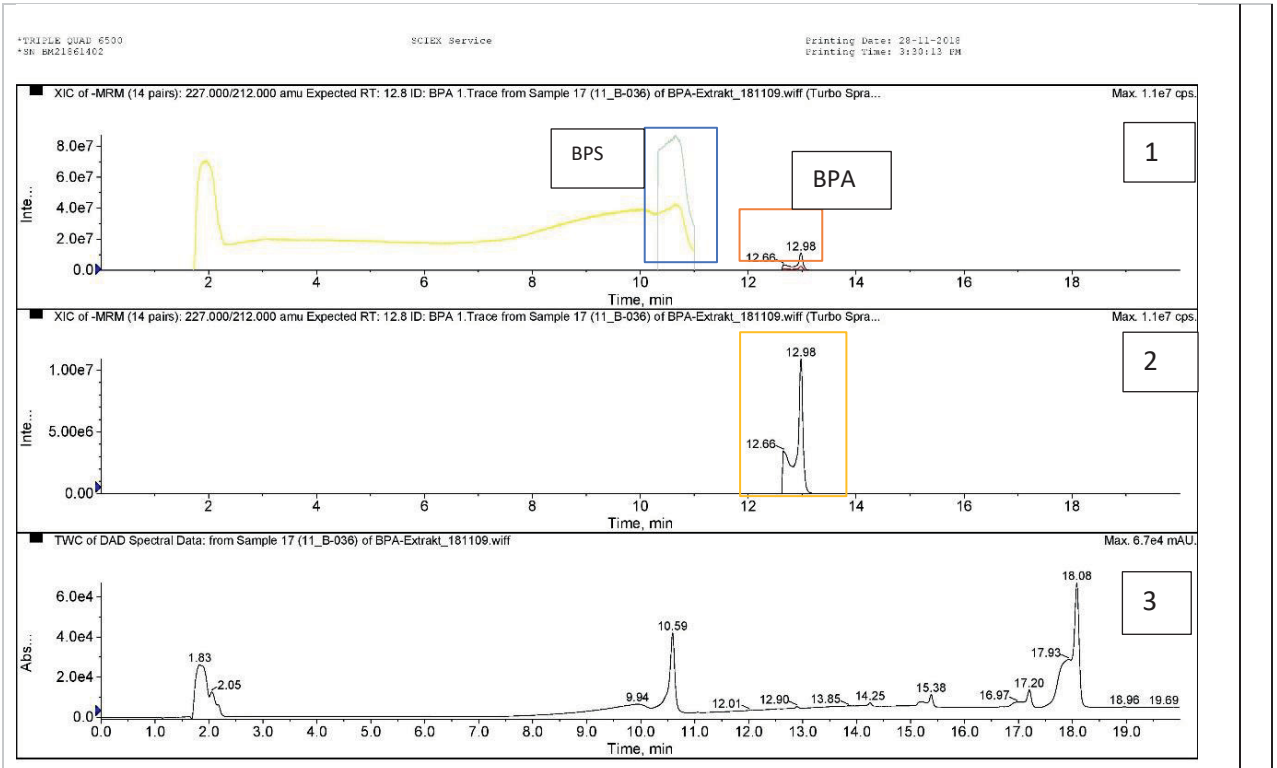

A. Thermal receipt paper BE [163]

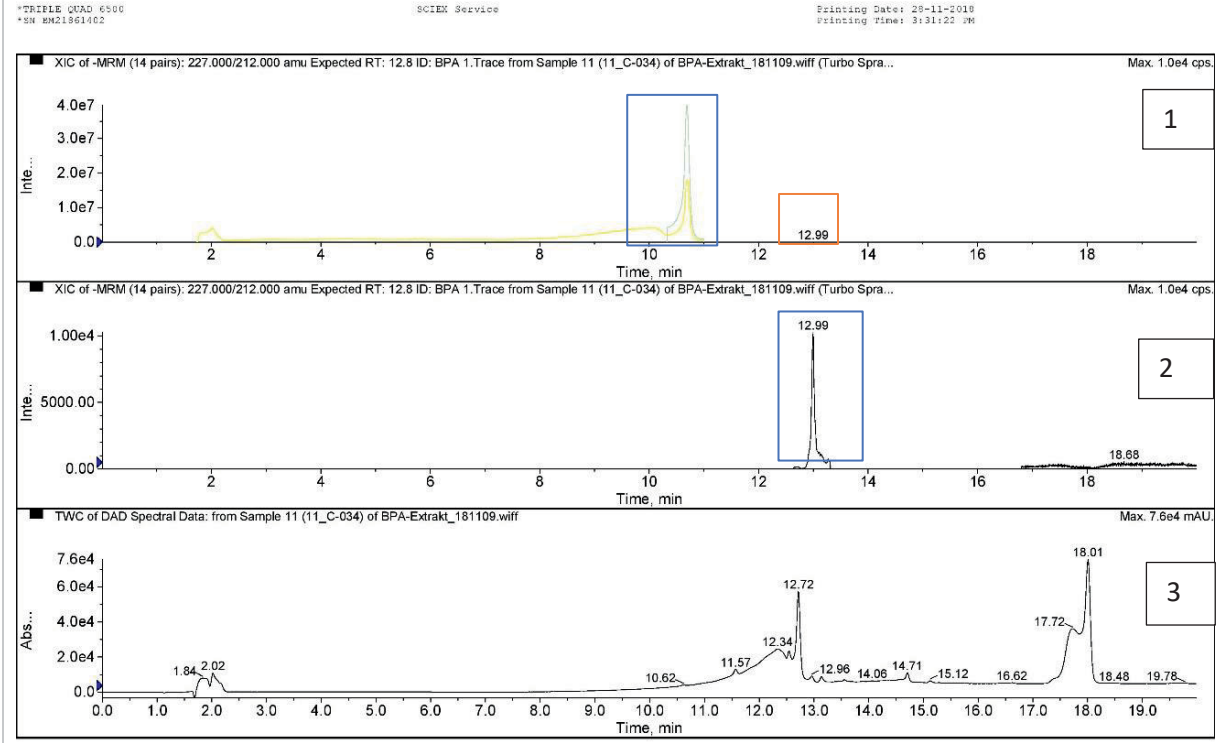

C. Thermal receipt paper DE [163]

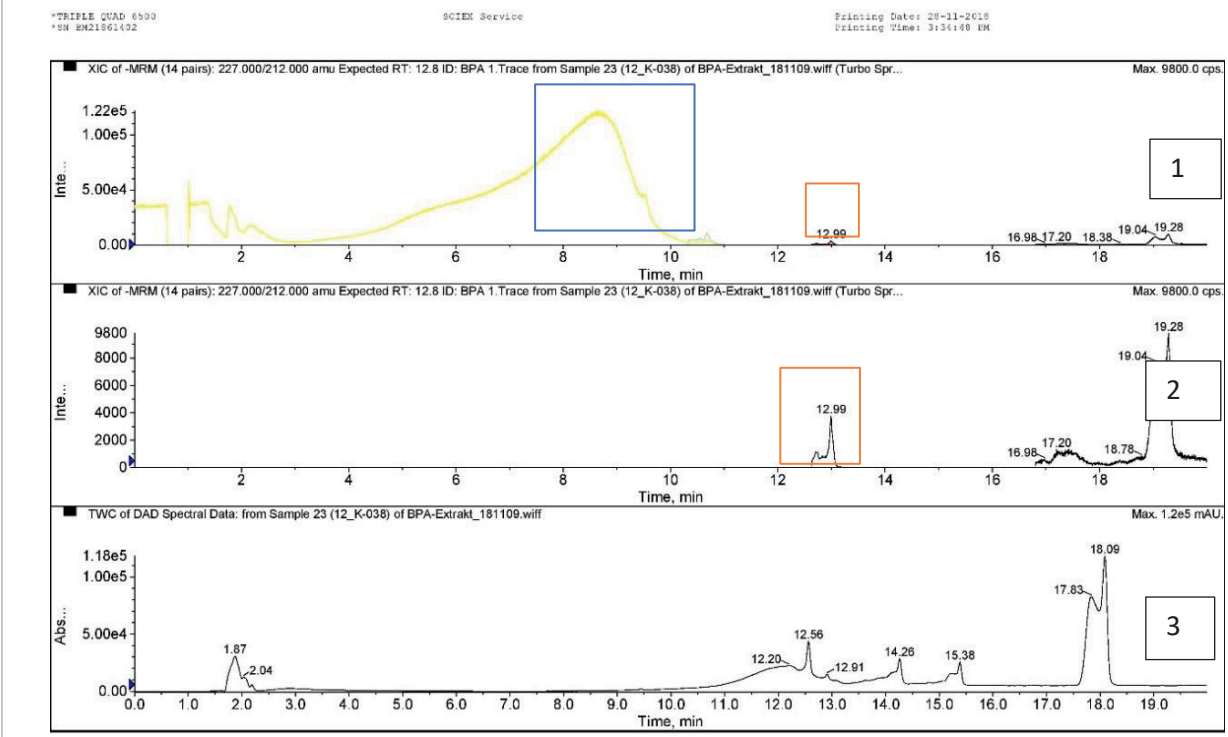

D. Thermal receipt paper RU

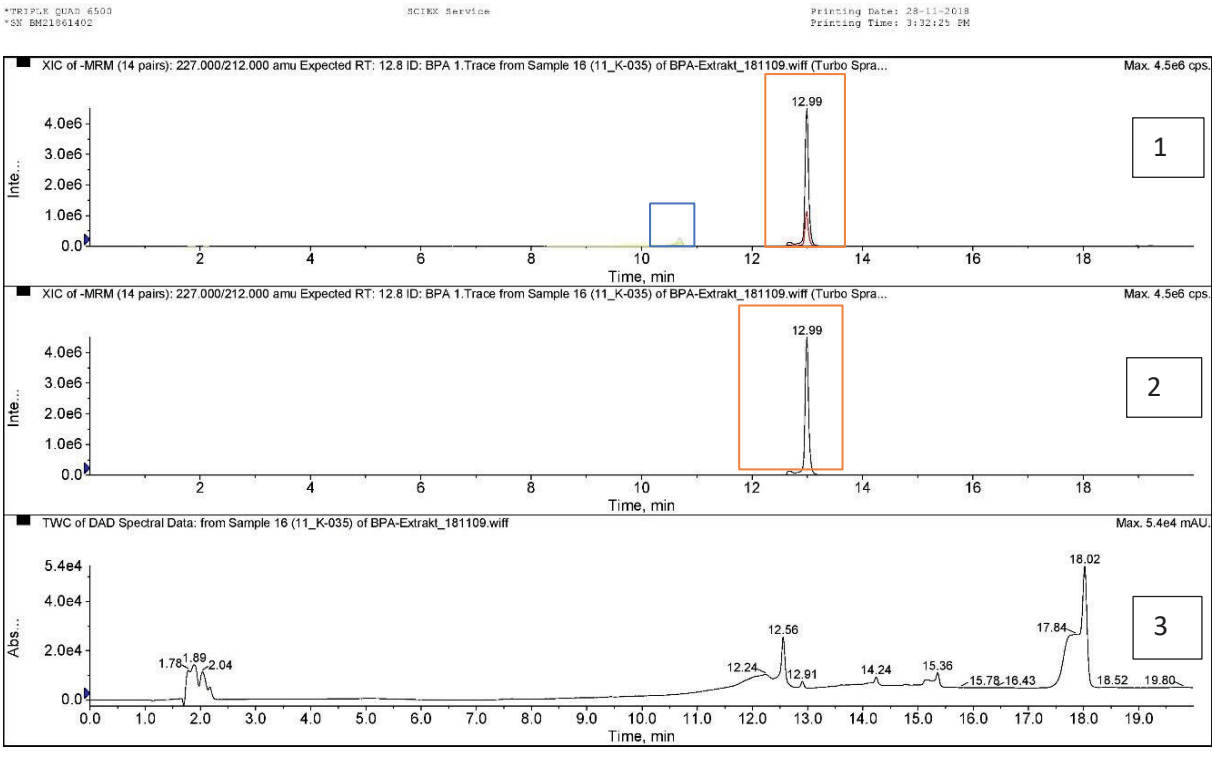

E. Flyer DE

Figure S 11. Chromatograms of BPA and BPS 1. XIC (extracted ion chromatogram) showing the peak of the desired BPA at 12.99 and BPS at 10.47 min. 2. XIC (extracted ion chromatogram) showing the peak of the desired BPA at 12.99. 4. HPLC chromatogram, DAD trace, showing a signal at RT = 12.56.

LIST OF FIGURES

LIST OF TABLES

REFERENCES

1. Almeida, S.; Raposo, A.; Almeida-González, M.; Carrascosa, C., Bisphenol A: Food exposure and impact on human health. *Comprehensive reviews in food science and food safety* **2018,** *17* (6), 1503-1517.
2. EFSA CEF Panel (EFSA Panel on Food Contact Materials, E., Flavourings and Processing Aids), Scientific Opinion on the risks to public health related to the presence of bisphenol A (BPA) in foodstuffs: Part I – Exposure assessment. *EFSA Journal 2015, 13.* **2015**.
3. Biedermann, S.; Tschudin, P.; Grob, K., Transfer of bisphenol A from thermal printer paper to the skin. *Analytical and Bioanalytical Chemistry* **2010,** *398* (1), 571-576.
4. Rykowska, I.; Wasiak, W., Properties, threats, and methods of analysis of bisphenol A and its derivatives. *Acta chromatographica* **2006,** *16*, 7.
5. Mehr, M. Y.; van Driel, W. D.; Jansen, K. M. B.; Deeben, P.; Zhang, G. Q., Lifetime assessment of Bisphenol-A Polycarbonate (BPA-PC) plastic lens, used in LED-based products. *Microelectronics Reliability* **2014,** *54* (1), 138-142.
6. Smith, M. E.; Ishida, H., Chromatographic Analysis of Oligomer Structures during the Copolymerization of Epoxy with Bisphenol-A. *Abstracts of Papers of the American Chemical Society* **1991,** *202*, 227-Poly.
7. Parker, R. E.; Isaacs, N. S., Mechanisms of Epoxide Reactions. *Chemical Reviews* **1959,** *59* (4), 737-799.
8. Okada, H.; Tokunaga, T.; Liu, X.; Takayanagi, S.; Matsushima, A.; Shimohigashi, Y., Direct evidence revealing structural elements essential for the high binding ability of bisphenol A to human estrogen-related receptor-γ. *Environmental health perspectives* **2008,** *116* (1), 32-38.
9. Acconcia, F.; Pallottini, V.; Marino, M., Molecular mechanisms of action of BPA. *Dose-response* **2015,** *13* (4).
10. Ben-Jonathan, N., Endocrine disrupting chemicals and breast cancer: The saga of Bisphenol A. *Estrogen Receptor and Breast Cancer* **2019**, 343-377.
11. Nagel, S. C.; Bromfield, J. J., Bisphenol A: A Model Endocrine Disrupting Chemical With a New Potential Mechanism of Action. *Endocrinology* **2013,** *154* (6), 1962-1964.
12. Rochester, J. R., Bisphenol A and human health: A review of the literature. *Reproductive Toxicology* **2013,** *42*, 132-155.
13. Munro, I. C.; Haighton, L. A.; Lynch, B. S.; Hlywka, J. J.; Doull, J.; Kroes, R., Response to "Does exposure to bisphenol A represent a human health risk?". *Regulatory Toxicology and Pharmacology* **2003,** *37* (3), 409-410.
14. Chemicals Management Plan of Canada, (2008) (Last accessed on November 30, 2017). https://www.canada.ca/en/healthcanada/.

15. European Commission. Commission Regulation (EU) 2018/832 of 12 February 2018 on the Use of Bisphenol A in Varnishes and Coatings Intended to Come into Contact with Food and Amending Regulation (EU) No 10/2011 as Regards the Use of That Substance in Plastic Food Contact Materials; Official Journal of the European Union: Brussels, Belgium, 2018; p. 7.

16. FAO/WHO Food and Agricultural Organization/World Health Organization, Expert Meeting to Review Toxicological and Health Aspects of Bisphenol A, (2011) Available from: http://www.who.int/foodsafety/publications/bisphenol-a/en/

(Last accessed on November 30, 2017).
17. FDA report, Draft Assessment of Bisphenol A for Use in Food Contact Applications, (2008) www.fda.gov

18. FDA Science Board Subcommittee on Bisphenol A, Scientific Peer-Review of the Draft Assessment of Bisphenol A for Use in Food Contact Applications, (2018) Available from: www.fda.gov.
19. Vandenberg, L. N.; Hauser, R.; Marcus, M.; Olea, N.; Welshons, W. V., Human exposure to bisphenol A (BPA). *Reproductive toxicology* **2007,** *24* (2), 139-177.
20. Watabe, Y.; Hosoya, K.; Tanaka, N.; Kondo, T.; Morita, M.; Kubo, T., LC/MS determination of bisphenol A in river water using a surface-modified molecularly-imprinted polymer as an on-line pretreatment device. *Analytical and Bioanalytical Chemistry* **2005,** *381* (6), 1193-1198.
21. Horie, M.; Yoshida, T.; Ishii, R.; Kobayashi, S.; Nakazawa, H., Determination of bisphenol A in canned drinks by LC MS. *Bunseki Kagaku* **1999,** *48* (6), 579-587.
22. Khedr, A., Optimized extraction method for LC-MS determination of bisphenol A, melamine and di(2-ethylhexyl) phthalate in selected soft drinks, syringes, and milk powder. *Journal of Chromatography B-Analytical Technologies in the Biomedical and Life Sciences* **2013,** *930*, 98-103.
23. Narasaki, H., Determination of bisphenol A in river-waters samples by LC/MS using solid-phase sorbents. *Bunseki Kagaku* **2002,** *51* (11), 1027-1035.
24. Volkel, W.; Bittner, N.; Dekant, W., Quantitation of bisphenol A and bisphenol A glucuronide in biological samples by high performance liquid chromatography-tandem mass spectrometry. *Drug Metabolism and Disposition* **2005,** *33* (11), 1748-1757.
25. Viñas, P.; Campillo, N.; Martínez-Castillo, N.; Hernández-Córdoba, M., Comparison of two derivatization-based methods for solid-phase microextraction–gas chromatography–mass spectrometric determination of bisphenol A, bisphenol S and biphenol migrated from food cans. *Analytical and Bioanalytical Chemistry* **2010,** *397* (1), 115-125.
26. Deceuninck, Y.; Bichon, E.; Marchand, P.; Boquien, C.-Y.; Legrand, A.; Boscher, C.; Antignac, J. P.; Le Bizec, B., Determination of bisphenol A and related substitutes/analogues in human breast milk using gas chromatography-tandem mass spectrometry. *Analytical and Bioanalytical Chemistry* **2015,** *407* (9), 2485-2497.
27. De Nys, S.; Putzeys, E.; Vervliet, P.; Covaci, A.; Boonen, I.; Elskens, M.; Vanoirbeek, J.; Godderis, L.; Van Meerbeek, B.; Van Landuyt, K. L.; Duca, R. C., A novel high sensitivity UPLC-MS/MS method for the evaluation of bisphenol A leaching from dental materials. *Scientific Reports* **2018,** *8* (1), 6981.
28. Vela-Soria, F.; Ballesteros, O.; Zafra-Gómez, A.; Ballesteros, L.; Navalón, A., UHPLC–MS/MS method for the determination of bisphenol A and its chlorinated derivatives, bisphenol S, parabens, and benzophenones in human urine samples. *Analytical and Bioanalytical Chemistry* **2014,** *406* (15), 3773-3785.
29. Xiao, Z.; Wang, R.; Suo, D.; Li, T.; Su, X., Trace analysis of bisphenol A and its analogues in eggs by ultra-performance liquid chromatography-tandem mass spectrometry. *Food Chemistry* **2020,** *327*, 126882.
30. Reyes-Gallardo, E. M.; Lucena, R.; Cardenas, S.; Valcarcel, M., Dispersive micro-solid phase extraction of bisphenol A from milk using magnetic nylon 6 composite and its final determination by HPLC-UV. *Microchemical Journal* **2016,** *124*, 751-756.
31. Wild, D., *The immunoassay handbook: theory and applications of ligand binding, ELISA and related techniques*. Newnes: 2013.

32. Vashist, S. K.; Luong, J. H., *Handbook of immunoassay technologies: approaches, performances, and applications*. Academic Press: 2018.
33. Elgert, K. D., Antibody structure and function. In *Immunology: Understanding The Immune System*, Wiley-Blackwell: 2009.
34. Arruebo, M.; Valladares, M.; Gonzalez-Fernandez, A., Antibody-Conjugated Nanoparticles for Biomedical Applications. *Journal of Nanomaterials* **2009**.
35. Dankwardt, A., Immunochemical assays in pesticide analysis. *Encyclopedia of Analytical Chemistry: Applications, Theory and Instrumentation* **2006**.
36. Hock, B.; Giersch, T.; Kramer, K.; Dankwardt, A., Antibody production and progress in hybridoma technology by immunomagnetic screening. **1995**.
37. Kohler, G.; Milstein, C., Continuous Cultures of Fused Cells Secreting Antibody of Predefined Specificity. *Nature* **1975,** *256* (5517), 495-497.
38. Littlefield, J. W., Selection of Hybrids from Matings of Fibroblasts in Vitro + Their Presumed Recombinants. *Science* **1964,** *145* (363), 709-&.
39. Littlefield, J. W.; Sarkar, P. F., Mouse Fibroblasts Partially Deficient in Thymidine Kinase. *Federation Proceedings* **1964,** *23* (2p1), 169-&.
40. Kim, Y. J.; Cho, Y. A.; Lee, H. S.; Lee, Y. T.; Gee, S. J.; Hammock, B. D., Synthesis of haptens for immunoassay of organophosphorus pesticides and effect of heterology in hapten spacer arm length on immunoassay sensitivity. *Analytica Chimica Acta* **2003,** *475* (1-2), 85-96.
41. Omi, K.; Ando, T.; Sakyu, T.; Shirakawa, T.; Uchida, Y.; Oka, A.; Ise, N.; Aoyagi, K.; Goishi, K., Noncompetitive immunoassay detection system for haptens on the basis of antimetatype antibodies. *Clinical chemistry* **2015,** *61* (4), 627-635.
42. Lan, X.; Zhu, L.; Xu, W., Novel immuno-nucleic acid cooperative detection technology for food safety. *Food and Agricultural Immunology* **2020,** *31* (1), 789-802.
43. Hage, D. S., Immunoassays. *Anal Chem* **1999,** *71* (12), 294R-304R.
44. Dandliker, W. B.; Feigen, G. A., Quantification of the antigen-antibody reaction by the polarization of fluorescence. *Biochem Biophys Res Commun* **1961,** *5*, 299-304.
45. Oberleitner, L.; Grandke, J.; Mallwitz, F.; Resch-Genger, U.; Garbe, L. A.; Schneider, R. J., Fluorescence polarization immunoassays for the quantification of caffeine in beverages. *J Agric Food Chem* **2014,** *62* (11), 2337-2343.
46. Beloglazova, N. V.; Eremin, S. A., Rapid screening of aflatoxin B1 in beer by fluorescence polarization immunoassay. *Talanta* **2015,** *142*, 170-175.
47. Dandliker, W. B.; Kelly, R. J.; Dandliker, J.; Farquahar, J.; Levin, J., Fluorescence polarization immunoassay. Theory and experimental method. *Immunochemistry* **1973,** *10* (4), 219-227.
48. Jameson, D. M.; Ross, J. A., Fluorescence polarization/anisotropy in diagnostics and imaging. *Chemical reviews* **2010,** *110* (5), 2685-2708.
49. Oberleitner, L.; Dahmen-Levison, U.; Garbe, L. A.; Schneider, R. J., Improved strategies for selection and characterization of new monoclonal anti-carbamazepine antibodies during the screening process using feces and fluorescence polarization immunoassay. *Analytical Methods* **2016,** *8* (38), 6883-6894.
50. Oberleitner, L.; Eremin, S. A.; Lehmann, A.; Garbe, L. A.; Schneider, R. J., Fluorescence polarization immunoassays for carbamazepine - comparison of tracers and formats. *Analytical Methods* **2015,** *7* (14), 5854-5861.
51. Leuvering, J. H. W.; Thal, P. J. H. M., Colloidal Gold Particles Coated with Monoclonal-Antibodies - Preparation and Shelf-Life. *Ultramicroscopy* **1984,** *14* (4), 412-413.

52. Mabey, D.; Peeling, R. W.; Ustianowski, A.; Perkins, M. D., Diagnostics for the developing world. *Nat Rev Microbiol* **2004,** *2* (3), 231-240.
53. Law, J. W. F.; Ab Mutalib, N. S.; Chan, K. G.; Lee, L. H., Rapid methods for the detection of foodborne bacterial pathogens: principles, applications, advantages and limitations. *Frontiers in Microbiology* **2015,** *5*.
54. Eltzov, E.; Guttel, S.; Kei, A. L. Y.; Sinawang, P. D.; Ionescu, R. E.; Marks, R. S., Lateral Flow Immunoassays - from Paper Strip to Smartphone Technology. *Electroanalysis* **2015,** *27* (9), 2116-2130.
55. Wild, D., *The immunoassay handbook : theory and applications of ligand binding, ELISA, and related techniques*. 4th ed.; Elsevier: Oxford ; Waltham, MA, 2013; p xxi, 1013 p.
56. Wong, R. C.; Tse, H. Y., *Lateral flow immunoassay*. Springer: New York, NY, 2009; p xii, 223 p.
57. Guler, E.; Sengel, T. Y.; Gumus, Z. P.; Arslan, M.; Coskunol, H.; Timur, S.; Yagci, Y., Mobile Phone Sensing of Cocaine in a Lateral Flow Assay Combined with a Biomimetic Material. *Analytical Chemistry* **2017,** *89* (18), 9629-9632.
58. Hsieh, H. V.; Dantzler, J. L.; Weigl, B. H., Analytical Tools to Improve Optimization Procedures for Lateral Flow Assays. *Diagnostics* **2017,** *7* (2).
59. Houghton, R. L.; Reed, D. E.; Hubbard, M. A.; Dillon, M. J.; Chen, H. J.; Currie, B. J.; Mayo, M.; Sarovich, D. S.; Theobald, V.; Limmathurotsakul, D.; Wongsuvan, G.; Chantratita, N.; Peacock, S. J.; Hoffmaster, A. R.; Duval, B.; Brett, P. J.; Burtnick, M. N.; AuCoin, D. P., Development of a Prototype Lateral Flow Immunoassay (LFI) for the Rapid Diagnosis of Melioidosis. *Plos Neglected Tropical Diseases* **2014,** *8* (3).
60. Moon, J.; Kim, G.; Lee, S., A Gold Nanoparticle and Aflatoxin B1-BSA Conjugates Based Lateral Flow Assay Method for the Analysis of Aflatoxin B1. *Materials* **2012,** *5* (4), 634-643.
61. Li, B.; Shao, W.; Wang, Y.; Xiao, D.; Li, C.; Kan, C., Facile synthesis and characterization of covalently colored polyurethane latex based on the chain extension of water-soluble dye monomer. *Progress in Organic Coatings* **2019,** *129*, 140-146.
62. Millipore, Rapid Lateral Flow Test Strips: Considerations for Project Development. **2008:**, 1-39.
63. Mansfield, Michael A., The Use of Nitrocellulose Membranes in Lateral-Flow Assays. *Wong R.C., Tse H.Y. (eds) Drugs of Abuse. Forensic Science and Medicine. Humana Press* **2005,** *20* 71-85.
64. Bahadir, E. B.; Sezginturk, M. K., Lateral flow assays: Principles, designs and labels. *Trac-Trends in Analytical Chemistry* **2016,** *82*, 286-306.
65. O'Farrell, Brendan., Lateral Flow Technology for Field-Based Applications-Basics and Advanced Developments. *Top Companion Anim Med* **2015,** *30* (4), 139-147.
66. Ye, H. H.; Xia, X. H., Enhancing the sensitivity of colorimetric lateral flow assay (CLFA) through signal amplification techniques. *Journal of Materials Chemistry B* **2018,** *6* (44), 7102-7111.
67. Banerjee, R.; Jaiswal, A., Recent advances in nanoparticle-based lateral flow immunoassay as a point-of-care diagnostic tool for infectious agents and diseases. *Analyst* **2018,** *143* (9), 1970-1996.
68. Posthuma-Trumpie, G. A.; Korf, J.; van Amerongen, A., Lateral flow (immuno) assay: its strengths, weaknesses, opportunities and threats. A literature survey. *Analytical and Bioanalytical Chemistry* **2009,** *393* (2), 569-582.

69. Wang, C.; Li, X. M.; Peng, T.; Wang, Z. H.; Wen, K.; Jiang, H. Y., Latex bead and colloidal gold applied in a multiplex immunochromatographic assay for high-throughput detection of three classes of antibiotic residues in milk. *Food Control* **2017,** *77*, 1-7.
70. Zhu, M. S.; Jia, Y. R.; Peng, L. Z.; Ma, J. F.; Li, X. R.; Shi, F., A highly sensitive dual-color lateral flow immunoassay for brucellosis using one-step synthesized latex microspheres. *Analytical Methods* **2019,** *11* (22), 2937-2942.
71. Vashist, S. K., Comparison of 1-Ethyl-3-(3-Dimethylaminopropyl) Carbodiimide Based Strategies to Crosslink Antibodies on Amine-Functionalized Platforms for Immunodiagnostic Applications. *Diagnostics (Basel)* **2012,** *2* (3), 23-33.
72. Hermanson, G. T., Bioconjugate Techniques, 3rd Edition. *Bioconjugate Techniques, 3rd Edition* **2013**, 1-1146.
73. Di Nardo, F.; Cavalera, S.; Baggiani, C.; Giovannoli, C.; Anfossi, L., Direct vs Mediated Coupling of Antibodies to Gold Nanoparticles: The Case of Salivary Cortisol Detection by Lateral Flow Immunoassay. *Acs Applied Materials & Interfaces* **2019,** *11* (36), 32758-32768.
74. Cvak, B.; Pum, D.; Molinelli, A.; Krska, R., Synthesis and characterization of colloidal gold particles as labels for antibodies as used in lateral flow devices. *Analyst* **2012,** *137* (8), 1882-1887.
75. Gwyn, S.; Mitchell, A.; Dean, D.; Mkocha, H.; Handali, S.; Martin, D. L., Lateral flow-based antibody testing for Chlamydia trachomatis. *Journal of Immunological Methods* **2016,** *435*, 27-31.
76. Damborsky, P.; Koczula, K. M.; Gallotta, A.; Katrlik, J., Lectin-based lateral flow assay: proof-of-concept. *Analyst* **2016,** *141* (23), 6444-6448.
77. Mthembu, C. L.; Sabela, M. I.; Mlambo, M.; Madikizela, L. M.; Kanchi, S.; Gumede, H.; Mdluli, P. S., Google Analytics and quick response for advancement of gold nanoparticle-based dual lateral flow immunoassay for malaria - Plasmodium lactate dehydrogenase (pLDH). *Analytical Methods* **2017,** *9* (41), 5943-5951.
78. Maiolini, E.; Ferri, E.; Pitasi, A. L.; Montoya, A.; Di Giovanni, M.; Errani, E.; Girotti, S., Bisphenol A determination in baby bottles by chemiluminescence enzyme-linked immunosorbent assay, lateral flow immunoassay and liquid chromatography tandem mass spectrometry. *Analyst* **2014,** *139* (1), 318-324.
79. Mei, Z.; Qu, W.; Deng, Y.; Chu, H.; Cao, J.; Xue, F.; Zheng, L.; El-Nezamic, H. S.; Wu, Y.; Chen, W., One-step signal amplified lateral flow strip biosensor for ultrasensitive and on-site detection of bisphenol A (BPA) in aqueous samples. *Biosens Bioelectron* **2013,** *49*, 457-461.
80. Dudley, R. A.; Edwards, P.; Ekins, R. P.; Finney, D. J.; McKenzie, I. G.; Raab, G. M.; Rodbard, D.; Rodgers, R. P., Guidelines for immunoassay data processing. *Clin Chem* **1985,** *31* (8), 1264-1271.
81. Andreasson, U.; Perret-Liaudet, A.; van Doorn, L. J. C. V.; Blennow, K.; Chiasserini, D.; Engelborghs, S.; Fladby, T.; Genc, S.; Kruse, N.; Kuipenj, H. B.; Kulic, L.; Lewczuk, P.; Mollenhauer, B.; Mroczko, B.; Pametti, L.; Vanmechelen, E.; Verbeek, M. M.; Winblad, B.; Zetterberg, H.; Koel-Simmelink, M.; Teunissen, C. E., A practical guide to immunoassay method validation. *Frontiers in Neurology* **2015,** *6*.
82. Winklmair, M., Weller, M.G., Mangler, J., Schlosshauer, B., und Niessner, R.,, Development of a highly sensitive enzyme-immunoassay for the determination of triazine herbicides. *Fresenius J Anal Chem* **1997,** *2* (358), 614-622.

83. Weller, M. G.; Schuetz, A. J.; Winklmair, M.; Niessner, R., Highly parallel affinity sensor for the detection of environmental contaminants in water1. *Analytica Chimica Acta* **1999,** *393* (1–3), 29-41.
84. Grandke, J.; Oberleitner, L.; Resch-Genger, U.; Garbe, L. A.; Schneider, R. J., Quality assurance in immunoassay performance--comparison of different enzyme immunoassays for the determination of caffeine in consumer products. *Anal Bioanal Chem* **2013,** *405* (5), 1601-1611.
85. Ekins, R. P., The precision profile: its use in RIA assessment and design. *Ligand Quarter* **1981,** *4*, 33–44.
86. Hoffmann, H.; Baldofski, S.; Hoffmann, K.; Flemig, S.; Silva, C. P.; Esteves, V. I.; Emmerling, F.; Panne, U.; Schneider, R. J., Structural considerations on the selectivity of an immunoassay for sulfamethoxazole. *Talanta* **2016,** *158*, 198-207.
87. Geiß, S.; Einax, J., Comparison of detection limits in environmental analysis–is it possible? An approach on quality assurance in the lower working range by verification. *Fresenius' journal of analytical chemistry* **2001,** *370* (6), 673-678.
88. Shrivastava, A.; Gupta, V., Methods for the determination of limit of detection and limit of quantitation of the analytical methods. *Chronicles of young scientists* **2011,** *2* (1), 21-21.
89. Connolly, R.; O'Kennedy, R., Magnetic lateral flow immunoassay test strip development - Considerations for proof of concept evaluation. *Methods* **2017,** *116*, 132-140.
90. Meulenberg, E. P., *Antibodies Applications and New Developments*. Bentham Science Publishers: 2012.
91. Gosling, J. P., Standardization of Immunoassays for Hapten Analytes. *Scandinavian Journal of Clinical & Laboratory Investigation* **1991,** *51*, 95-104.
92. Bergeron, S.; Laforte, V.; Lo, P.-S.; Li, H.; Juncker, D., Evaluating mixtures of 14 hygroscopic additives to improve antibody microarray performance. *Analytical and bioanalytical chemistry* **2015,** *407* (28), 8451-8462.
93. Feng, Y.; Ning, B.; Su, P.; Wang, H.; Wang, C.; Chen, F.; Gao, Z., An immunoassay for bisphenol A based on direct hapten conjugation to the polystyrene surface of microtiter plates. *Talanta* **2009,** *80* (2), 803-808.
94. Lu, Y.; Peterson, J. R.; Gooding, J. J.; Lee, N. A., Development of sensitive direct and indirect enzyme-linked immunosorbent assays (ELISAs) for monitoring bisphenol-A in canned foods and beverages. *Anal Bioanal Chem* **2012,** *403* (6), 1607-1618.
95. Manclus, J. J.; Moreno, M. J.; Montoya, A., Validation of an immunoassay for fast screening of bisphenol A in canned vegetables. *Analytical Methods* **2013,** *5* (16), 4244-4251.
96. Moreno, M. J.; D'Arienzo, P.; Manclus, J. J.; Montoya, A., Development of monoclonal antibody-based immunoassays for the analysis of bisphenol A in canned vegetables. *J Environ Sci Health B* **2011,** *46* (6), 509-517.
97. Yang, F. F.; Xu, L.; Zhu, L. X.; Zhang, Y.; Meng, W.; Liu, R. R., Competitive immunoassay for analysis of bisphenol A in children's sera using a specific antibody. *Environmental Science and Pollution Research* **2016,** *23* (11), 10714-10721.
98. Peng, C. F.; Pan, N.; Xie, Z. J.; Liu, L. Q.; Xiang, J.; Liu, C. L., Determination of Bisphenol A by a Gold Nanoflower Enhanced Enzyme-Linked Immunosorbent Assay. *Analytical Letters* **2016,** *49* (10), 1492-1501.
99. Huang, P.; Zhao, S.; Eremin, S. A.; Zheng, S.; Lai, D.; Chen, Y.; Guo, B., A fluorescence polarization immunoassay method for detection of the bisphenol A residue

in environmental water samples based on a monoclonal antibody and 4′-(aminomethyl)fluorescein. *Anal. Methods* **2015,** *7* (10), 4246-4251.
100. Wu, X.; Wang, L.; Ma, W.; Zhu, Y.; Xu, L.; Kuang, H.; Xu, C., A simple, sensitive, rapid and specific detection method for Bisphenol A based on Fluorescence Polarization Immunoassay. *Immunol Invest* **2012,** *41* (1), 38-50.
101. Zhang, J.; Zhao, S. Q.; Zhang, K.; Zhou, J. Q., Cd-doped ZnO quantum dots-based immunoassay for the quantitative determination of bisphenol A. *Chemosphere* **2014,** *95*, 105-110.
102. Peng, X. Y.; Kang, L. C.; Pang, F. Q.; Li, H. M.; Luo, R. F.; Luo, X. L.; Sun, F. X., A signal-enhanced lateral flow strip biosensor for ultrasensitive and on-site detection of bisphenol A. *Food and Agricultural Immunology* **2018,** *29* (1), 216-227.
103. Sheng, W.; Liu, Y.; Li, S. J.; Lu, Y.; Chang, Q.; Zhang, Y.; Wang, S., Lateral Flow Quantum-Dot-Based Immunochromatographic Assay and Fluorescence Quenching Immunochromatographic Assay with Quantum Dots as Fluorescence Donors to Visually Detect Bisphenol A in Food and Water Samples. *Food Analytical Methods* **2018,** *11* (3), 675-685.
104. Lin, L. K.; Uzunoglu, A.; Stanciu, L. A., Aminolated and Thiolated PEG-Covered Gold Nanoparticles with High Stability and Antiaggregation for Lateral Flow Detection of Bisphenol A. *Small* **2018,** *14* (10).
105. Lin, L. K.; Huang, P. Y.; Dutta, S.; Rochet, J. C.; Stanciu, L. A., Tuning a Bisphenol A Lateral Flow Assay Using Multiple Gold Nanosystems. *Particle & Particle Systems Characterization* **2019,** *36* (7).
106. Zhang, H. Y.; Yang, S. P.; De Ruyck, K.; Beloglazova, N. V.; Eremin, S. A.; De Saeger, S.; Zhang, S. X.; Shen, J. Z.; Wang, Z. H., Fluorescence polarization assays for chemical contaminants in food and environmental analyses. *Trac-Trends in Analytical Chemistry* **2019,** *114*, 293-313.
107. Jiang, X. M.; Li, X. M.; Yang, Z.; Eremin, S. A.; Zhang, X. Y., Evaluation and Optimization of Three Different Immunoassays for Rapid Detection Zearalenone in Fodders. *Food Analytical Methods* **2017,** *10* (1), 256-262.
108. Ediage, E. N.; Di Mavungu, J. D.; Goryacheva, I. Y.; Van Peteghem, C.; De Saeger, S., Multiplex flow-through immunoassay formats for screening of mycotoxins in a variety of food matrices. *Analytical and Bioanalytical Chemistry* **2012,** *403* (1), 265-278.
109. Ramachandran, S.; Singhal, M.; McKenzie, K. G.; Osborn, J. L.; Arjyal, A.; Dongol, S.; Baker, S. G.; Basnyat, B.; Farrar, J.; Dolecek, C.; Domingo, G. J.; Yager, P.; Lutz, B., A Rapid, Multiplexed, High-Throughput Flow-Through Membrane Immunoassay: A Convenient Alternative to ELISA. *Diagnostics (Basel)* **2013,** *3* (2), 244-260.
110. Burmistrova, N. A.; Rusanova, T. Y.; Yurasov, N. A.; Goryacheva, I. Y.; De Saeger, S., Multi-detection of mycotoxins by membrane based flow-through immunoassay. *Food Control* **2014,** *46*, 462-469.
111. Xu, Z.; Xu, L. G.; Zhu, Y. Y.; Ma, W.; Kuang, H.; Wang, L. B.; Xu, C. L., Chirality based sensor for bisphenol A detection. *Chemical Communications* **2012,** *48* (46), 5760-5762.
112. Zhou, J. Q.; Zhao, S. Q.; Zhang, J.; Zhang, L.; Cai, Y. F.; Zhou, L. H., An indirect competitive enzyme-linked immunosorbent assay for bisphenol-A based on the synthesis of a poly-L-lysine-hapten conjugate as a coating antigen. *Analytical Methods* **2013,** *5* (6), 1570-1576.

113. Mercader, J. V.; Agullo, C.; Abad-Somovilla, A.; Abad-Fuentes, A., A Monoclonal Antibody-Based Immunoassay for Mepanipyrim Residue Sensitive Analysis in Grape Juice and Wine. *Food Analytical Methods* **2020,** *13* (3), 770-779.
114. Schmidt, S.; Hanelt, S.; Canitz, C.; Hoffmann, H.; Garbe, L. A.; Schneider, R. J., Synthetic Strategies for the Modification of Diclofenac. *Synlett* **2017,** *28* (15), 1984-1989.
115. M.M., B., A rapid and sensitive method for the quantitation of microgram quantities of protein utilizing the principle of protein-dye binding. *Anal. Biochem* **1976,** *72*, 248–254.
116. Boroduleva, A. Y.; Manclus, J. J.; Montoya, A.; Eremin, S. A., Fluorescence polarization immunoassay for rapid screening of the pesticides thiabendazole and tetraconazole in wheat. *Analytical and Bioanalytical Chemistry* **2018,** *410* (26), 6923-6934.
117. Di Pasqua, A. J.; Mishler, R. E.; Ship, Y. L.; Dabrowiak, J. C.; Asefa, T., Preparation of antibody-conjugated gold nanoparticles. *Materials Letters* **2009,** *63* (21), 1876-1879.
118. Liu, E. Y.; Jung, S.; Yi, H. M., Improved Protein Conjugation with Uniform, Macroporous Poly(acrylamide-co-acrylic acid) Hydrogel Microspheres via EDC/NHS Chemistry. *Langmuir* **2016,** *32* (42), 11043-11054.
119. Sastre, P.; Gallardo, C.; Monedero, A.; Ruiz, T.; Arias, M.; Sanz, A.; Rueda, P., Development of a novel lateral flow assay for detection of African swine fever in blood. *Bmc Veterinary Research* **2016,** *12*.
120. Koniev, O.; Wagner, A., Developments and recent advancements in the field of endogenous amino acid selective bond forming reactions for bioconjugation (vol 44, pg 5495, 2015). *Chemical Society Reviews* **2015,** *44* (15), 5743-5743.
121. Holstein, C. A.; Chevalier, A.; Bennett, S.; Anderson, C. E.; Keniston, K.; Olsen, C.; Li, B.; Bales, B.; Moore, D. R.; Fu, E.; Baker, D.; Yager, P., Immobilizing affinity proteins to nitrocellulose: a toolbox for paper-based assay developers. *Analytical and Bioanalytical Chemistry* **2016,** *408* (5), 1335-1346.
122. Dias, T. M.; Fernandes, E.; Cardoso, S.; Monteiro, G.; Freitas, P. P., One-step trapping of droplets and surface functionalization of sensors using gold-patterned structures for multiplexing in biochips (vol 7, pg 43273, 2017). *Rsc Advances* **2017,** *7* (73), 46124-46124.
123. Urusov, A. E.; Zherdev, A. V.; Dzantiev, B. B., Towards lateral flow quantitative assays: detection approaches. *Biosensors* **2019,** *9* (3), 89.
124. Nečas, D.; Klapetek, P., Gwyddion: an open-source software for SPM data analysis. *Open Physics* **2012,** *10* (1), 181-188.
125. Balázs, B.; Szalay, T.; Takács, M. In *Investigation of micro milled surface characteristics*, Proceedings of International Conference on Innovative Technologies, 2017; pp 161-164.
126. Wu, X.; Wang, L.; Ma, W.; Zhu, Y.; Xu, L.; Kuang, H.; Xu, C., A simple, sensitive, rapid and specific detection method for bisphenol A based on fluorescence polarization immunoassay. *Immunological investigations* **2012,** *41* (1), 38-50.
127. Karir, T.; Samuel, G.; Kothari, K.; Sivaprasad, N.; Venkatesh, M., Studies on the influence of the structural modifications in the tracer on the immunoassay of progesterone. *Journal of Immunoassay & Immunochemistry* **2006,** *27* (2), 151-171.
128. Chen, J.; Shanin, I. A.; Lv, S.; Wang, Q.; Mao, C.; Xu, Z.; Sun, Y.; Wu, Q.; Eremin, S. A.; Lei, H., Heterologous strategy enhancing the sensitivity of the

fluorescence polarization immunoassay of clinafloxacin in goat milk. *J Sci Food Agric* **2016,** *96* (4), 1341-1346.
129. Smith, D. S.; Eremin, S. A., Fluorescence polarization immunoassays and related methods for simple, high-throughput screening of small molecules. *Analytical and bioanalytical chemistry* **2008,** *391* (5), 1499-1507.
130. Wang, Q. A.; Haughey, S. A.; Sun, Y. M.; Eremin, S. A.; Li, Z. F.; Liu, H.; Xu, Z. L.; Shen, Y. D.; Lei, H. T., Development of a fluorescence polarization immunoassay for the detection of melamine in milk and milk powder. *Analytical and Bioanalytical Chemistry* **2011,** *399* (6), 2275-2284.
131. Chen, Y. S.; Cui, X. P.; Wu, P. P.; Jiang, Z. Y.; Jiao, L. Y.; Hu, Q. Q.; Eremin, S. A.; Zhao, S. Q., Development of a Homologous Fluorescence Polarization Immunoassay for Diisobutyl Phthalate in Romaine Lettuce. *Food Analytical Methods* **2017,** *10* (2), 449-458.
132. Hoffmann, H.; Knizia, C.; Kuhne, M.; Panne, U.; Schneider, R. J., LC-ELISA as a contribution to the assessment of matrix effects with environmental water samples in an immunoassay for estrone (E1). *Accreditation and Quality Assurance* **2018,** *23* (6), 349-364.
133. Safenkova, I. V.; Zherdev, A. V.; Dzantiev, B. B., Factors influencing the detection limit of the lateral-flow sandwich immunoassay: a case study with potato virus X. *Analytical and Bioanalytical Chemistry* **2012,** *403* (6), 1595-1605.
134. Guo, Y. R.; Liu, S. Y.; Gui, W. J.; Zhu, G. N., Gold immunochromatographic assay for simultaneous detection of carbofuran and triazophos in water samples. *Analytical Biochemistry* **2009,** *389* (1), 32-39.
135. Bell, N. C.; Minelli, C.; Shard, A. G., Quantitation of IgG protein adsorption to gold nanoparticles using particle size measurement. *Analytical Methods* **2013,** *5* (18), 4591-4601.
136. Monopoli, M. P.; Walczyk, D.; Campbell, A.; Elia, G.; Lynch, I.; Bombelli, F. B.; Dawson, K. A., Physical-chemical aspects of protein corona: relevance to in vitro and in vivo biological impacts of nanoparticles. *J Am Chem Soc* **2011,** *133* (8), 2525-2534.
137. Bell, N. C.; Minelli, C.; Tompkins, J.; Stevens, M. M.; Shard, A. G., Emerging Techniques for Submicrometer Particle Sizing Applied to Stober Silica. *Langmuir* **2012,** *28* (29), 10860-10872.
138. Mansfield, M. A., The use of nitrocellulose membranes in lateral-flow assays. In *Drugs of abuse*, Springer: 2005; pp 71-85.
139. Laitinen, M. P. A.; Vuento, M., Affinity immunosensor for milk progesterone: Identification of critical parameters. *Biosensors & Bioelectronics* **1996,** *11* (12), 1207-1214.
140. Anfossi, L.; Di Nardo, F.; Cavalera, S.; Giovannoli, C.; Baggiani, C., Multiplex Lateral Flow Immunoassay: An Overview of Strategies towards High-throughput Point-of-Need Testing. *Biosensors-Basel* **2018,** *9* (1).
141. Le, T. T.; Chang, P. X.; Benton, D. J.; McCauley, J. W.; Iqbal, M.; Cass, A. E. G., Dual Recognition Element Lateral Flow Assay Toward Multiplex Strain Specific Influenza Virus Detection. *Analytical Chemistry* **2017,** *89* (12), 6781-6786.
142. Molinelli, A.; Grossalber, K.; Krska, R., A rapid lateral flow test for the determination of total type B fumonisins in maize. *Analytical and Bioanalytical Chemistry* **2009,** *395* (5), 1309-1316.

143. Shim, W. B.; Kim, J. S.; Kim, M. G.; Chung, D. H., Rapid and Sensitive Immunochromatographic Strip for On-site Detection of Sulfamethazine in Meats and Eggs. *Journal of Food Science* **2013,** *78* (10), M1575-M1581.
144. Sajid, M.; Kawde, A. N.; Daud, M., Designs, formats and applications of lateral flow assay: A literature review. *Journal of Saudi Chemical Society* **2015,** *19* (6), 689-705.
145. Wang, Z. H.; Mi, T. J.; Beier, R. C.; Zhang, H. Y.; Sheng, Y. J.; Shi, W. M.; Zhang, S. X.; Shen, J. Z., Hapten synthesis, monoclonal antibody production and development of a competitive indirect enzyme-linked immunosorbent assay for erythromycin in milk. *Food Chemistry* **2015,** *171*, 98-107.
146. Burkin, M. A.; Galvidis, I. A.; Eremin, S. A., Specific and Generic Immunorecognition of Glycopeptide Antibiotics Promoted by Unique and Multiple Orientations of Hapten. *Biosensors-Basel* **2019,** *9* (2).
147. Guo, L. L.; Liu, L. Q.; Cui, G.; Ma, S. F.; Wu, X. L.; Kuang, H., Gold immunochromatographic assay for kitasamycin and josamycin residues screening in milk and egg samples. *Food and Agricultural Immunology* **2019,** *30* (1), 1189-1201.
148. Xu, Z.-L.; Wang, Q.; Lei, H.-T.; Eremin, S. A.; Shen, Y.-D.; Wang, H.; Beier, R. C.; Yang, J.-Y.; Maksimova, K. A.; Sun, Y.-M., A simple, rapid and high-throughput fluorescence polarization immunoassay for simultaneous detection of organophosphorus pesticides in vegetable and environmental water samples. *Analytica chimica acta* **2011,** *708* (1-2), 123-129.
149. Kolosova, A. Y.; Park, J.-H.; Eremin, S. A.; Park, S.-J.; Kang, S.-J.; Shim, W.-B.; Lee, H.-S.; Lee, Y.-T.; Chung, D.-H., Comparative study of three immunoassays based on monoclonal antibodies for detection of the pesticide parathion-methyl in real samples. *Analytica Chimica Acta* **2004,** *511* (2), 323-331.
150. Lee, H.-B.; Peart, T. E., Bisphenol A contamination in Canadian municipal and industrial wastewater and sludge samples. *Water Quality Research Journal* **2000,** *35* (2), 283-298.
151. Zalko, D.; Jacques, C.; Duplan, H.; Bruel, S.; Perdu, E., Viable skin efficiently absorbs and metabolizes bisphenol A. *Chemosphere* **2011,** *82* (3), 424-430.
152. Kruger, T.; Long, M.; Bonefeld-Jorgensen, E. C., Plastic components affect the activation of the aryl hydrocarbon and the androgen receptor. *Toxicology* **2008,** *246* (2-3), 112-123.
153. Huang, H.; Feng, Z.; Li, Y.; Liu, Z.; Zhang, L.; Ma, Y.; Tong, J., Highly sensitive detection of bisphenol A in food packaging based on graphene quantum dots and peroxidase. *Analytical Methods* **2015,** *7* (7), 2928-2935.
154. Troiano, R.; Goodman, W., UHPLC Separation and Detection of Bisphenol A (BPA) in Plastics. *Lc Gc North America* **2009**, 56-56.
155. Lv, T.; Zhao, X. E.; Zhu, S. Y.; Qu, F.; Song, C. H.; You, J. M.; Suo, Y. R., Determination of bisphenol A, 4-octylphenol, and 4-nonylphenol in soft drinks and dairy products by ultrasound-assisted dispersive liquid-liquid microextraction combined with derivatization and high-performance liquid chromatography with fluorescence detection. *Journal of Separation Science* **2014,** *37* (19), 2757-2763.
156. Yiantzi, E.; Psillakis, E.; Tyrovola, K.; Kalogerakis, N., Vortex-assisted liquid-liquid microextraction of octylphenol, nonylphenol and bisphenol-A. *Talanta* **2010,** *80* (5), 2057-2062.

157. Lopez-Cervantes, J.; Paseiro-Losada, P., Determination of bisphenol A in, and its migration from, PVC stretch film used for food packaging. *Food Additives and Contaminants* **2003,** *20* (6), 596-606.
158. Biles, J. E.; McNeal, T. P.; Begley, T. H.; Hollifield, H. C., Determination of bisphenol-A in reusable polycarbonate food-contact plastics and migration to food-simulating liquids (vol 45, pg 3541, 1997). *Journal of Agricultural and Food Chemistry* **1998,** *46* (7), 2894-2894.
159. Mendum T, S. E., Vanbenschoten H, Warner JC, Concentration of bisphenol a in thermal paper. *Green Chem Lett Rev 1*, 81-86.
160. Russo G, B. F., Grumetto L. , Monitoring of bisphenol A and bisphenol S in thermal paper receipts from the Italian market and estimated transdermal human intake. A pilot study. *Sci Total Environ* **2017,** *599–600*, 68-75.
161. Synthesis of haptens and production of antibodies to bisphenol A.
162. Lin, Z. K.; Cheng, W. J.; Li, Y. Y.; Liu, Z. R.; Chen, X. P.; Huang, C. J., A novel superparamagnetic surface molecularly imprinted nanoparticle adopting dummy template: An efficient solid-phase extraction adsorbent for bisphenol A. *Analytica Chimica Acta* **2012,** *720*, 71-76.
163. Xiao, P.; Weibel, N.; Dudal, Y.; Corvini, P. F. X.; Shahgaldian, P., A cyclodextrin-based polymer for sensing diclofenac in water. *Journal of Hazardous Materials* **2015,** *299*, 412-416.
164. Calafat, A. M.; Weuve, J.; Ye, X. Y.; Jia, L. T.; Hu, H.; Ringer, S.; Huttner, K.; Hauser, R., Exposure to Bisphenol A and Other Phenols in Neonatal Intensive Care Unit Premature Infants. *Environmental Health Perspectives* **2009,** *117* (4), 639-644.
165. Nam, K.; Kimura, T.; Kishida, A., Controlling coupling reaction of EDC and NHS for preparation of collagen gels using ethanol/water co-solvents. *Macromolecular Bioscience* **2008,** *8* (1), 32-37.
166. Yan, Q.; Zheng, H. N.; Jiang, C.; Li, K.; Xiao, S. J., EDC/NHS activation mechanism of polymethacrylic acid: anhydride versus NHS-ester. *Rsc Advances* **2015,** *5* (86), 69939-69947.
167. Ramireddy, A.; Chugh, H.; Reinier, K.; Ebinger, J.; Park, E.; Thompson, M.; Cingolani, E.; Cheng, S.; Marban, E.; Albert, C. M.; Chugh, S. S., Experience with Hydroxychloroquine and Azithromycin in the COVID-19 Pandemic: Implications for QT Interval Monitoring. *J Am Heart Assoc* **2020**, e017144.
168. Teng, C.; Goodwin, B.; Shockley, K.; Xia, M.; Huang, R.; Norris, J.; Merrick, B. A.; Jetten, A. M.; Austin, C. P.; Tice, R. R., Bisphenol A affects androgen receptor function via multiple mechanisms. *Chemico-biological interactions* **2013,** *203* (3), 556-564.
169. Lee, S.; Kim, G.; Moon, J., Performance Improvement of the One-Dot Lateral Flow Immunoassay for Aflatoxin B1 by Using a Smartphone-Based Reading System. *Sensors* **2013,** *13* (4), 5109-5116.
170. Zhao, Y.; Zhang, Q.; Meng, Q. F.; Wu, F. L.; Zhang, L. H.; Tang, Y.; Guan, Y. Y.; An, L. X., Quantum dots-based lateral flow immunoassay combined with image analysis for semiquantitative detection of IgE antibody to mite. *International Journal of Nanomedicine* **2017,** *12*, 4805-4812.
171. Liu, C. Y.; Jia, Q. J.; Yang, C. H.; Qiao, R. R.; Jing, L. H.; Wang, L. B.; Xu, C. L.; Gao, M. Y., Lateral Flow Immunochromatographic Assay for Sensitive Pesticide Detection by Using Fe_3O_4 Nanoparticle Aggregates as Color Reagents. *Analytical Chemistry* **2011,** *83* (17), 6778-6784.

ACKNOWLEDGEMENTS

Numerous great names in the history of science are closely associated with the city of Berlin. All of this inspired me to choose Berlin as the place to do my PhD.

For this I will be eternally grateful to and indebted to my research supervisor Dr. Rudolf J. Schneider who not only gave me the opportunity to work in his group but also gave me the freedom to develop and pursue my own ideas. I will always remember that it was you who opened the door for my academic career.

I would also like to express my most sincere gratitude to my supervisor Prof. Dr. Kannan Balasubramanian for his continuous support, advice, and the many intensive discussions with him that helped to finish this thesis.

I would like to thank Prof. Dr. Sergei A. Eremin for triggering my interest onto the field of immunoassays already when I was an undergraduate student and for fueling my enthusiasm for the importance of immunoanalytical technology.

Very special thanks to Dr. Dirk Tuma for his encouraging support and sharing my daily frustrations as well as my successes throughout the last several years.

And I would like to thank my teacher of chemistry at school Olga Liboratovna Ulukhanova, PhD; without her, I would not have discovered the beauty of chemistry and science.

I had the great pleasure to work with many wonderful people at BAM over the years and I am grateful to each of them for their support. I would like to express my special thanks to those extraordinary scientists: Ander Chapartegui Arias and Teodor Tchipilov for their efforts that successfully yielded publications. I am grateful for the opportunity of being co-author. Thank you, Dr. Peter Carl, for the nice chats in the lab, your help, and sharing your contagious enthusiasm for science.

This thesis could not have been completed without the support of the devoted laboratory workers, many thanks to Dr. Andreas Lehmann, Tanja Westphalen, and Christoph Wilming, whose support and knowledge of LC-MS/MS helped in my research studies, and to Sabine Flemig and Jan Ole Kaufmann for MALDI-TOF measurements. My deep

gratitude extends to other colleagues who have already left BAM and started their careers: Dr. Nahala Abdel-Shafi, Dr. Inês Ramos, Dr. Margarida Carvalho, and Dr. Holger Hoffmann which were colleagues in our group, and, among other BAM members, Dr. Estela Climent, Marco Wilke, and Martin Paul, who shared their knowledge with me.

I am especially grateful to Anka Kohl for her support and endless patience with all IT-related issues.

I would like to thank Nadine Scheel. Without her, I am not sure whether I would ever have discovered the path of finding a balance in between private and professional life.

This journey could not be possible without Bianca Coesfeld. Without her assistance, I would have failed with managing the experimental work. I express my thanks for your help and support. I am also very thankful to have a friend like you. Very special thanks go to Dr. Stephan Schmidt, who helped me in the first few months in the field of immunoassays and protein conjugates.

Finally, I express my deepest gratitude to my family. I simply can't imagine having achieved all this without your devoted support. Thank you, my mother Heghine Frunziki Bagratuni Durgaryan and my father Sargis Beglari Raysyan for patiently listening to all the details of my experiments; you never stopped believing in me at a time when I didn't believe in myself. Thank you for taking the strenuous flights to visit me in Berlin, for mailing me fancy bits of Russia and Armenia, that nurtured me with strength and optimism. And for supporting me since I am still spending my time with growing and learning to be myself. To my uncle in law Igor Scheer, for your wisdom and the right words that always encouraged me and for the large library in which I spent my entire childhood.

The importance of friendship in our life is beyond any description. Friends always provide us with good guidance, and we may rely on them for solving our problems. Friends can solve all our problems as well as share good times that will multiply our happiness. To my childhood friends Arsen Mirzayan and Dzhamal Bakriev, I very grateful to have you in my life since my young age.

Last but not least, funding by BAM's MI program (BAM/BMWi, Grant No. Ideen_2015_55 to A.R.) is gratefully acknowledged.

Vielen Dank, Спасибо, Շնորհակալություն, Thank you